

QUEEN'S UNIVERSITY BELFAST

**Electronic structure of certain
Titanium-Aluminium superalloys: from
first principles to Bond Order Potentials**

Dimitar Lyubomirov Pashov
BSc in Chemistry

A thesis submitted to
the School of Mathematics and Physics
in partial fulfilment of the requirements for the degree
of
Doctor of Philosophy

November 12, 2012

Abstract

At the outset of the project it was intended to find a bond order potential, such as first proposed by Stefan Znam, that will describe the titanium aluminides across the stoichiometry Ti - TiAl - Ti₃Al. Znam's BOP model was not fitted to Ti₃Al, nevertheless it showed some promising results for D0₁₉. It was first discovered that Znam's BOP failed to predict the stability of D0₁₉ α_2 phase, instead D0₂₂ was dramatically stabilised. The search for a remedy for this was long and hard and, essentially, in this thesis I investigate in detail the sources of uncertainty contributing to the problem. At the end of this exercise I had a potential for α_2 and this in itself is a significant advance. We can now proceed to make atomistic simulations of dislocation core structures in the monolithic α_2 phase but we require a new strategy for the γ/α_2 interfaces. Because the polysynthetically twinned titanium aluminide is of less pressing interest to metallurgists than it was three years ago, it was decided to change the course of the research and in the final chapter, rather than report any atomistic simulations, I derive the formulas needed to implement the new strategy. By writing a general computer program to make the BOP / TB hybrid embedding I will provide the platform for the next generation of atomistic simulation planned in the Atomistic Simulation Centre.

Contents

Abstract	i
I Introduction and background	1
I.1 Ti-Al microstructure	4
I.1.1 Defects	5
I.1.2 gamma-Ti-Al deformation modes	12
I.1.3 alpha ₂ -Ti-Al deformation modes	14
I.1.4 PST TiAl/Ti ₃ Al deformation modes	15
I.2 Modelling	17
II Electronic structure and BOP	22
II.1 Introduction	22
II.2 Density Functional Theory	25
II.3 Tight Binding	36
II.4 Bond Order Potentials	42
II.5 Classical potential terms	58
III Pairwise functions in TB/BOP	61
III.1 Cutoffs	64
III.1.1 The Augmentative Cut-off	64
III.1.2 The Multiplicative Cut-off	65
III.1.3 Proof of eligibility	67
III.1.4 Type II	69
III.1.5 Comparison	70
III.2 GSP revisited	73

CONTENTS	iii
III.3 Matching cosines	76
IV Finding Parameters	78
IV.1 Introduction	78
IV.2 From LMTO-ASA	81
IV.2.1 Structural Energy Difference and RS-LMTO-ASA	89
IV.2.2 Less-Than-Minimal Basis	94
IV.2.3 Moments Horizon	100
IV.2.4 TB-ASA fundamental integrals	103
IV.2.5 Fitting to the ASA bandstructure	110
IV.3 Fitting the Classical Terms	114
V Exact Embedding with BOP	120
V.1 Introduction	121
V.2 Perturbative representation	122
V.3 Direct block-matrix solution	125
V.4 Extension to embedded surface	128
V.5 Overlap	129
VI Conclusions	132
Appendix	135
Bibliography	155
Acknowledgements	156

Chapter I

Introduction and background

Metals have had wide spectrum of application since ancient times. From soft plastic lead pencils and fine brass pieces of art to steel weaponry, metals have been utilised in almost every aspect of life. The development of metallurgy has played an important role in shaping today's world. By the end of the second quarter of the XX century the then newly invented Ni based high-performance (super)alloys[1] filled the need for material capable of enduring some of the most challenging industrial environments. For nearly 60 years by now[2] these superalloys have been serving under enormous stresses, blazing temperatures and high pressures of reactive gases in aircrafts, jet propulsion, internal combustion engines and gas turbines in power-plants(fig. I.1).

The extraordinary mechanical properties leading to the “super-alloy” name are largely due to the presence of intermetallic compound γ' -Ni₃Al. Probably its most interesting properties are the ability to stay ordered up to melting and the yield strength anomaly[6] i.e. the applied stress necessary to initiate a plastic deformation increases with the temperature, contrary to the norm in metals. Many other intermetallic compounds have been found to possess similar mechanical properties and have been subject of industrial

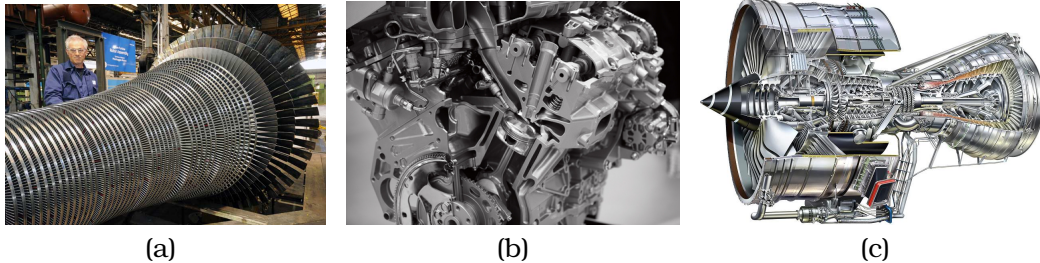


Figure I.1: Applications of “superalloys”. (a) Steam turbine rotor[3]. (b) Internal combustion engine found in vehicles[4]. (c) The Rolls-Royce Trent 900 engine[5].

interest and active research since. Unfortunately none has been found to match and improve overall the mechanical strength, high temperature creep, and chemical/corrosion resistance offered by the Ni-superalloys and yet be ductile enough at room temperature to endure treatment with established conventional technologies. The current efforts are mostly focused on developing specialised materials which could replace or be used in combination with Ni-superalloys in applications, like protective coatings and very specific construction elements. The most prominent alternatives are Ni-Al, Fe-Al, Mo-Si, Nb-Si, Ti-Al, Pt-Al and others[7, 8, 9, 10].

Of these, Ti-Al based alloys offer a balance of the mechanical properties mentioned as shown in I.1 and I.2. What makes them stand out is their very low density, about half the Ni alloy’s density.

Lower weight of construction elements increases efficiency and decreases overall wear extending the lifespan of a machine. These considerations gain importance in times of rising fuel costs and environmental responsibility. Ti and Al are also cheaper and more abundant than the more exotic Ta, Nb, Zr, Re, and of course Pt. There have been a few shortcomings, which have made the handling and working with these alloys difficult and expensive, and have practically prevented any sizable application for many years.

	Density [g/cm ³]	Elastic Modulus [Mbar]	Fracture Toughness [MN/m ^{3/2}]	Tensile Creep Limit, [°C]	Oxidation Limit, [°C]
Ti super-alloys	4.5	1.10	35-60	600	600
Ni super-alloys	8.3	1.25	30-35	1100	>1100
Ti ₃ Al(α_2)	4.3	1.45	25	800	650
TiAl (γ)	3.8	1.76	25	950	900
NiAl	5.9	1.93	12-15	1100	...
MoSi ₂	6.5	3.79	4-5	...	> 1700
Nb ₉ Si	7.5	1.45	25	...	≈ 400

Table I.1: Selected properties of various intermetallic materials for turbine engine applications[10]. Fracture toughness measured at room temperature

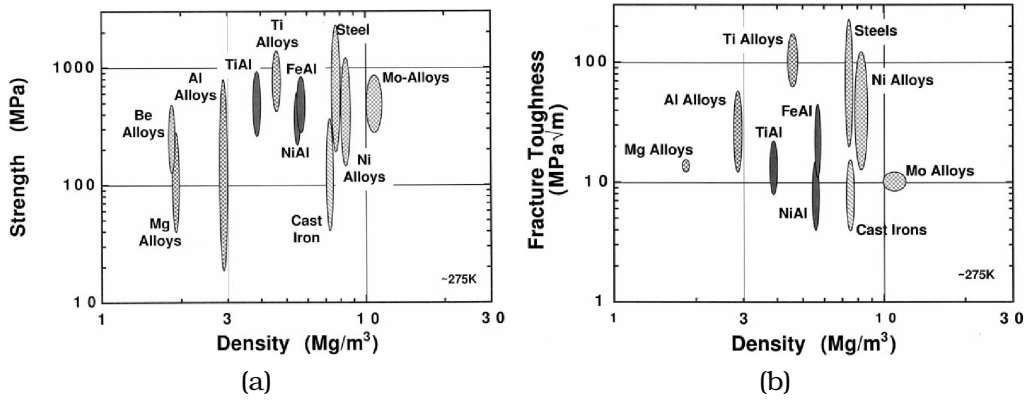


Figure I.2: Cross-plot of room temperature strength (a) and fracture toughness (b) vs density [8].

The major problem is the brittleness, at moderate to low(room) temperatures, of the most prevalent pure γ -TiAl phase[11]. The ductility has been improved with the advent of the so-called polysynthetically twinned (PST) alloy[12, 11]. It was only a few years ago when “General Electric” announced their new gas turbine engine “GEnx”, highlighting the use of TiAl in the low pressure turbine blades[13].

I.1 Ti-Al microstructure

One of the determining factors for the mechanical properties of a material is its microstructure. Depending on the composition and temperature the Ti-Al binary system forms a variety of phases (fig. I.3): α -Ti-(A3), β -Ti-(A2), α_2 -Ti₃Al-(D0₁₉), γ -TiAl-(L1₀), TiAl₃-(D0₂₂) (fig. I.4) and others. A large number of experimental and theoretical studies on the phase equilibria has been published [14, 15, 16, 17, 18, 19, 20, 21, 22, 23, 24, 25, 26, 27, 11]. While there had been some disagreements in the high temperature zones attributed to oxygen contamination [28], the equilibrium between the most interesting phases, γ and α_2 , has been confirmed [26].

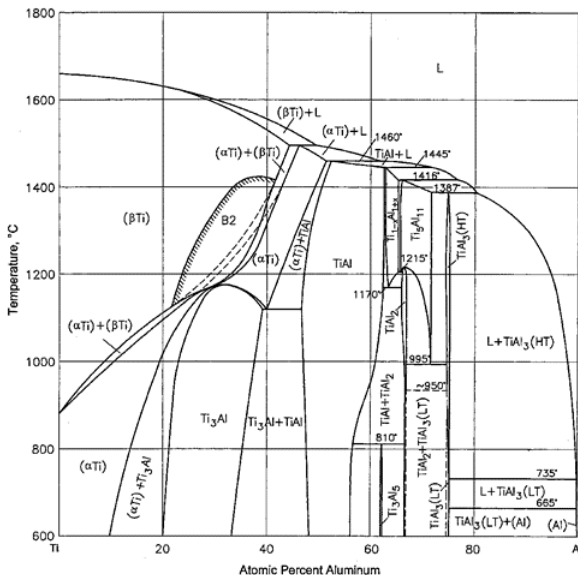


Figure I.3: Phase-diagram for the Ti-Al system.[27]

The predominant phase in Ti-Al alloys is γ -TiAl-(L1₀). It is obtained when the mixture is richer in Al, up to about 55%. It has a f.c.c. derived tetragonal cell built by stacking pure Al and pure Ti {002} layers in the $\langle 001 \rangle$ directions in alternating order leading to axial ratio different than 1, $c/a = 1.016$ [30]. The stacking order along the $\langle 111 \rangle$ directions is ...ABCABC Environments

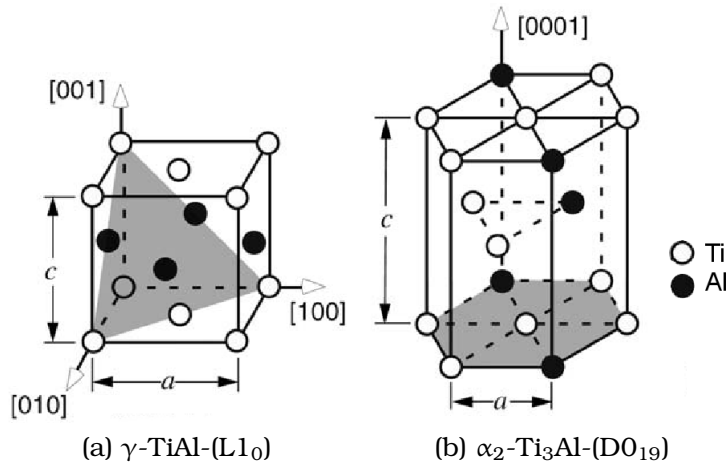


Figure I.4: Most important structures in the Ti-Al binary system. (Graphics courtesy of [29])

slightly richer in Ti or near 1:1 produce lamellar structure of γ and α_2 phases and duplex microstructure composed of lamellar grains and pure γ grains. The $\alpha_2\text{-Ti}_3\text{Al-(D}0_{19}\text{)}$ phase has a hexagonal cell with stacking ...ABAB.... The axial ratio $c/a = 0.804$ is close to the ideal 0.8165. The (0001) plane is compatible with the (111) in the γ phase. Although both phases are extremely brittle in ambient temperature, the lamellar(fig. I.5) and duplex structures are more ductile[11].

I.1.1 Defects

Ductility in ordered phases is strongly influenced by the defects in the crystal lattice, their creation, motion and interactions. In three dimensional lattice there are defects of all dimensions: point, line, plane and bulk.

Point defects are related to a single lattice position. A missing atom is a vacancy or sometimes called Schottky defect, an additional atom is an interstitial defect. An atom replaced with one of

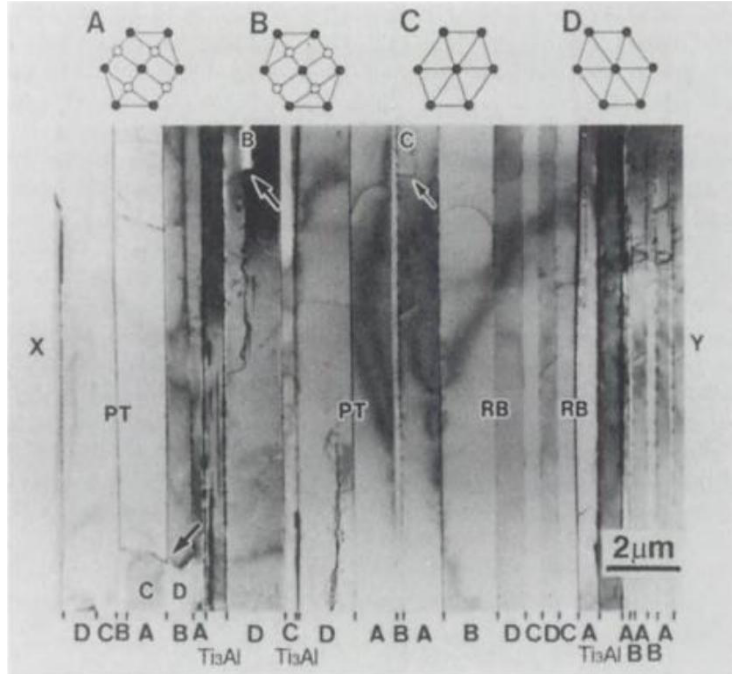


Figure I.5: Lamellar polysynthetically twinned (PST) Ti-Al.

different type caused by impurity is a substitutional defect. A pair of atoms with swapped positions is an antisite defect. A vacancy nearby an interstitial is called a Frenkel defect or pair [31].

The presence of a certain number of structural point defects lowers the free energy of a crystal due to an increase of entropy. Appreciable number of point defects then may be present in a crystal in thermodynamic equilibrium. One and two dimensional defects on the other hand always raise the free energy of the system. The motion of vacancies facilitates diffusion in solids.

A line defect can be created if a two parts of a crystal, separated by a finite surface, are displaced with respect to each other by vector \vec{b} and any overlapping material is removed and voids are filled in. If the displacement amount \vec{b} is multiple of the lattice vectors then only the atoms near the boundary of the surface are significantly displaced from ideal positions. The line bounding the

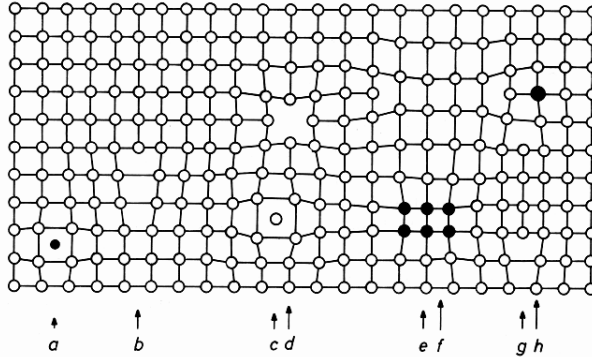


Figure I.6: Examples of crystal defects: a) interstitial impurity atom, b) edge dislocation, c) self interstitial atom, d) vacancy, e) precipitate of impurity atoms, f) Vacancy type dislocation loop, g) interstitial type dislocation loop, h) substitutional impurity atom [32]

surface is a dislocation line[33]. The displacement \vec{b} is called Burgers vector. It does not change during motion and is a characteristic quantity of the dislocation.

There are two basic types of dislocations(fig. I.7) depending on the relation between the dislocation line and the burgers vector: edge and screw.

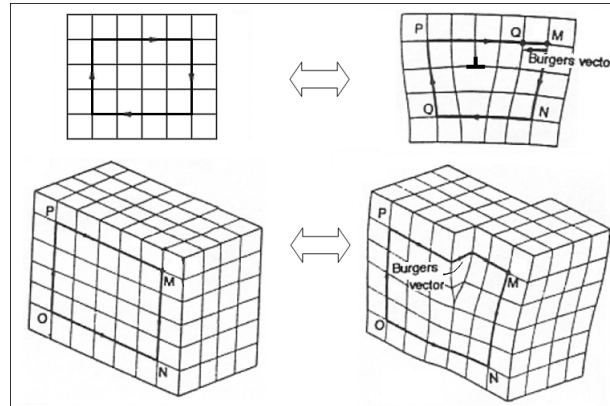


Figure I.7: Dislocations: top: edge; bottom: screw

An edge dislocation is formed when an extra plane (edge) is inserted in or removed from the crystal (fig. I.7). The Burgers vector

is perpendicular to the dislocation line. A screw dislocation may be visualised as the result of shearing a crystal twisting (partially and displacing) the two parts in direction parallel to the line of the shearing edge. The Burgers vector of a screw dislocation is parallel to the dislocation line. A mixed dislocation combines characteristics of both types. The line of mixed dislocation may be curved and the tangents at different points form different angles with the Burgers vector.

A motion accompanied with adding or removing atoms around the dislocation line is called climb. It is a slow and difficult process relying on diffusion to handle the addition or disposal of atoms displaced. At low temperatures it is usually faster to "glide" on the slip plane containing the dislocation line and the Burgers vector without change in the volume. Such plane is well defined in edge dislocations because the Burgers vector and the dislocation line are perpendicular while in screw dislocations the plane of motion may be any crystallographic plane containing the dislocation line. During ideal glide the stress applied has to overcome the hills on the potential energy surface created by the bonding between atoms. The energy surface features are named after R. Peierls: Peierls barrier, Peierls valley, etc. and the necessary minimal stress Peierls stress. In practice the dislocation line moves stepwise by the random formation of kink pairs. A kink is a defect of the dislocation line, a step which lies in the slip plane. A kink is a special case of a jog, a step in the line which does not necessarily lie in the slip plane. Kinks facilitate glide while jogs are related with climb. Jogs require the absorption or emission of vacancies or interstitials to move. A comparatively slower process at low temperatures makes jogs rather immobile. Kinks appear spontaneously because they decrease the free energy of a dislocation under stress, much like point defect do for the bulk crystal at finite temperature. Jogs may form when edge and screw dislocations intersect. Each obtains a

jog the size of the other dislocation's Burgers vector. They may also appear from point defects accumulation on a dislocation. Kinks are an important facilitator of creep. Creep occurs when stress, lower than the critical needed to overcome the Peierls barrier, is applied for very long time. It is rarely visible on simple inspection until fracture and disasters happen.

Dislocation loops may form when a dislocation is pinned by sessile jogs at some distance apart. Kinks expand and bend the dislocation line under the load stress until the two fronts meet. They may be seen as separate parallel dislocations in the same slip plane with opposite Burgers vectors which annihilate. The resulting pinned dislocation inside the loop may undergo the same process many times. This mechanism is commonly called Frank-Read source [33].

Dislocation loops can be observed under electron microscope. The line looks curved macroscopically but the curvature is in fact a perception of the concentration of many tiny kinks much like a curved or diagonal line is drawn on pixel screen.

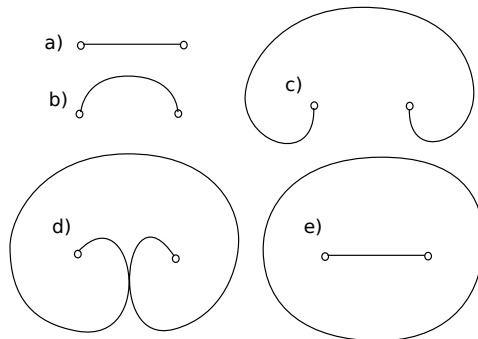


Figure I.8: Consecutive phases of a dislocation loop: a), b), c), d), e)

A dislocation may dissociate into partial dislocations with planar defect between them[33]. These partial dislocations are often called just "partials". Their Burger's vectors are fractions of

the ideal lattice vectors instead of multiples. The planar defects possible are various shifts or rearrangement between inequivalent planes generally called stacking faults and interfaces between grains of different crystal phases called grain boundaries. For example the {111} planes in the fcc lattice have ...ABCABC... stacking order while in the hcp lattice the equivalent planes, {0001} follow ...ABABAB... order. If an edge dislocation is fictionally made by removing or inserting a {111} plane in fcc structure in fashion similar to the one mentioned above then the Burgers vector will be $\pm 1/3\langle 111 \rangle$. Such dislocation is Frank's partial. If instead of removal or addition of a plane one of the halves is displaced so that the order is shifted in one part of the crystal, for example ...ABC|BCA..., we would have a Shockley partial. Since partial dislocations are created after the dissociation of 'perfect' dislocations, the sum of the Burgers vectors of the resulting partial dislocations is the Burgers vector of the original dislocation. Whether a dislocation will dissociate depends on the energies of the stacking fault and of the dislocation before and after dissociation. The stacking fault energies are usually local minima on the energy surface made by shifting part of a crystal with respect to neighbouring part on sharing the slip plane plane and calculating/"measuring" the energy at each point. This interfacial potential energy surface is called γ -surface [34].

Another interesting planar defect is the "twin". A twinned crystal has at least two parts separated by a plane and related to each other with some symmetry rule[33]. The plane of contact is sometimes called twinning plane or compositional plane. In the most common case parts of a twinned crystal are mirror images of one another. This twinning may be seen as rotational planar defect which turns the two halves to 180° with respect to each other. Twinning can be caused by applied shear stress and can also appear spontaneously during solidification from liquid phase or de-

position from gas phase. Many naturally occurring crystals have repeating mirror planes separated by layers of twins. They are commonly called *polysynthetically twinned*[33]. Polysynthetical twinning may also occur after specific heat treatments and tempering. A deformation twinning(fig. I.9b), resulting from straining a crystal may occur in cases when there are few other deformation modes available due to lower symmetry or when the stress application is very quick. During deformation twinning partial dislocations in many planes move collectively a distance smaller than the lattice vector. If the Peierls stress for the partials is lower than for the corresponding perfect dislocation at low temperature then twinning may occur in crystals of higher symmetry[35]. The swift collective motion may lead to phonon propagation and distinctive audible sound[36]. Famous example is the "tin cry" which can also be heard from zinc, indium and other materials.

A dislocation's mobility is mostly influenced by its core structure. A planar core structure enables it to glide. A sessile dislocation's core, on the other hand, is spread across many planes considerably constraining its motion. High fraction of mobile dislocations makes for a plastically deformable material. Under stress crystalline materials initially deform elastically. After certain stress is reached a ductile material deforms plastically while brittle one is likely to suffer fracture before reaching yielding. Dislocations' interactions with other defects, may lead to changes in their core structure and, consequently, behaviour. These interactions are numerous and complex, and generally temperature dependent. A detailed description of the theory of dislocations is given in [35].

I.1.2 γ -TiAl deformation modes

The slip and twinning deformation modes occur on the close packed $\{111\}$ planes in the γ phase. The twinning is of type $\{111\}\langle 11\bar{2} \rangle$ and is not active at room temperature. Slip occurs through the $1/2\langle 110 \rangle$ and $1/2\langle 112 \rangle$ ordinary dislocations and a $\langle 101 \rangle$ superdislocation (fig. I.9).

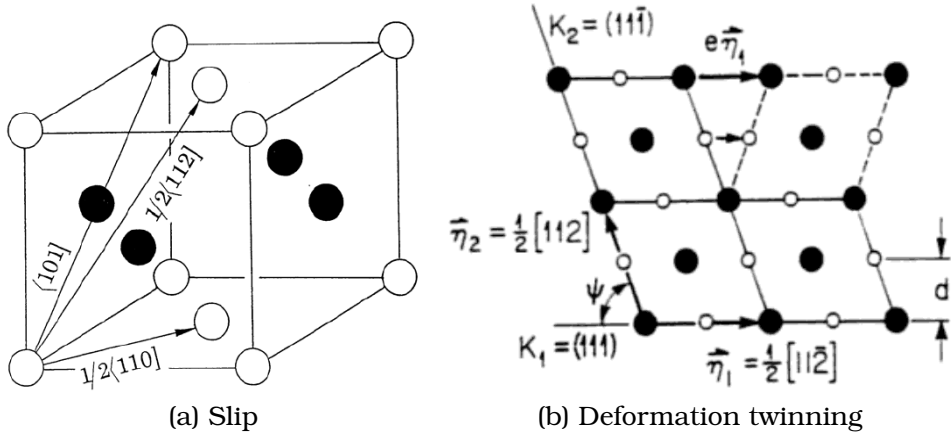


Figure I.9: Deformation modes in the γ phase. **(a)** $1/2\langle 110 \rangle$ and $1/2\langle 112 \rangle$ ordinary and $\langle 101 \rangle$ superdislocation's Burgers vectors. **(b)** Twinning. The filled circles are on the plane of shear $(1\bar{1}0)$ and the open circles are on the adjacent $(1\bar{1}0)$ plane [37].

The $1/2\langle 112 \rangle$ dislocation has fairly long Burgers vector and is not observed to glide. The $1/2\langle 110 \rangle$ dislocation is not active at low temperatures and only the $\langle 101 \rangle$ superdislocation is involved in slip [38]. Its critical resolved shear stress (CRSS) is very dependent on the loading axis angle. The twinning and the $1/2\langle 110 \rangle$ dislocations are activated at higher temperature and becomes dominant while the superdislocation becomes less active and eventually the hardest deformation mode [39, 38].

Theoretical studies [40, 41, 42] have shown the $1/2\langle 110 \rangle$ screw dislocation has non-planar core structure and is spread symmet-

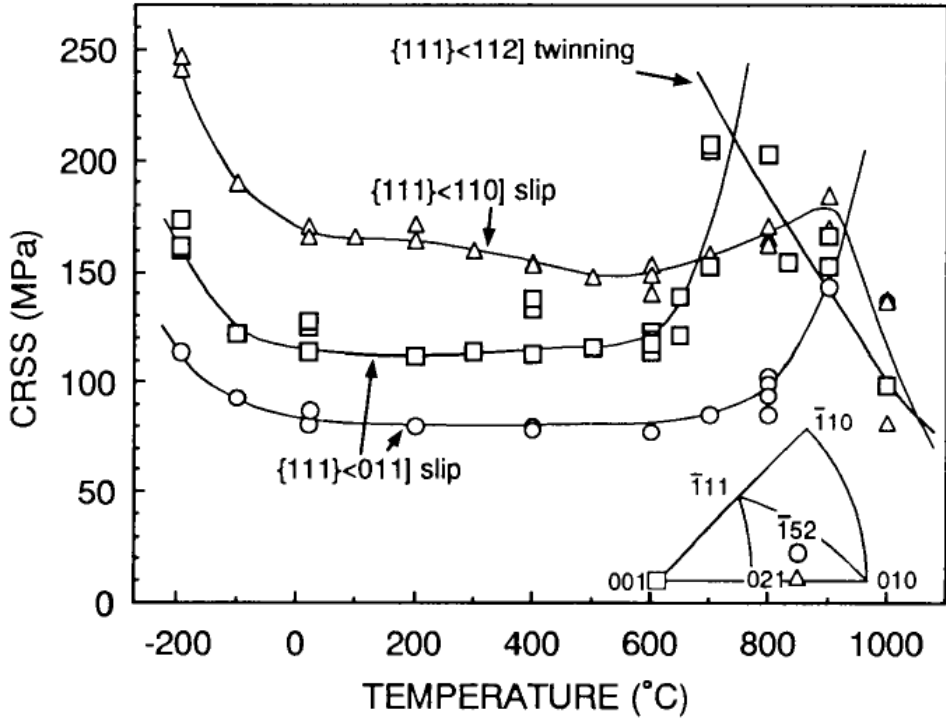


Figure I.10: Yield stress as a function of temperature for single crystals of TiAl(56% at.) with three different orientations[39]

rically on two $\{111\}$ planes. Under the application of gradually increasing shear stress in the $[1\bar{1}0]$ direction on the (111) plane the dislocation initially distorts and spreads asymmetrically on the $\{111\}$ planes then starts to move at CRSS of about 1 GPa. Continued increase of the stress extends the displacements along the cross-slip plane. Due to the localisation of strain on the (111) plane the dislocation cross-slips to the conjugated $(11\bar{1})$ plane. Further cross-slip was observed after short gliding[40].

The $\langle 101 \rangle$ superdislocation has planar and non-planar alternative core structures. The planar is the result of splitting into three partials with superlattice intrinsic and complex stacking fault type planar defects (SISF and CSF) on (111) between them. Its energy barrier/Peierls stress is lower than the one for the non-planar

which corresponds to splitting to three partials with two SISFs between them. The non-planar core is sessile but is the one more likely to move when the resolved stress is too low for the planar core. The planar core structure is short lived and transforms to non-planar after short glide[42, 40].

I.1.3 α_2 -Ti₃Al deformation modes

Due to its hcp derived lattice, D0₁₉ the α_2 -Ti₃Al phase has strongly anisotropic mechanical properties. The limiting symmetry and the lack of deformation twinning in D0₁₉ are thought to contribute to the high brittleness. The slip systems found are {1̄100}⟨11̄20⟩ (prism **a**-slip), (0001)⟨11̄20⟩ (basal **a**-slip), {0̄221}⟨11̄26⟩ (type **I** pyramidal **2c+a**-slip) and {11̄21}⟨11̄26⟩ (type **II** pyramidal **2c+a**-slip)[43, 44, 45, 46, 47]. Similarly to hcp Ti, the prismatic **a**-slip is the easiest to operate followed by the basal **a**-slip. Both of them are caused by the motion of the 1/3⟨11̄20⟩ superdislocations in the prism and the basal planes. The pyramidal **2c+a**-slip is considerably harder to activate and also has anomalous temperature dependence up to 700°C depending on the exact stoichiometry. 1/3⟨1̄126⟩ superdislocations generally exist as pairs of superpartials bounding antiphase boundaries (APB) of varying widths at relatively low temperatures. At temperatures centering at the peak yield-stress temperature but not so high as 900°C, the superpartials of the opposite sign are coupled by APBs about 300 nm wide. Edge segments of these unlike superpartials are thought to be locked by climb dissociation into partials and prevent the unlike superpartials from combining together and being annihilated. At much higher temperatures, pyramidal slip occurs but superpartials are no longer stable under the unstressed conditions. The superpartials decompose into **a/2** and **c** component dislocations. The APB on {1121} associated with the superpartials is generally so wide that it is difficult to find any relationship between the APB and the yield stress

anomaly[48]. Above 900°C the basal and pyramidal slip systems glide easily and the material is fairly ductile (fig. I.11).

Unlike hcp Ti, stoichiometric Ti_3Al does not undergo deformation twinning. It occurs only in compositions with more than 34at.% Al at temperatures higher than 1000°C and compression axis close to **c** [49, 50]. The compositional deviation to the Al-rich side was found to be harmful for ductility of Ti_3Al and coarse slip bands on the basal plane often act as a trigger for crack nucleation [45]. A tensile deformation study at room temperature[51] finds that fracture precedes yielding for specimens with a thickness greater than 300 μm and plastic flow only occurs when the thickness is reduced to 150 μm .

There are few theoretical studies on the α_2 phase. They are ab-initio and thus mostly concerned with calculations which do not need more than a few hundred atoms. The electronic structure, phase stability, planar defects and interface boundary energies [53, 54, 55] are available and it is our intention to contribute with more investigations of the dislocations and their interaction with the various interfaces.

I.1.4 PST $TiAl/Ti_3Al$ deformation modes

The lamellar structure is composed of γ and α_2 phase lamellae (fig. I.5) with thickness of approximately 1 μm . The predominant phase is γ . The α_2 lamellae are thinner and stand at considerable distance apart. The predominant interfaces are γ/γ . The different domains in each lamella form different angles with their neighbours from the neighbouring lamellae. The domain boundaries in each lamella are also not correlated with the ones in the neighbouring lamellae. These observations apply to both γ and α_2 domains. The contact (composition) planes face the {111} planes of the γ lamellae with their basal plane (0001). The lamellae are composed of

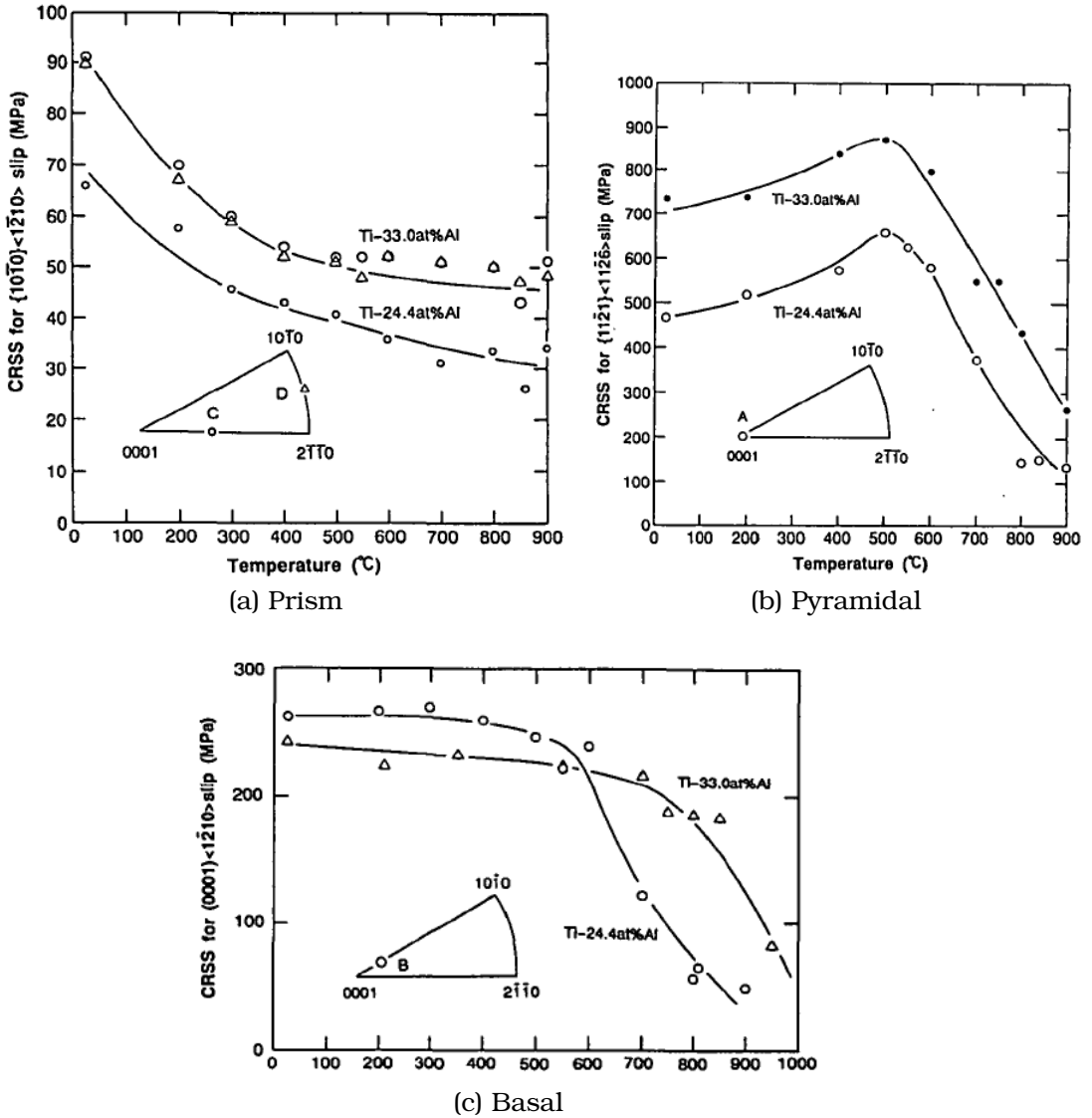


Figure I.11: CRSS for the three slip systems in the α_2 phase as a function of the temperature[52].

domains with different orientations (fig. I.12). Many of the γ/γ interfaces between thin layers are twins similar in appearance to some naturally occurring *polysynthetically twinned* crystals leading to the name *PST Ti-Al*, but the different domains also form 60° and 120° interfaces.

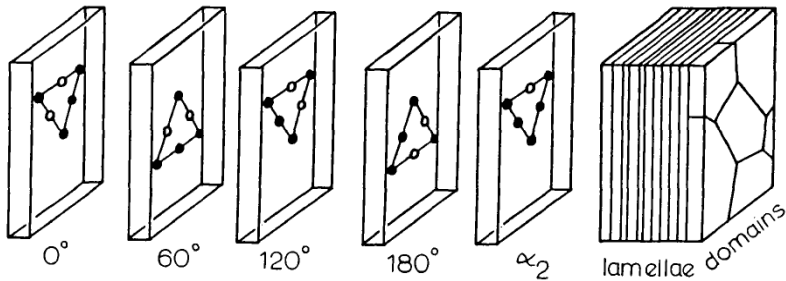


Figure I.12: Lamellar geometry in PST[56].

The presence of interfaces leads to strongly anisotropic deformation behaviour and influences the mechanical properties significantly. An inverse relation has been found between the thickness of the lamellae and the ductility of the PST Ti-Al. Glide is easier when parallel to the lamellar boundaries than perpendicular and the lowest yield stress is found when the loading axis is at 45° with respect to the lamellar boundaries. Large number of dislocations are concentrated and emitted from the interfaces during plastic deformation increasing the interactions between them and the boundaries. The 60° and 120° interfaces lower the energy of the CSF in the γ lamellae and thus stabilise the glissile planar core structure of the [101] superdislocation. 180° interfaces on the other hand increase the energy of CSF. The 60° and 120° interfaces are also found to reduce the Peierls stress of the dislocations lying in the lamellar boundaries[57]. A twin near a 60° ordinary dislocation preserves the dislocation's planar core structure under applied stress with loading axis parallel to the lamellae[58].

I.2 Modelling

Dislocations create long ranged elastic fields which are described well by analytic expressions provided by the continuum elasticity theory. Close to the dislocation core the continuum model is not

applicable but it is the core structure which defines the characteristics of the defect. There are solid sphere models with limited applicability because the arrangements of the atoms in the core structure depend highly on their quantum chemical character. Experimental observations are very difficult if possible at all and the only viable options left for looking into these small worlds are the computer simulations.

Usually a starting simulation block containing a defect is prepared by following an analytic model. Depending on the objects of interest and the computational method's limitations periodic boundary conditions may be required or inevitable. A relaxation algorithm and method for calculation of the energies and forces on the atoms are chosen. Depending on the whether temperature effects or meaningful time evolution steps are required one may carry out molecular dynamics, molecular statics (MS), or Monte Carlo simulation (MC). Molecular dynamics moves the atoms according to Newton's laws of motion with variety of particle ensembles. It requires the forces on the atoms to be consistent with the energy calculated and results in realistic temperature and time dependence. Molecular statics and Monte Carlo simulations are faster methods useful for finding the energy of a local minimum in the atomic positions space near the starting configuration by allowing physically meaningless intermediate steps predicted by an optimisation algorithm. The method for calculation of the energy for a given atomic configuration is the non-trivial part of a simulation. A balance has to be struck between the speed, scaling, features and accuracy offered. The choice depends on the specific material simulated and on the properties of interest. The existence of significant covalent, directional bonding for example is not well described by simple and fast models while the long range elastic fields dislocations create requires large simulation boxes with very many atoms.

The simplest atomistic simulations can be performed with simple pairwise potentials. These are most applicable to materials close to the fictitious jellium: a system of uniform electron gas engulfing a lattice of atom cores. There are generally two contributors to the energy: a pairwise term expressing the rearrangement energy and average density dependent term accounting for the volume dependence. While such models may shed some light on the bulk properties of metals like Cu, Ag, Au they are not applicable to any cells with non-uniform arrangement or containing any amount of covalent bonding.

Addition of a local atomic (also as representation of electron) density term somewhat expands the applicability of simple models to systems with less uniform distribution of atoms. While still severely limited the value of these methods, when applicable, is in their simplicity. The high speed of computation allows simulations with millions of atoms on modest hardware. Due to the analytical representation the calculations of forces are fast and consistent which is important in molecular dynamics. The locality of the terms allows for relatively easy implementations on parallel machines with ideal scalability of resources used.

The most widely used potentials for atomistic modelling of metals are the embedded atom method (EAM) [59] and the Finnis-Sinclair (FS) method [60]. While developed separately they are very similar in form. They consist of pairwise interactions and a functional dependent on the local density. The functional in FS is square root and in EAM its definition is part of the specific model. The EAM looks at each atom as being embedded in its surrounding with related embedding energy hence the name: embedded atom method. The FS potential was derived from the analytical expansion up to the second moment of the density of electronic states in the tight binding theory. The density of states is a distribution of the number of available states at certain energy and it represents

the electronic structure. The second moment of a distribution is its variance or root mean square width. The applicability of FS then depends on how well the second moment describes the density of states for certain material. Higher moment terms are usually significant in more directional covalent bonding formed by electrons in partially filled d orbitals thus unfortunately the FS/EAM rarely provide adequate description there. For example the difference in the cohesive energy of polytypes is usually contributed by the fourth and higher moments[61, 62].

The methods based on arbitrary moment expansion are called Bond Order Potentials (BOP/s) or often Tight Binding moment expansion in the French speaking world[61, 62]. An analytical derivation for higher than second moments is possible, albeit difficult. Models have been made for sp-bonded carbon and silicon structures[63] and there are efforts to extend it to d-bonded transition metals but they are not yet practical for transitional metals and very much a theoretical work in progress. The numerical expansion on the other hand is practical and can achieve up to 11 to 17 moments at the level of precision and performance offered by the current computers. Due to the better description of the electronic structure BOPs are more suitable for simulations of defects and dislocations in transition metals than the EAM/FS potentials. An important success of their application is the correct core structure in TiAl obtained with expansion of up to the 9-th moment. Most often 9 or 13 moments are used in models for transition metals and alloys Mo-Si, W, Ti-Al ... The numerical BOPs are understandably slower than EAM/FS but they still retain the locality of interactions and allow for simple parallel implementations with very good scalability. A common observation is that the portability of a model is inversely proportional to its simplicity. The BOPs provide a variable for continuous adjustment between faster, simpler models and slower, higher moment but more portable models. Hence they are

suitable for simulations which include interfaces between different structures such as the ones in PST. A downside to the numerical BOPs is the difficulty of calculations of forces which makes their application in molecular dynamics risky. This problem is addressed by the analytic BOP[64, 65, 66].

A BOP with infinite moment shall give the same result as the Tight Binding (TB) method from which it is derived. BOP is practically real space implementation of a simple TB model with constraint of local charge neutrality (LCN). TB is a bandstructure method and as such it works ordinarily in reciprocal space. The hopping integrals are short ranged but an atom's orbital contribution to the wavefunction in the whole space is always calculated irrespective of how insignificant it may be. BOPs linear scaling with respect to the number of atoms is precisely due to this truncation of the interactions through the moment expansion. The heaviest step in a TB calculation is the diagonalisation whose computational effort increases proportionally to the cube of the rank of the Hamiltonian matrix. Parallelisation of diagonalisation is notoriously difficult and is an area of research[67]. Currently this is only practical for up to a few thousand atoms. The TB model implements the more correct charge transfer self-consistency in comparison with BOP's LCN, there is also multipole electrostatic interactions, ion polarisability etc..[68] but they are often not needed in the modelling of metals and alloys. The empirical hopping parameters are common for TB and BOP.

Chapter II

Electronic structure and BOP

II.1 Introduction

The state of the art description of matter is presently provided by the quantum mechanical "*ab initio*" methods. As the name "from beginning" suggests everything is computed from first principles with minimal input and assumptions. The usual picture consists of a set of particles residing in an external electrostatic and/or magnetic field optionally. The state of a system is fully defined by a wave function. In a time independent description, standing waves are formed and only discrete stationary energy levels/states are allowed. They are solutions of the time independent Schrödinger equation[69].

$$\hat{H}\Psi = E\Psi \quad (\text{II.1})$$

Each state has its energy E and is expressed by its wave function Ψ . Ψ contains the information for all particles in the whole space.

$$\Psi = \Psi(\vec{r}_1, \vec{r}_2, \vec{r}_3, \dots, \vec{r}_N) \quad (\text{II.2})$$

Its modulus squared over a region is the probability of finding particles in this space. The lowest energy state is called *ground state*

and the higher states are said to be *excited*.

The Hamiltonian operator \hat{H} consists of kinetic \hat{T} and potential \hat{V} energy operators. The potential energy is the electrostatic interactions U between the particles and their interaction with some externally imposed potential v_{ext} .

$$\hat{H} = \hat{T} + \hat{U} = \sum_i \frac{-\hbar^2}{2m_e} \nabla_i^2 + \frac{1}{2} \sum_{i \neq j} \frac{q_i q_j}{4\pi\epsilon_0 |\vec{r}_j - \vec{r}_i|} + \sum_i q_i v_{\text{ext}}(\vec{r}_i)$$

A choice of units is usually made to remove all boilerplate constants/coefficients/factors for reasons of brevity and simplicity. In *atomic units* $e = m = \hbar = 4\pi\epsilon_0 = 1$, the energy is measured in Hartree $1\text{Ha} = 2\text{Ry} = 27.2\text{eV}$, 1Ry is the first energy level in the hydrogen atom, the unit for length is the Bohr radius $a_0 = 4\pi\epsilon_0\hbar^2/me^2 = 0.53\text{\AA}$ which is the position of the electron occupying the first level in the H atom. All subsequent equations will be written in the atomic units. Again for reasons of brevity and simplicity the Dirac or *bra-ket* notation is introduced. A row vector is written as $\langle v |$ and column vector is $| u \rangle$. The dot or inner product $\langle v | u \rangle$ results in a scalar and the tensor/dyadic or outer product $| u \rangle \langle v |$ leads to an operator.

Solving the Schrödinger equation is a quantum many body problem. It has been solved exactly only for a small number of small systems. Analytical solution exists for hydrogen like atoms. Numerical direct solutions are severely restricted by the present computational resources to only a few particles. There are approaches for finding the ground state wave function directly through optimisation techniques for example the Quantum Monte-Carlo methods but they are still only recently applicable to a few atoms. To reach bigger more complex systems a number of different levels of approximations are usually applied. They greatly simplify the description of a system and allow for the construction of more trans-

parent effective interatomic potentials for practical purposes.

An electron is more than 1836 times lighter than a proton[70]. The electrons' speed is also in most cases much higher than the speed of the nuclei. Any change in their positions is assumed to be accounted for by the electrons instantaneously. From electrons' point of view the nuclei are static and only provide potential in which to move. This is the Born-Oppenheimer approximation[71] and is successful in most applications. Since the nuclei are treated as classical particles the kinetic energy operator is only responsible for the electrons. The nuclei-nuclei electrostatic energy is then constant and the electron-nuclei merges with the external potential term. An important result is that the energy of the system is a function of the nuclear positions and an external potential only.

After the nuclei are removed the electrons are modelled as independent charged particles moving in an effective potential made out of the external potential and the potential of the charge density. The interdependence of the electrons' motion arising from the presence of spin is added in the form of exchange energy. Only one electron can occupy a quantum state and 2 electrons can be at the same energy level only if they have opposite spin.

The decoupling of the electrons allows the many body wave function to be written in terms of single particle wave functions. Depending on the level of approximation it can be expressed as product, determinant or combinations of determinants. The ground state is found from the minimisation of the energy with respect to the wave function. The computational effort is considerable as the wave function's number of degrees of freedom is three times as many as the number of electrons.

II.2 Density Functional Theory

There was an idea in the early days of quantum mechanics that the electron density

$$\rho = N \int |\Psi|^2 d\vec{r}_1 d\vec{r}_2 \dots d\vec{r}_N \quad (\text{II.3})$$

is a fundamental quantity and every other quantity could be represented as unique functional of the density, even the wave function itself[72]. The idea was realised in the Thomas-Fermi (TF) model for the ground state without proof of the existence or the uniqueness of the density functional. These points were cleared later and form the basis for the modern Density Functional Theory (DFT)[73, 74, 75].

Once the energy is written as a density functional,

$$\begin{aligned} E[\rho] &= T[\rho] + U[\rho] = \\ &= T[\rho] + E_H[\rho] + E_{xc}[\rho] + E_{ext} \end{aligned} \quad (\text{II.4})$$

the task is to minimise it with respect to its single variable the density by solving

$$\frac{\delta}{\delta \rho} \left(E[\rho] - \mu \left(N - \int \rho(\vec{r}) d\vec{r} \right) \right) = 0 \quad (\text{II.5})$$

subject to a few constraints: $\rho(\vec{r})$ should integrate to the number of electrons N , and it should have smooth physically justified shape

$$N - \int \rho(\vec{r}) d\vec{r} = 0; \quad \int |\nabla \rho(\vec{r})| d\vec{r} < \infty \quad (\text{II.6})$$

The quantity μ is the chemical potential and it represents the energy dependence on the number of electrons.

The potential energy terms have explicit density functional ex-

pressions.

$$E_H[\rho] = \int \rho(\vec{r}) v_H(\vec{r}) d\vec{r} = \frac{1}{2} \iint \frac{\rho(\vec{r}) \rho(\vec{r}')}{|\vec{r} - \vec{r}'|} d\vec{r} d\vec{r}' \quad (\text{II.7})$$

$$E_{\text{ext}}[\rho] = \int \rho(\vec{r}) v_{\text{ext}}(\vec{r}) d\vec{r} \quad (\text{II.8})$$

The exchange term is not calculated exactly as in Hartree-Fock theory and being correlative in nature is combined with the more dubious correlation term leading to exchange-correlation energy. In DFT the exchange-correlation partially subtracts the unphysical terms in the Hartree energy arising from electron self-interaction. Due to the less deterministic nature of the exchange-correlation there is a proliferation of expressions. One simple form is the local density approximation. It is based on the assumption that the density is varying slowly and the exchange-correlation depends on the local density only (eq. II.9) and is parametrised and fitted to exact calculations for homogeneous electron gas. While fairly successful for metals where density indeed does not vary sharply it is superseded by expressions including the density gradient and possibly higher derivatives and in even more sophisticated schemes hybrid functionals are prepared by mixing with exact exchange from Hartree-Fock calculation. In the local density approximation

$$E_{xc}[\rho] = \int \rho(\vec{r}) \epsilon_{xc}(\rho) d\vec{r} \quad (\text{II.9})$$

The local density approximation was also applied to the kinetic energy in the TF model which was its major source of error. In DFT, however, the kinetic energy does not have an explicit density functional form and its functional derivative cannot be taken directly. Then to solve the Euler-Lagrange equation (eq. II.5) in its current form,

$$\frac{\delta E[\rho]}{\delta \rho} = \frac{\delta T[\rho]}{\delta \rho} + v_H + v_{\text{ext}} + \frac{\delta E_{xc}[\rho]}{\delta \rho} = \mu \quad (\text{II.10})$$

T is set to the kinetic energy of a system of non-interacting electrons with the same density in an effective potential $v_{\text{eff}} = v_H + v_{\text{ext}} + v_{xc}$. Any many body effects on the kinetic energy are swept into the exchange-correlation term. The Schrödinger equation for such system is called the Kohn-Sham equation and it is much easier to solve.

$$\left(-\frac{1}{2} \nabla^2 + v_{\text{eff}}(\vec{r}) \right) \psi_n(\vec{r}) = \varepsilon_n \psi_n(\vec{r}) \quad (\text{II.11})$$

The single electron wavefunctions ψ_n reproduce the electron density of the interacting system

$$\rho(\vec{r}) = \sum_n f_n |\psi_n(\vec{r})|^2 \quad (\text{II.12})$$

after finding the occupancy from the Fermi-Dirac distribution,

$$f_n \equiv f(\varepsilon_n); \quad f(\varepsilon) = 2f_F(\varepsilon); \quad f_F(\varepsilon) = \frac{1}{1 + e^{\frac{\varepsilon - \varepsilon_f}{k_B t}}} \quad (\text{II.13})$$

where k_B is the Boltzmann constant, t is the temperature, and ε_f is the occupancy level named after E. Fermi. At $t = 0$ the distribution becomes a step function. The Fermi level ε_f is chosen to satisfy (eq. II.6)

Self consistency between the density and the effective potential is reached through iterative procedure. The basic steps are as follows:

1. Starting from some sensible ρ^{in} , often an overlap of electron densities of free atoms, the effective potential $v_{\text{eff}}(\rho^{in})$ is calculated.
2. Then the Schrödinger like Kohn-Sham equation (eq. II.11) is solved for this effective potential. The output density ρ^{out} is then calculated according to (eq. II.12)
3. Substituting the kinetic energy $\sum_n f_n \varepsilon_n - \int \rho^{out} v_{\text{eff}}^{in} dr$ and the

density in (eq. II.4) leads to the total energy for the iteration.

$$\begin{aligned} E = \sum_n f_n \varepsilon_n + \frac{1}{2} \int \frac{\rho(\vec{r})\rho(\vec{r}')}{|\vec{r} - \vec{r}'|} d\vec{r}d\vec{r}' - \int \frac{\rho(\vec{r})\rho^{in}(\vec{r})}{|\vec{r} - \vec{r}'|} d\vec{r}d\vec{r}' \\ + E_{xc} - \int \rho(\vec{r})v_{xc}^{in}(\vec{r}) d\vec{r} + E_{nuclear} \end{aligned} \quad (\text{II.14})$$

4. This is the end of a single calculation. The self-consistency problem is non-linear and there is a variety of methods for solving it. The simplest is to use the resultant output density as input for the new cycle. Better results may be obtained if a linear combination (mixing) of the old input density and the output density is taken. Yet more advanced procedures like Anderson's[76] and Broyden's[77] are usually used in practical calculations. The stability and convergence may strongly depend on the mixing scheme.

If the output density is written as a small perturbation to the input $\rho = \rho^{out} \equiv \rho^{in} + \delta\rho$, and the terms in (eq. II.14) are expanded e.g.:

$$E_H[\rho] = E_H[\rho^{in}] + \int \delta\rho(\vec{r})v_H^{in} d\vec{r} + \frac{1}{2} \int \frac{\delta\rho(\vec{r})\delta\rho(\vec{r}')}{|\vec{r} - \vec{r}'|} d\vec{r}d\vec{r}'$$

then the terms first order in $\delta\rho$ disappear and the following useful expression is obtained.

$$E^{HKS}[\rho] = \sum_n f_n \varepsilon_n + E_{xc}^{in} - \int \rho^{in}(\vec{r})v_{xc}^{in} d\vec{r} - E_H^{in} + E_{ncl} \quad (\text{II.15})$$

$$\begin{aligned} &+ \frac{1}{2} \int \delta\rho(\vec{r})\delta\rho(\vec{r}') \left(\frac{1}{|\vec{r} - \vec{r}'|} + \frac{\delta^2 E_{xc}}{\delta\rho(\vec{r})\delta\rho'} \right) d\vec{r}d\vec{r}' \quad (\text{II.16}) \\ &+ O[\delta\rho^3(\vec{r})] \end{aligned}$$

For sufficiently good guess ρ^{in} the first order terms contain the

most significant part of the energy and they are consistent with the first order potential so the iterative solution only affects the second order terms. A number of simplified models can be derived from this expression by approximation or neglecting some of the terms. The Harris-Foulkes functional[78, 79] for example keeps only the first order terms and decouples the potential from the density. If applied on every iteration in the self consistent scheme the energy fluctuates less than the Hohenberg-Kohn-Sham energy and is closer to the exact value near completion. The last two of the first order terms are essentially screened pairwise interactions. Adding the empirically parametrised second order terms is one step towards a branch of self consistent of tight binding models.

The solution of the single particle Schrödinger like Kohn-Sham equation is also a difficult problem. The operators' matrices are usually expanded and solutions found in terms of basis functions. From a mathematical point of view any complete set is sufficient and orthogonal-complete such as plane waves is preferable. From a physical point of view though a set of functions which can be interpreted physically, even if they are more cumbersome to handle, is sometimes more valuable. Examples are functions related to the solution of neutral atoms, spherical harmonics, Bessel functions, and Gaussians. Since bound atoms still resemble free atoms it makes to use the free atom solutions as basis because very few functions are expected to be enough for reasonably realistic description. In addition it is simpler to judge the contributions of each function and devise further approximations.

The atomic like basis functions are composed of angular and radial parts,

$$\phi_{nlm}(r, \theta, \varphi) = V_n(r)Y_{lm}(\theta, \varphi) \quad (\text{II.17})$$

The angular dependent functions are spherical harmonics. $n \in [1, \infty)$, $l \in [0, n]$ and $m \in [-l, l]$ are the principal, orbital and mag-

netic quantum numbers. The first few orbitals with respect to the l number are also named with the letters s , p , d , f , g ... All of the quantum numbers will be combined in single index i or j in the following and when necessary l .

The eigenfunctions ψ_n are written as linear combinations of the basis functions. The expansion coefficients are generally complex numbers.

$$|\Psi_n\rangle = \sum_i |\phi_i\rangle C_{i,n}; \quad \langle \Psi_n | = \sum_i C_{n,i}^* \langle \phi_i | \quad (\text{II.18})$$

The omnipresent $|\psi_{n/m/..}\rangle$ and $|\phi_{i/j/..}\rangle$ will be shortened to simply $|n/m/..\rangle$ and $|i/j/..\rangle$ respectively.

Operators may also be expanded in the chosen basis in terms of their expansion coefficients,

$$\hat{H} = \sum_{i,j} |i\rangle H^{ij} \langle j| \quad (\text{II.19})$$

The states are orthogonal

$$\langle n|m\rangle = \delta_{nm} = \sum_{i,j} C_{n,i}^* \langle i|j\rangle C_{j,m} \quad (\text{II.20})$$

but the local orbitals are generally not and may form an overlap matrix,

$$\langle i|j\rangle = S_{ij} \quad (\text{II.21})$$

In case of orthogonality the overlap becomes an unit matrix. The partial sums in (eq. II.20) when $m = n$ may be seen as weights of state n on orbital i for example,

$$w_{n,i} = \sum_j C_{n,j}^* S_{ji} C_{i,n}; \quad \sum_i w_{n,i} = 1 \quad (\text{II.22})$$

The operators are written in matrix form for the numerical solution of the single particle equation. The matrix elements are obtained by left and right multiplication by the basis vectors,

$$H_{ij} = \langle i|\hat{H}|j\rangle = \langle i|\hat{T}|j\rangle + \langle i|\hat{V}_{\text{eff}}|j\rangle \quad (\text{II.23})$$

$$\sum_j H_{ij} C_{j,n} = \sum_j S_{ij} C_{j,n} \varepsilon_n \quad (\text{II.24})$$

The calculation of the Hamiltonian matrix elements and the following numerical solution of the eigenvalue problem on each self consistency iteration are the two most time consuming operations in DFT calculations. Depending on the specific approach either one may be more expensive. If simple floating basis functions are used for describing the whole space the construction is simpler but the often huge number of functions needed shifts the burden onto the secular equation. If a more sophisticated atom based basis is used much fewer functions are needed but due to their complexity the effort for computing the matrix elements often outweighs many times the eigenproblem. Methods using the atom based basis and optionally floating functions are usually implemented by splitting the space in atom based spheres and interstitial regions[80]. The matching between the different regions then introduces dependence of the Hamiltonian on the eigenvalues. The resulting nonlinear eigenvalue problem may be solved approximately by linearising the energy dependence near some appropriately guessed values[80].

The solution of the eigenvalue problem consists of finding basis of vectors in which the Hamiltonian takes diagonal form. The vectors are eigen vectors and the diagonal elements of the Hamiltonian in basis of the eigen vectors are eigenvalues.

Useful quantities are the density expansion coefficients ρ_{ij} and

the density of states (DOS) $\mathcal{D}(\varepsilon)$. By definition the density operator in the eigen vector basis is diagonal and contains the occupancy values f_n ,

$$\begin{aligned}\hat{\rho} &= \sum_n |n\rangle f_n \langle n| = \sum_n \sum_{i,j} |i\rangle C_{i,n} f_n C_{n,j}^* \langle j| \equiv \sum_{i,j} |i\rangle \rho^{ij} \langle j| \\ \rho^{ij} &= \sum_n C_{i,n} f_n C_{n,j}^*\end{aligned}\quad (\text{II.25})$$

Following the usual definition, the trace of the density operator in the eigen vectors' basis is the total number of electrons. When written in terms of the expansion coefficients ρ^{ij} the trace nicely expands to charges accumulating in orbitals and atoms,

$$\begin{aligned}N &= \text{Tr}(\hat{\rho}) = \sum_n \langle n | \hat{\rho} | n \rangle = \sum_n \sum_{i,j} \langle n | i \rangle \rho^{ij} \langle j | n \rangle \\ &= \sum_{i,j} \rho^{ij} \langle j | i \rangle \sum_n |n\rangle \langle n| = \sum_{i,j} \rho^{ij} S_{ji}\end{aligned}\quad (\text{II.26})$$

The indices i and j are substituted now with the respective atom site R and all quantum numbers are combined in the orbital index L ,

$$q_{RL} = \sum_{R'L'} \rho^{RL,R'L'} S_{R'L',RL} \quad (\text{II.27})$$

The partial charges may alternatively be seen as weighted sum of the occupancies following (eq. II.22) and (eq. II.25),

$$q_{RL} = \sum_{R'L'} \rho^{RL,R'L'} S_{R'L',RL} = \sum_n \sum_{R'L'} C_{RL,n} f_n C_{n,R'L'}^* S_{R'L',RL} = \sum_n f_n w_{n,RL} \quad (\text{II.28})$$

$$q_R = \sum_L q_{RL}; \quad N = \sum_R q_R \quad (\text{II.29})$$

In very large systems the energies of the states are closely spaced on the energy axis and, in the limit of infinite systems, they form continuous bands. In such a case an important quantity is the density of states. This is a distribution plotting the number of states happening to fall in an infinitesimally small interval of energy. Each state is written as a delta function located at its eigenvalue and plotted on the energy axis,

$$\mathcal{D}(\varepsilon) = \sum_n \delta(\varepsilon - \varepsilon_n) \quad (\text{II.30})$$

the eigenvalues are the Hamiltonian expansion coefficients in basis of the eigenfunctions:

$$\hat{H} = \sum_n |n\rangle \varepsilon_n \langle n|$$

$$\mathcal{D}(\varepsilon) = \text{Tr}(\delta(\varepsilon - \hat{H})) = \text{Tr}(\hat{\mathcal{D}}) \quad (\text{II.31})$$

This is analogous to the the density expansion coefficients, but employing ε_n instead of f_n . Partial densities of states can be written as a weighted sum in a fashion similar to the partial charges,

$$\mathcal{D}_{RL}(\varepsilon) = \sum_n \delta(\varepsilon - \varepsilon_n) w_{n,RL} \quad (\text{II.32})$$

$$\mathcal{D}_R(\varepsilon) = \sum_L \mathcal{D}_{RL}(\varepsilon); \quad \mathcal{D}(\varepsilon) = \sum_R \mathcal{D}_R(\varepsilon) \quad (\text{II.33})$$

The sum of the occupied energy states is the band energy. It is the first term in (eq. II.14) and is usually the most significant structurally dependent contribution of the total electron energy. Since the DOS is a distribution of the states the band energy may

be written as an integral over it.

$$E_{\text{band}} = \sum_{\text{occ.}} \varepsilon_n = \sum_n f_n \varepsilon_n = \int f(\varepsilon) \varepsilon D(\varepsilon) d\varepsilon \quad (\text{II.34})$$

Using the operator form of band energy it is possible to expand it in a sum of contributions from different atoms and orbitals like the density and the DOS but a more interesting property appears when it is expanded in the local basis.

$$\begin{aligned} E_{\text{band}} &= \sum_n f_n \varepsilon_n = \sum_n \langle n|n \rangle f_n \langle n|n \rangle \varepsilon_n \langle n|n \rangle \\ &= \sum_n \langle n|\hat{\rho}\hat{H}|n \rangle = \text{Tr}(\hat{\rho}\hat{H}) \\ &= \sum_n \langle n|\hat{\rho}\hat{H}|n \rangle = \sum_n \sum_{i,j} \langle n|i \rangle \rho^{ij} \langle j|\hat{H}|n \rangle \\ &= \sum_n \sum_{i,j} \rho^{ij} \langle j|\hat{H}|n \rangle \langle n|i \rangle = \sum_{ij} \rho^{ij} H_{ji} \end{aligned} \quad (\text{II.35})$$

There is an equivalence between the band energy calculated from eigenvalues on the one hand and the density matrix and the Hamiltonian in the local basis on the other. The two can be seen as different representations of the same operator,

$$\hat{E}_{\text{band}} = \hat{\rho}\hat{H} = \sum_n |n\rangle f_n \varepsilon_n \langle n| \quad (\text{II.36})$$

When large systems of atoms have periodicity a huge amount of calculations can be saved by looking only at the unit cell since the density follows the periodicity of the potential. To satisfy this requirement a unit cell wave function can be multiplied by a complex factor with unit modulus. Then the probability density remains the same in any image of the cell but the wavefunction is not constrained by the same periodicity. According to Bloch's theorem[81]:

$$\psi_k(\vec{r} + \vec{a}) = e^{i\vec{k} \cdot \vec{a}} \psi_k(\vec{r}) \quad (\text{II.37})$$

where \vec{a} is a unit cell lattice vector or an integer combination of lattice vectors. The Hamiltonian has to be Bloch-transformed and the Kohn-Sham equation solved for each \vec{k} every iteration. A problem of infinite size is in this way mapped to infinitely many solutions of a finite problem. An important point in (eq. II.37) is that \vec{k} does not need to sample the whole space but similarly to \vec{r} in (eq. II.37) it can be limited. If a reciprocal lattice vector \vec{G} is introduced such that

$$\vec{G} \cdot \vec{a} = 2\pi n \quad (\text{II.38})$$

where n is integer, then any vector \vec{k}_n can be folded back to a vector \vec{k} in the first Brilouin zone:

$$\vec{k}_n = \vec{k} + \vec{G} \quad (\text{II.39})$$

and \vec{G} can be expressed more conveniently in basis of the primitive vectors of the reciprocal lattice \vec{b} ,

$$\vec{G} = \sum_{i=1}^3 n_i \vec{b}_i \quad (\text{II.40})$$

If \mathbf{a} is a matrix formed by the direct lattice vectors \vec{a} , then \mathbf{b} will be composed of the reciprocal lattice vectors \vec{b} in the same order:

$$\mathbf{b} = 2\pi (\mathbf{a}^\top)^{-1}; \quad (\text{II.41})$$

Since closely spaced \vec{k} vectors shift the eigenvalues smoothly the periodic solution can be interpolated reasonably well from a relatively small sample. If any symmetry of the unit cell is found the number of \vec{k} points can be reduced significantly. An energy band is formed by the set of \vec{k} along a certain axis in the reciprocal cell. A plot of the bands along lines of high symmetry, weighted by contributions from the different atomic orbitals may be useful in assessing the significance of certain orbitals.

II.3 Tight Binding

The tight binding method initially started as a transparent empirical method for electronic structure calculations[82]. Atomic like orbitals are placed on the atoms and electrons are allowed to hop from orbital to orbital with predefined probabilities. Pairwise repulsive terms are used to balance the attractive energy. Diagonalisation of the Hamiltonian yields the eigen values and vectors and charges, densities of states, energies and forces are found with the outlined formalism.

Tight binding approaches were later derived from the Harris-Foulkes and the second order functionals[83]. A number of common approximations are applied, but there are some variations between different TB models. As a general point, all TB methods are defined within minimal atomic like basis resulting in a small Hamiltonian matrix. The construction of the Hamiltonian is also parametrised requiring very small computational effort unlike the corresponding DFT methods using local atomic functions. In the most basic non self consistent TB all terms except the band energy in (eq. II.15) are replaced by pairwise repulsive terms between the atoms. A form of self consistent TB may be constructed by approximating the second order terms (eq. II.16) [68].

The parametrisation of the Hamiltonian consists of fundamental bond integrals between the orbitals, and on-site energies for these orbitals. The number of fundamental bond integrals and on-site energies in minimal basis is small. For most elements only a selection of s, p and/or d orbitals is used. Assuming a fixed bond vector there are up to 10 different bonds which can be formed: $ss\sigma$, $sp\sigma$,

$pp\sigma$, $pp\pi$, $sd\sigma$, $pd\sigma$, $pd\pi$, $dd\sigma$, $dd\pi$ and $dd\delta$. The convention to define a bond integral between sites $R\ell$ and $R'\ell'$ is to place R at the origin of the coordinate system and R' at the equilibrium distance on the z axis, then decorate them with the appropriate orbitals(fig. II.1). All other orientations are linear combinations of these bond integrals. The coefficients are simple functions of the direction cosines and are given by the famous Slater-Koster tables[82]. The direction cosines are the relative projections of the bond vector on the Cartesian axes. The dependence on the length is modelled by multiplying the equilibrium bond integral by a scaling function. There are a few scaling expressions which bring a handful of new parameters to the set: r^n , e^{-nr} , $r^ne^{-mr}\dots$ More flexibility is provided by the the Goodwin-Skinner-Pettifor[84] (GSP) function:

$$\ell\ell'm = v_0 \left(\frac{r_0}{r}\right)^n e^{n[(\frac{r_0}{r_c})^{n_c} - (\frac{r}{r_c})^{n_c}]}$$

The decay is quicker after r_c and setting $n_c = 0$ produces power law scaling. It is also possible to cut the functions at certain distance r_1 and augment with some tail expression matching the first few derivatives at r_1 and smoothly vanishing at certain r_{cut} . Another option to make the scaling vanish between r_1 and r_{cut} is to multiply by a polynomial with value 1 and a specified number of derivatives set to 0 at the left end and value and derivatives set to 0 at the right end. The second option keeps the character of the original function and is preferable for other reasons in most cases as will be shown in the next chapter. It can alternatively be seen as somewhat similar in spirit to the GSP where both are factors introduced to smear a base function.

The hopping integrals in an orthogonal TB model are usually assumed to be environmentally independent. This limits the transferability and applicability to intermetallics or materials with properties significantly affected by core screening. Often the non bond-

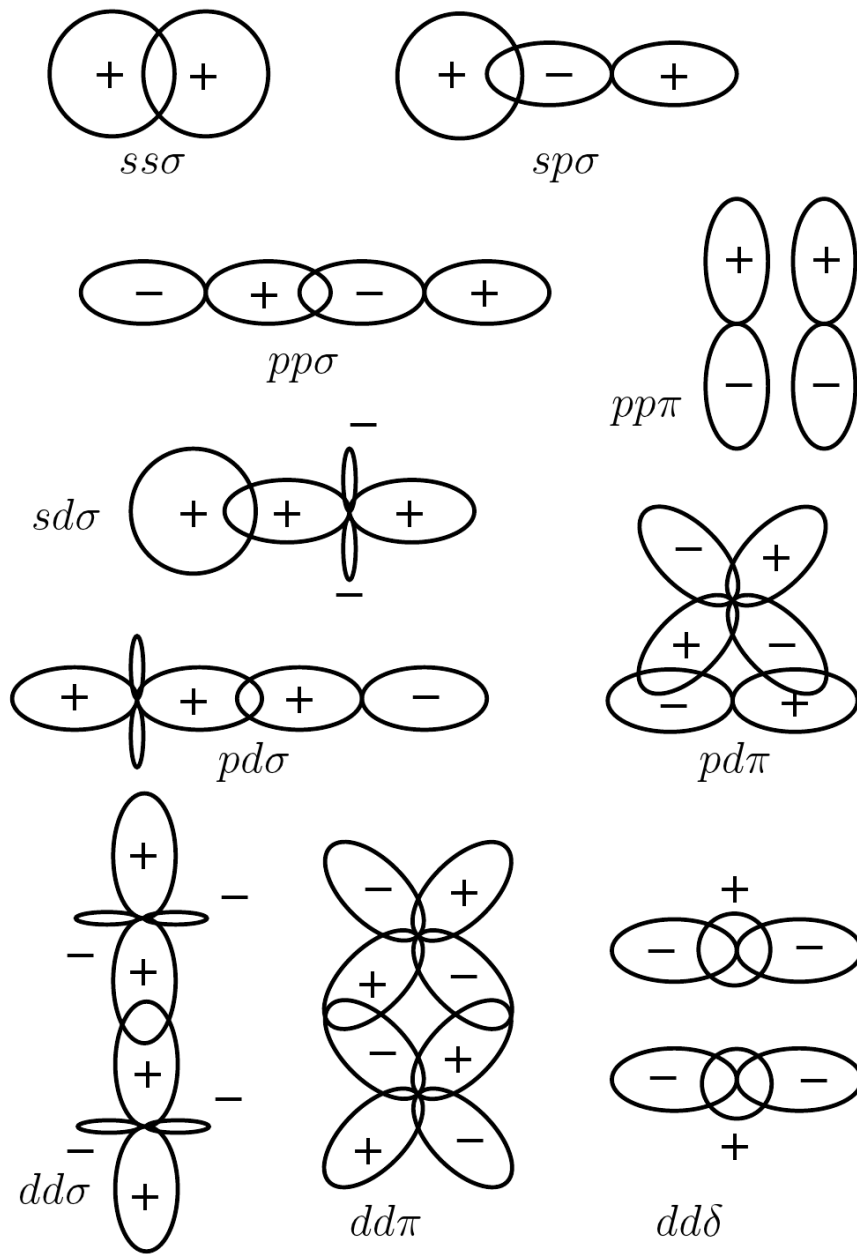


Figure II.1: Bond integrals[85].

ing s orbitals are left out of TB/BOP models but their contribute to the cohesion or rather against it is accounted for by screening of the covalent bonding and the pairwise repulsion. The former is

more prominent in bcc metals where there difference in the distance to the nearest neighbour and the next one is not big but the environments are different as is the case in BCC metals. In these cases bond scalings from DFT calculations show clear discontinuity and explicitly screened hopping integrals may be necessary. Such screened TB/BOP models have been developed for Mo[86, 87], MoSi₂[88], W[89] etc with hoppings dependent on the nearest neighbour environment.

In contrast, the distance between the first and second nearest neighbours in close packed crystals is significantly larger and the discontinuity in the scalings is somewhat less obvious but some physical properties like the Cauchy pressures are influenced. A screened addition to the repulsive potential may be appropriate in modelling these materials.

Assuming the effective potential can be expanded in contributions from different sites the TB Hamiltonian matrix elements contain one centre integrals of the potential $\langle i|\hat{V}_i|i\rangle$ on the diagonals and two centre ones $\langle i|\hat{V}_i|j\rangle$ in the off diagonal elements. The Slater-Koster table is intrinsically spherically symmetric and 2-centre because three centre integrals $\langle i|\hat{V}_k|j\rangle$ are discarded as they require more effort to calculate and the parametrisation may become more obfuscated. Having this in mind it does not make very much sense to extend the hopping integrals much beyond the first or second nearest neighbours because the neglected three centre contributions of the near atoms may be bigger than any gain from more distant atoms.

An orthogonal basis is assumed in the simple TB models but it is possible to construct an overlap matrix in fashion similar to the one for the Hamiltonian.

A parametrised approximation of the second order terms in the

HKS functional may be added by:

$$E_2 = \frac{1}{2} \sum_i U_i \delta q_i^2 + \frac{1}{2} \sum_{i \neq j} U_{ij} \delta q_i \delta q_j \quad (\text{II.42})$$

δq_i are the charges accumulated on the sites i . The charge differences change the potential at the sites i which in turn drives the flow. Iterations continue until charge transfers stabilise. This may result in some atoms being completely stripped of electrons and others accumulating them all. The U_i parameters act as inhibitors to charge transfer from or to site i and thus prevent such rarely physical picture. This is the basic self consistent charge transfer model.

If the Hubbard U parameters are set to very high value effectively no transfers are allowed. This leads to a more basic approximation called local charge neutrality (LCN). In metals it is not unreasonable if the bound atoms are more or less neutral due to significant screening. To satisfy the atom neutrality the onsite energies on each site are shifted uniformly, in response to the change of the potential with respect to charge, to adjust the number of electrons associated with the atom.

All other terms in (eq. II.15) and (eq. II.16) are approximated with pair potentials and optionally screened multi atom potentials,

$$E_{\text{pair}} = \frac{1}{2} \sum_{ij} V_{ij}^{\text{pair}} \quad (\text{II.43})$$

The form of the pairwise functions is often the one used for the hopping integral scalings but not necessarily. The only requirements are to be smooth, repulsive and vanish at certain distance. The terminal cutoff may be more distant than the hopping integrals because the Coloumbic ion-ion interactions should be included.

The total energy in ordinary TB is written as:

$$E_{\text{tot}} = E_{\text{band}} + E_{\text{pair}} \quad (\text{II.44})$$

This is the tight binding band model. It emphasises the quantum mechanical character through E_{band} . Equally if not more important is the cohesive or binding energy,

$$\begin{aligned} E_{\text{bind}} &= E_{\text{tot}} - E_{\text{atom}} = E_{\text{band}} - E_{\text{atom}} + E_{\text{pair}} = \\ &= \sum_{ij} \rho^{ij} H_{ij} - \sum_i \varepsilon_i^0 f_i + E_{\text{pair}} = \\ &= \sum_{i \neq j} \rho^{ij} H_{ij} + \sum_i \rho^{ii} H_{ii} - \sum_i \varepsilon_i^0 f_i + E_{\text{pair}} = \\ &= \sum_{i \neq j} \rho^{ij} H_{ij} + \sum_i q_i \varepsilon_i^0 - \sum_i N_i \varepsilon_i^0 + E_{\text{pair}} = \\ &= \sum_{i \neq j} \rho^{ij} H_{ij} + \sum_i (q_i - N_i) \varepsilon_i^0 + E_{\text{pair}} = \\ &= E_{\text{bond}} + E_{\text{prom}} + E_{\text{pair}} \end{aligned} \quad (\text{II.45})$$

This is the tight binding bond model (TBBM)[83]. ε_i^0 are the on-site energies at combined index i and N_i the number of electron in the neutral free atoms.

The bond energy and promotion energies are the new entities here. From its defining expression the bond energy can be seen as a sum over the energies of all bonds $i-j$. A simple interpretation of a bond's energy is the product between the probability of a single electron hopping through the bond and the number of electrons which are there to hop. This is particularly important because the bond energies are localised effective interactions formally similar to the pair potentials.

The promotion energy represents the energy shift due to accumulated change in the orbitals i , that is, the promotion of the orbitals for bonding. The promotion energy is used in the local charge

neutrality self consistency model. The core charges are balanced by the same number of electrons and charge transfers are not allowed but the effective potential now represented solely by the on-site terms is adjusted in order to be consistent. In practice the charge transfers are calculated on every iteration and the on-site energies on every atom changed accordingly by some scheme to minimise the transfers.

The TBBM bridges the quantum mechanical and the effective potentials description of a system of atoms. It is the starting point for further development of more approximate models.

II.4 Bond Order Potentials

The bond order potentials (BOP)[90] formally continue the line of thought of the tight binding bond model. The off diagonal density expansion coefficients taking the part of the bond energy are also called bond orders when the model is orthogonal.

$$E_{\text{bond}} = \sum_{i \neq j} \rho^{ij} H_{ji} = \frac{1}{2} \sum_{i \neq j} (\rho^{ij} + \rho^{ji}) H_{ij} = \sum \Theta^{ij} H_{ij} \quad (\text{II.46})$$

$$\Theta^{ij} = \frac{1}{2} (\rho^{ij} + \rho^{ji}) \quad (\text{II.47})$$

They are real numbers and are conceptually linked to the older idea of bond multiplicity(eq. II.48) dating back to the valence theory and molecular orbital (MO) theories in chemistry[91]. Bond multiplicities are still written in structural formulas for example: H-H, O=C=O, N≡N.

$$\Theta = \frac{1}{2} (N^{\text{bonding}} - N^{\text{antibonding}}) \quad (\text{II.48})$$

The strength of a bond, according to MO, depends on its order and contributes to the binding energy. A bond was defined to link

two atoms and it was known that elements could engage in a specific number of bonds which would be decreased when their order is higher than one. In the molecular orbital theory, during bonding the atomic orbitals were split/combined resulting in molecular orbitals. These were then populated with electrons according to the *aufbau* rules[92]. The molecular orbitals with lower energy than the their parent atomic orbitals are called bonding because electrons landing on them stabilise the bound system. The molecular orbitals with higher energy are called anti bonding(fig. II.2) because filling them with electrons leads to destabilisation. Orbitals which do not take part in the bonding process are said to be non bonding. The difference between the number of electron pairs in bonding and anti bonding orbitals is the order of the bond(eq. II.48).

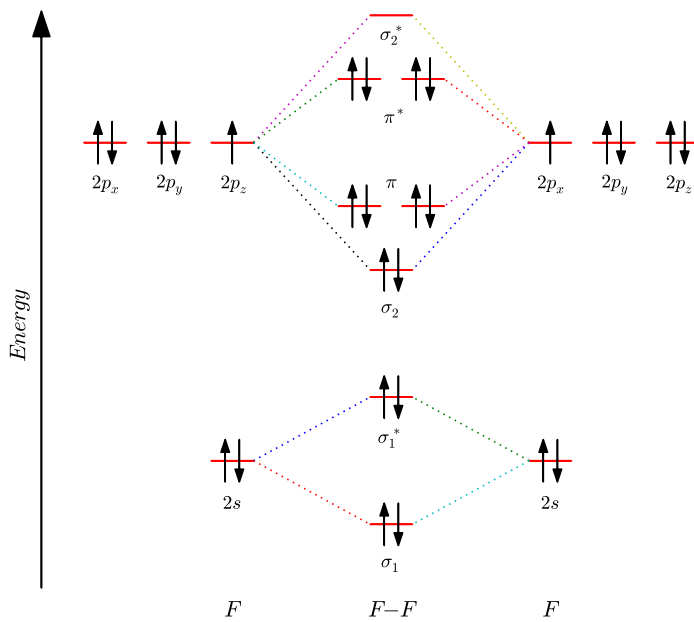


Figure II.2: Bonding in the F_2 molecule, MO diagram.

The BOP model is sometimes called tight binding expansion or moment expansion because it is formally derived from and very

much a branch in the tight binding method. It always uses an orthogonal TB Hamiltonian although approximations to nonorthogonality [87] as well as explicitly nonorthogonal models[93] have been developed. A distinctive feature is that BOP is implemented in real space and does not use the Bloch transformation for periodic systems, which is otherwise common practice in TB and many DFT programs. This keeps the Hamiltonian matrix elements as real numbers.

A defining feature and one which substantiates the name "TB expansion" is that the heavy numerical diagonalisation, which is the bottleneck in TB's performance, is avoided and replaced with expansion in moments of the DOS. The eigen values and vectors are not explicitly calculated. The density of states, bond orders and energies are approximated up to a certain level through the moments theorem[94]. The equivalence between the band energy found through the DOS (eq. II.34) and bond + promotional energy is a convergence criterion rather than identity in BOP. The first involves only on-site quantities and the later inter site.

The DOS is a histogram, it is non-negative on the real line. Since only a finite basis is used the DOS is defined only in a finite range of energies. There is a lower bound and possibly one or more band gaps. Its moments are thus finite. Here they are defined about the origin. The definition of the p^{th} moment around 0 is

$$\mu_i^{(p)} = \int_{-\infty}^{\infty} \varepsilon^p \mathcal{D}_i(\varepsilon) d\varepsilon; \quad \mu^{(p)} = \sum_i \mu_i^{(p)} \quad (\text{II.49})$$

The relation between the moments and the Hamiltonian operator follows from their definition, the definition of the DOS and the eigenvalues presented as Hamiltonian matrix elements in the eigenvector basis,

$$\mu^{(p)} = \int_{-\infty}^{\infty} \varepsilon^p \sum_n \delta(\varepsilon - \varepsilon_n) d\varepsilon = \sum_n \varepsilon_n^p = \sum_n \langle n | \hat{H}^p | n \rangle = \text{Tr}(\hat{H}^p) \quad (\text{II.50})$$

A more interesting expression is the partial moment expansion through the insertion of the identity, $\sum_j |j\rangle\langle j|$, $p - 1$ times between the factors of \hat{H}^p ,

$$\mu_i^{(p)} = \langle i | \hat{H}^p | i \rangle = \sum_{jkl\dots} \langle i | \hat{H}^p | j \rangle \langle j | \hat{H}^p | k \rangle \dots \langle l | \hat{H}^p | i \rangle \quad (\text{II.51})$$

Each term of the sum is formed by a closed path starting from index i hopping p times through the neighbouring j, k, l, \dots , and eventually returning to the starting point. In-place hops are included; they correspond to the on-site energies.

The practical significance is in the fact that they can be calculated locally within the reach of a neighbour table cutoff, independent for every atom and orbital, and without diagonalisation. While the calculation of the high moments may be a fairly time consuming task it is not dependent on the total number of atoms in the cell thus they can be computed simultaneously and the effort is linear with respect to the number of atoms.

The first moment is simply an on-site Hamiltonian matrix element. The second moment involves only steps to the nearest neighbours and so on... The Finnis-Sinclair method for example is derived from the second moment approximation. The first few moments are frequently used named quantities

- 0: norm
- 1: mean; centre of gravity
- 2: variance; root mean square width
- 3: skewness
- 4: bimodality

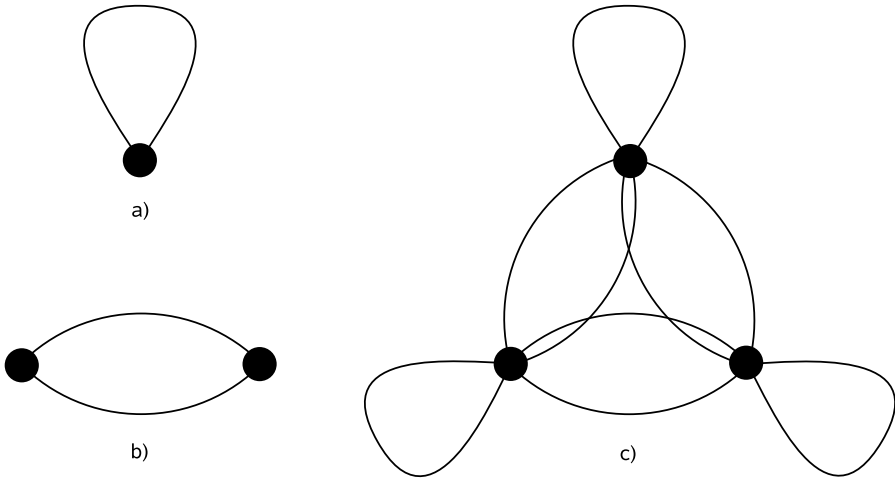


Figure II.3: Hopping paths for a) $p=1$, b) $p=2$ and c) $p=3$.

While these hops give visual insight and may lead to interesting analyses on trends in stability, electronic structure and topology, it quickly becomes impractical for computation of higher moments, say, greater than the tenth; and the nontrivial problem of reconstruction of the DOS from the moments is still outstanding.

The reconstruction of a function from its moments, the moment problem, has been a research topic in mathematics since the end of XIX century[95, 96]. The moments of a function are uniquely defined but there is an infinite number of functions corresponding to the same moments. A knowledge of the specific requirements in a particular case is usually necessary for successful reconstruction. Solutions are usually developed for concrete problem and there are also more general approaches[97, 98]. In general introducing additional information or expectation into the reconstruction may reduce the number of required moments significantly.

In the case of the density of states suitable basis functions like Gaussians were initially fitted to the low moments and more complex functions were used for the higher moments but this process

may tend to be more arbitrary than appreciated.

One way to attempt a reconstruction is to use the Green function of the Hamiltonian operator.

$$\hat{G}(\varepsilon) = (\varepsilon - \hat{H})^{-1} \quad (\text{II.52})$$

Taylor expansion around $\varepsilon = 0$ results in a power series and the Hamiltonian powers can be substituted with the corresponding moments,

$$(\varepsilon - \hat{H})^{-1} \approx \frac{1}{\varepsilon} + \frac{\hat{H}}{\varepsilon^2} + \frac{\hat{H}^2}{\varepsilon^3} \dots = \sum_{p=0}^{\infty} \frac{\hat{H}^p}{\varepsilon^{p+1}} \quad (\text{II.53})$$

This is a problematic step because it introduces significant numerical error if it is possible to evaluate at all and may not be convergent. Other ways of finding the Green function have been developed so the following expressions are still useful.

$$G_{ii}(\varepsilon) = \sum_{p=0}^{\infty} \frac{\mu_i^{(p)}}{\varepsilon^{p+1}} \quad (\text{II.54})$$

Using the following formulas for the delta function and the Green function expanded in local basis

$$\delta(\varepsilon) = -\frac{1}{\pi} \lim_{\eta \rightarrow 0} \text{Im} \frac{1}{\varepsilon + i\eta} \quad (\text{II.55})$$

$$G_{ij}(\varepsilon) = \langle i | \hat{G}(\varepsilon) | j \rangle = \sum_n \frac{C_{i,n} C_{j,n}^*}{\varepsilon - \varepsilon_n} \quad (\text{II.56})$$

the DOS is then

$$\mathcal{D}_i(\varepsilon) = -\frac{1}{\pi} \text{Im} G_{ii}(\varepsilon^+) \quad (\text{II.57})$$

If the density expansion coefficients are written similarly to the band energy in (eq. II.34), in terms of the weighted DOS, then they can also be linked with the Green function. Since the local or-

bitals in BOP are assumed to be orthogonal there is no distinction between expansion coefficients and matrix elements here.

$$\rho_{ij} = \sum_n \int f_n C_{i,n} C_{j,n} \delta(\varepsilon - \varepsilon_n) d\varepsilon = \int f(\varepsilon) D_{ij}(\varepsilon) d\varepsilon = -\frac{1}{\pi} \text{Im} \int f(\varepsilon) G_{ij}(\varepsilon^+) d\varepsilon \quad (\text{II.58})$$

Here, ε^+ is the complex number $\varepsilon + i\eta$ and η is a positive infinitesimal. The imaginary part smears the reconstructed function. Too small η makes the DOS too spiky and too large too featureless.

A systematic approach tackling both issues of the calculation of the moments and reconstruction of the DOS was found by Haydock in 1972 and is now known as the "recursion method"[90, 99]. A procedure of recursive application of the Hamiltonian on a vector and subsequent orthogonalisation is used to calculate its powers indirectly and encode them in series of recursion coefficients. The link between the recursion coefficients and the moments was known for long time already[96]. The algorithm is similar to Lanczos' recursive tridiagonalisation[100] and it does end up finding a basis set in which the Hamiltonian is tridiagonal with these recursion coefficients in the diagonals. The calculation of the diagonal Greenian matrix elements is then simple because the diagonal of the inverse of a tridiagonal matrix is a continued fraction of the diagonal and off-diagonal elements.

The reach of the hopping integrals in a tight binding Hamiltonian is short and typically many atoms are included in a real space calculation. The matrix becomes very large but sparse and custom ordering and packing is vital for the efficiency of the matrix vector dot products.

The Lanczos recursion procedure starts with an arbitrary orthonormal vector $|u_0\rangle$ while in BOP it is an orbital state vector. The

next recursion vector $|u_1\rangle$ is obtained from the following expression

$$|\tilde{u}_1\rangle = H|u_0\rangle - a_0|u_0\rangle \quad (\text{II.59})$$

The tilde in \tilde{u}_1 is to note the vector is not normalised. The a_0 coefficient is the first of the recursion coefficients. It is obtained by left-multiplying by $\langle u_0|$. The normality of u_0 and the orthogonality requirement $\langle u_0|\tilde{u}_1\rangle = 0$ result in the expression for a_0 .

$$a_0 = \langle u_0|H|u_0\rangle \quad (\text{II.60})$$

The magnitude of \tilde{u}_1 is the next recursion coefficient b_1 .

$$b_1^2 = \langle \tilde{u}_1|\tilde{u}_1\rangle \quad (\text{II.61})$$

$$|u_1\rangle = \frac{1}{b_1}|\tilde{u}_1\rangle \quad (\text{II.62})$$

$$b_1 = \langle u_1|\tilde{u}_1\rangle \quad (\text{II.63})$$

Left-multiplying (eq. II.59) by $\langle u_1|$ yields another expression for b_1 .

$$b_1 = \langle u_1|H|u_0\rangle \equiv \langle u_0|H|u_1\rangle \quad (\text{II.64})$$

The algorithm continues according to the recursion steps (eq. II.65). Each application of the vector advances with one step in all possible paths beginning at the starting vector illustrated in (fig. II.3).

$$|\widetilde{u_{n+1}}\rangle = H|u_n\rangle - a_n|u_n\rangle - b_n|u_{n-1}\rangle \quad (\text{II.65})$$

$$a_n = \langle u_n|H|u_n\rangle \quad (\text{II.66})$$

$$b_n^2 = \langle \tilde{u}_n | \tilde{u}_n \rangle; \quad b_n = \langle u_n | H | u_{n-1} \rangle \quad (\text{II.67})$$

$$|u_n\rangle = \frac{1}{b_n} |\tilde{u}_n\rangle \quad (\text{II.68})$$

Every next state vector u_{n+1} is orthogonalised to the preceding u_n thus the vectors form orthogonal basis. It is automatically orthonormal to all previous vectors[101], a feature that distinguishes the recursion method from a Gram–Schmidt orthogonalisation. The orthogonality, however, it not maintained for long in finite precision algebra[101]. The series of recursion coefficients a_n and b_{n+1} form the diagonal and the off-diagonal elements of the tridiagonal Hamiltonian in the u_n basis.

$$H = \begin{pmatrix} a_0 & b_1 & 0 & 0 & 0 & \dots \\ b_1 & a_1 & b_2 & 0 & 0 & \dots \\ 0 & b_2 & a_2 & b_3 & 0 & \dots \\ 0 & 0 & b_3 & a_3 & b_4 & \dots \\ 0 & 0 & 0 & b_4 & a_4 & \ddots \\ \vdots & \vdots & \vdots & \vdots & \ddots & \ddots \end{pmatrix} \quad (\text{II.69})$$

This form of the Hamiltonian, in the context of the moments, suggests an image of a linear chain of states with on-site elements a_n and hopping integrals between the nearest neighbours b_n .

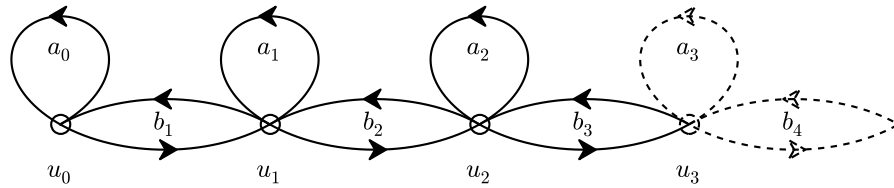


Figure II.4: The one-dimensional chain created by recursion.

The moments of this chain correspond to the moments of the

original system, the advantage for now is that the paths are easier to count. They are just the first element of the powers of the tridiagonal form.

$$\begin{aligned}
\mu^{(0)} &= 1 \\
\mu^{(1)} &= a_0 \\
\mu^{(2)} &= a_0^2 + b_1^2 \\
\mu^{(3)} &= a_0^3 + 2a_0b_1^2 + a_1b_1^2 \\
\mu^{(4)} &= a_0^4 + 3a_0^2b_1^2 + 2a_0a_1b_1^2 + a_1^2b_1^2 + b_i^4 + b_1^2b_2^2 \\
&\vdots
\end{aligned} \tag{II.70}$$

The first p recursion coefficient pairs fully define the $(2p + 1)^{\text{th}}$ moment. A relatively short chain is enough to approximate the high number of moments required for an accurate reconstruction. Expressing the recursion coefficients in terms of the moments by inverting the equations in (II.70) is a troublesome task. They can instead be found with the same recursion algorithm.

It has been discovered in the course of this work that if the recursion is carried out on an unknown matrix H and we additionally define unknown power matrices $H^p, p \in [0, \infty]$, for which only the $\langle 0 | H^p | 0 \rangle$ element is known from $\langle u_0 | H^p | u_0 \rangle = \mu^{(p)}$, the necessary elements of the matrices can be obtained from the recursion on H and then used in subsequent iterations. The procedure will fill in the diagonal and the two symmetric off diagonal elements of H corresponding to a_n and b_n respectively,

$$\begin{aligned}
\langle \tilde{n} | H^p | \tilde{n} \rangle &= \langle n - 1 | H^{p+2} | n - 1 \rangle - 2a_{n-1} \langle n - 1 | H^{p+1} | n - 1 \rangle \\
&\quad + a_{n-1}^2 \langle n - 1 | H^p | n - 1 \rangle + b_{n-1}^2 \langle n - 2 | H^p | n - 2 \rangle \\
&\quad - 2\widetilde{\langle n - 1 | H^{p+1} | n - 2 \rangle} + 2a_{n-1} \widetilde{\langle n - 1 | H^p | n - 2 \rangle}
\end{aligned} \tag{II.71}$$

$$\langle n|H^p|n\rangle = \frac{\langle \tilde{n}|H^p|\tilde{n}\rangle}{b_n^2}; \quad b_n^2 = \langle \tilde{n}|H^0|\tilde{n}\rangle; \quad a_n = \langle n|H^1|n\rangle \quad (\text{II.72})$$

The offdiagonal elements in (eq. II.71), of type $\langle \tilde{n}|H^p|n-1\rangle$ are also found recursively in terms of previously computed values by expanding the higher index only. The relation $|\tilde{n}\rangle = b_n|n\rangle$ has been used here.

$$\begin{aligned} \langle \tilde{n}|H^p|n-1\rangle &= \langle n-1|H^{p+1}|n-1\rangle - a_{n-1}\langle n-1|H^p|n-1\rangle \\ &\quad - \widetilde{\langle n-1|H^p|n-2\rangle} \end{aligned} \quad (\text{II.73})$$

This inversion of the recursion may be used to study the convergence of the moment expansion and reconstruction of a known distribution function. Examples of the application of this new formula will be shown in the next chapter.

The recursion coefficients may not be invariant with respect to rotation of the system. One way to guarantee such invariancy is to average the moments for orbital ℓ over all magnetic quantum numbers of the orbital.

$$\mu_\ell^{(p)} = \frac{1}{2\ell+1} \sum_{m=-\ell}^{\ell} \mu_{\ell m}^{(p)} \quad (\text{II.74})$$

This modification is further developed into the block-recursion method[102].

The DOS reconstruction from $\{a_n, b_n\}$ uses (eq. II.55) and (eq. II.57) but now the Greenian diagonal matrix elements are more stable to compute. The recursion coefficients and the tridiagonalisation are generated with the starting state $|u_0\rangle$ and then the Green function is

$$G_{00}(\varepsilon) = \frac{1}{\varepsilon - a_0 - \frac{b_1^2}{\varepsilon - a_1 - \frac{b_2^2}{\varepsilon - a_2 \dots}}} \quad (\text{II.75})$$

The continued fraction should be terminated after the appropriate number of recursion coefficients or moments is included. An appropriate termination is chosen according to the behaviour of the recursion coefficients' series. It depends on the distribution being reproduced. For single band DOS for example they tend to have damped oscillations approaching some constant values a_∞ and b_∞ which is the centre of the band and the band width. In DOS with band gaps the oscillations will not be damped. For more complex shapes more complex behaviour emerges for example high oscillation in the amplitude of the oscillations.

In the case of oscillations with constant amplitude and frequency the continued fraction can be successfully terminated by substituting the repeating pattern and obtaining a closed form. Solving the resulting quadratic equation gives the square root terminator. The repeating patterns are simply the terminal a_∞ and b_∞ .

$$t(\varepsilon) = \frac{1}{\varepsilon - a_\infty - b_\infty^2 \frac{1}{\varepsilon - a_\infty - \frac{b_\infty^2}{\varepsilon - \dots}}} = \frac{1}{\varepsilon - a_\infty - b_\infty^2 t(\varepsilon)} \quad (\text{II.76})$$

$$t(\varepsilon) = \frac{\varepsilon - a_\infty}{2b_\infty^2} \left(1 - \sqrt{1 - \left(\frac{2b_\infty}{\varepsilon - a_\infty} \right)^2} \right) \quad (\text{II.77})$$

Semiconductors may not be served well by the square root terminator and more sophisticated expressions have been developed to deal with multi gap DOSs[103, 104]

If the starting state was some atomic orbital $|RL\rangle$ then G_{00} corresponds to $G_{RL,RL}$ and the DOS obtained is the projection on the RL orbital. An important realisation is that the starting orbital may be more generally a linear combination of orbitals. The recursion method is not restricted to any particular starting vector. For example evaluating G_{00} starting from bonding or antibonding states, i.e. G_{++} and G_{--}

$$|+\rangle = \frac{1}{\sqrt{2}}(|\ell\rangle + |\ell'\rangle) \quad (\text{II.78})$$

$$|-\rangle = \frac{1}{\sqrt{2}}(|\ell\rangle - |\ell'\rangle) \quad (\text{II.79})$$

then taking half the difference between them in the spirit of valence bonds leads to an intersite Green function matrix element

$$\frac{1}{2} (\langle +|\hat{G}|+\rangle - \langle -|\hat{G}|-\rangle) = \langle \ell|\hat{G}|\ell'\rangle = G_{\ell\ell'} \quad (\text{II.80})$$

As an illustration, the bond order $\Theta_{\ell\ell'}$ may be computed as the half difference between the electrons found by integration of the DOSs projected from G_{++} and G_{--} ,

$$\Theta_{\ell\ell'} = -\frac{1}{\pi} \int f(\varepsilon) (G_{++}(\varepsilon^+) - G_{--}(\varepsilon^+)) d\varepsilon = \frac{1}{2}(N_+ - N_-) \quad (\text{II.81})$$

After finding the inter-site Green's function elements the density expansion coefficients are calculated by (eq. II.58) and from there on the bond orders and the inter-site representation of the band or bond energy constructed. The difference between the band energies computed in the both representations is a measure of the convergence of the intersite G_{nm} .

The intersite Green function elements converge slower with the number of recursion levels than the onsite elements and for this

reason the whole formalism was rewritten in strictly one-site expansion in an auxiliary space [105] and [106]. The development is rather involved but the result is faster offdiagonal convergence at the price of vastly increased memory usage. The dot product in the auxiliary space is generalised as a metric Λ .

$$\{w_n|w_m\} = \sum_{ij} \Lambda_{ij} \langle i_n | j_m \rangle \quad (\text{II.82})$$

The state vectors w are constructed from the initial orbitals i_n . And the recursion is carried out with them.

The Green function's intersite elements are written in terms of derivatives with respect to the recursion coefficients,

$$G_{RL,R'L'}(\varepsilon) = \sum_{n=0}^{\infty} \frac{\partial G_{00}^{\Lambda}(\varepsilon)}{\partial a_n^{\Lambda}} \frac{\partial a_n^{\Lambda}}{\partial \Lambda_{RL,R'L'}} + 2 \sum_{n=1}^{\infty} \frac{\partial G_{00}^{\Lambda}(\varepsilon)}{\partial b_n^{\Lambda}} \frac{\partial b_n^{\Lambda}}{\partial \Lambda_{RL,R'L'}} + G_{00}^{\Lambda}(\varepsilon) \delta_{RR} \delta_{LL'} \quad (\text{II.83})$$

The superscript Λ denotes quantities in the auxiliary space.

$$\frac{\partial G_{00}(\varepsilon)}{\partial a_n} = (G_{0n}(\varepsilon))^2; \quad \frac{\partial G_{00}(\varepsilon)}{\partial b_n} = 2G_{0n}(\varepsilon)G_{0,n-1}(\varepsilon) \quad (\text{II.84})$$

The G_{0n} elements are found from the following recurrence on the known G_{00} ,

$$G_{n+1,m}(\varepsilon) = \frac{\varepsilon - a_n}{b_{n+1}} G_{nm}(\varepsilon) - \frac{b_n}{b_{n+1}} G_{n-1,m}(\varepsilon) - \frac{\delta_{nm}}{b_{n+1}} \quad (\text{II.85})$$

Linear response functions and susceptibilities can be computed with these off diagonal elements. Density coefficients and bond orders can be written in terms of the susceptibilities and they can later be used to speed up the self consistency,

$$\chi_{0m,n0}^{\Lambda} = \frac{1}{\pi} \int f_n G_{0m}^{\Lambda}(\varepsilon^+) G_{n0}^{\Lambda}(\varepsilon^+) d\varepsilon \quad (\text{II.86})$$

$$\Theta_{RL,R'L'} = - \sum_{n=0}^{\infty} \chi_{0n,n0}^{\wedge} \frac{\partial a_n^{\wedge}}{\partial \Lambda_{RL,R'L'}} - 2 \sum_{n=1}^{\infty} \chi_{0,n-1,n0}^{\wedge} \frac{\partial b_n^{\wedge}}{\partial \Lambda_{RL,R'L'}} \quad (\text{II.87})$$

Another way to increase the convergence rate with respect to number of moments is to set a finite electronic temperature in the Fermi distribution from (eq. II.13). The electronic temperature localises the electron density and fewer moments should be sufficient for a realistic description. The introduction of temperature contributes an entropic band energy term,

$$U_{\text{ent}} = -T S(T) \quad (\text{II.88})$$

$$S(T) = -2k \sum_n (f_n \ln(f_n) + (1-f_n) \ln(1-f_n)) = -2k \int \sigma(\varepsilon) D(\varepsilon) d\varepsilon \quad (\text{II.89})$$

$$\sigma(\varepsilon) = f(\varepsilon) \ln(f(\varepsilon)) + (1-f(\varepsilon)) \ln(1-f(\varepsilon)) \quad (\text{II.90})$$

Simple self consistency is effected through local charge neutrality. The task is to minimise the charge transfers to some tolerance by finding suitable on-site energies. The number of iterations needed depends a lot on the scheme for adjustment of the on-site energies. Simple linear mixing yields very poor results requiring 50-60 iterations on average for tolerance 0.001 eV/atom. A secant algorithm applied to each atom individually was found to be much faster requiring around 10 iterations to satisfy a tiny tolerance, for example 0.000001 eV/atom for the Ti₃Al unit cells. Since the convergence is superlinear the number of steps needed for the conventional 0.01-0.001eV/atom tolerance is not much smaller, usually ≈ 7 . The change in onsite elements is calculated as follows:

$$H_{ii}^{(n+1)} = H_{ii}^{(n)} - \delta q_n \frac{H_{ii}^{(n)} - H_{ii}^{(n-1)}}{\delta q_n - \delta q_{n-1}} \quad (\text{II.91})$$

which is a discrete version of Newton's root finding method

$$x_{n+1} = x_n - \frac{f(x_n)}{f'(x_n)} \quad (\text{II.92})$$

with $f(x) = \delta q(H_{ii})$. The susceptibilities may help additionally here since the $\chi_{00,00}^\wedge = -\frac{1}{2} \frac{\partial q_{RL}}{\partial a_0^\wedge}$ and $a_0^\wedge = H_{RLRL}$ hence $\delta q'_R(H_{RR}) = -2 \sum_L \chi_{00,00}^\wedge$ [106], then:

$$H_{ii}^{(n+1)} = H_{ii}^{(n)} - \delta q_n / \delta q'(H_{ii}) = H_{ii}^{(n)} + \frac{\delta q_n}{2 \sum_L \chi_{00,00}^\wedge} \quad (\text{II.93})$$

For large systems the secant and Newton's methods may be unstable and linearly mixed Newton's algorithm using the response functions may be more appropriate.

A BOP calculation involves the following general steps:

1. Building the lists of neighbours and the Hamiltonian
2. Self-consistency cycle
 - (a) Calculation of the recursion coefficients
 - (b) Finding the Fermi level
 - (c) Computing the susceptibilities
 - (d) If the maximal charge accumulated on any atom meets the LCN tolerance exit, else shift the on-site energies appropriately and jump to 2a
3. Calculate the energies in the on-site and intersite representations, check the convergence and add the classical contributions

tions.

In every step contributions from different atoms are calculated independently, only numbers of electrons and the energies are collectively summed and require communication. Thereby the scheme is naturally parallelisable with very little communication and offers near ideal linear scaling. Parallel calculations on distributed memory machines additionally has the benefit of lowering the memory requirements per node. Another small speed-up comes from the fact that there is no requirement for a shared filesystem: these can introduce high latencies and low input-output rates on poorly configured and loaded clusters. There is in fact no strict requirement for having any file system on the computational nodes.

At 9 moments the building of the Hamiltonian is the most expensive step but it is carried out one time only. The subsequent iterations only update the on-site energies. The next most time consuming is the calculation of the recursion coefficients. About 80% of the time spent in calculation of the recursion coefficients goes in the matrix times vector products, $H|u_n\rangle$; as a part of the present work, this was hand optimised and pieces written in SSE2/3 assembly language.

II.5 Classical potential terms

The final ingredient in every TB model is the classical potential. Its physical role is to provide the core repulsion component of the energy. The core orbitals are not included in the quantum mechanical model because they are fairly rigid and insensitive to the states of the valence electrons. From this contribution comes the expectation that the classical potential should be always positive i.e. repulsive. Another, more difficult, role is to absorb all leftovers from the previous approximations that were not entirely covered

by the preceding terms. For example the 3-centre integral contributions that were not averaged over the 2-centre hopping integrals and the neglect of the overlap matrix. The classical potential in BOP sometimes also has the additional task to compensate for the lost bonding due to use of less than minimal basis. On that account it may no longer be strictly repulsive. In case that fitting "experimental" targets proves to be beyond the abilities of the potential then the bond model parameters have to be modified too in a feedback loop or together with the classical parameters.

The range of the pairwise functions of the classical repulsive potentials is expected not to be longer than the corresponding hopping integrals in the bonding part. Extending the repulsive potentials beyond the range of the bonding part providing cohesion may induce an unphysical behaviour. A longer ranged potential which is weakly attractive may have more merit and applicability.

A more sophisticated environmentally dependent repulsive term is sometime added to recover some of the effects of the approximation of the overlap matrix to identity and the neglect of low lying s and p orbitals. Particularly sensitive to these approximations are materials with negative Cauchy pressures, for example Ti-Al alloys like some other aluminides.

If bonding was to be correctly described by pair potentials the Cauchy pressures would have been zero. A more metallic model including density contributions was shown to only contribute to positive Cauchy pressures[107]. A screened Yukawa type potential was used to successfully fit the negative Cauchy pressures in tetragonal L1₀ TiAl,

$$\Phi(R_{ij}, \lambda_{ij}, r_{core}^{ij}) = \frac{A_{ij}}{R_{ij}} e^{-\lambda_{ij}(r_{ij} - 2r_{core}^{ij})} \quad (II.94)$$

$$\lambda_{ij} = \frac{\lambda_i + \lambda_j}{2} \quad (\text{II.95})$$

$$r_{core}^{ij} = \frac{r_{core}^i + r_{core}^j}{2} \quad (\text{II.96})$$

$$\lambda_i = \lambda_\infty^i + \left(\sum_k C_{ik} e^{-\nu_{ik} r_{ik}} \right)^{\frac{1}{m_{ik}}} \quad (\text{II.97})$$

Every pairwise interaction between i and j is being screened by a pairwise interaction with each k atom around it. The same environmental potential is also transferable to the secondary Ti-Al phase α_2 .

Further development of analytical many-body environmentally dependent potential from the overlap matrix is presented in [108].

All pair potentials have to be smoothly cut at appropriate distance. The smooth cutoff can be implemented similarly to that in the hopping integrals, either by augmenting the function with some polynomial smooth at the both ends and vanishing at the right, or more conveniently by multiplying the function by a smooth function which has values of 1 and 0 at the left and right ends, respectively, and vanishing derivatives up to a specified level at both ends, usually 2nd is required for correct description of the elastic properties.

The next chapter deals in more detail with the properties and the problems related with the pairwise functions commonly used in TB and BOP.

Chapter III

Pairwise functions in TB/BOP

The pairwise potentials are functions of the distance between a pair of atoms only. A number of functions can be used as pair potentials. They are generally decaying with different powers depending on the specific purpose. There may be case dependent allowances for negative regions too as described above. Pair potentials are written in terms of inverse power laws, exponents, products of the two, more sophisticated expressions or a combination of different terms. An interesting addition is the sum of left halves of shifted cubes of r [109]. Combinations of these various functions may introduce many linearly dependent parameters. In most fitting procedures it is preferable to minimise the number of dependent parameters.

If the potential is to be used in molecular dynamics simulations where atoms may cross the boundary of the sphere of influence of a neighbour, it is important that the potentials are continuously reduced to zero inside this boundary. The step in the force strength may otherwise be very large and lead to non preservation of the conserved quantities even for very small time steps. If the elastic properties of the system are important or if they have an important influence on the sought after observables, the continuity should be preserved up to the second derivative of the potential. Core struc-

tures of dislocations and their dissociations are dependent on the elastic field surrounding them[35] and it is necessary to ensure the potentials are smooth up to their second derivatives.

With the notable exception of the 'spline' type

$$\sum_i a_i (r_i - r)^3 \Theta(r_i - r) \quad (\text{III.1})$$

all other functions in common use, namely the inverse power law and exponentials, approach zero only asymptotically and need a little help to finally reach it in a reasonably finite distance.

The spline potential's main advantages are its great flexibility and the lack of discontinuities at the cutoff. The derivatives of the potential are also very simple and are also linear in $\{a_i\}$. These features are often used to simplify the fitting by writing the expressions for the target properties analytically for selected $\{r_i\}$ and solving the resulting linear system of equations for $\{a_i\}$ thus reducing the problem to only finding suitable selection of $\{r_i\}$. The knots should not be very close to each other because the corresponding coefficients may become nearly linearly dependent.

The splines' flexibility however is a double edged sword. Unless there are enough datapoints at different distances used in the fitting it may exhibit rather arbitrary behaviour. These points may be obtained by fitting to a number of different phases with different spacing of the neighbours, phase transition paths, other deformations or simply to randomly generated structures for which accurate results are available. BCC cells may be fitted without modifications because the separation between the first and second neighbours is small. If on the other hand the fitting relies only upon one to two neighbours in a close packed structure at or near equilibrium, shaping the potential away from the neighbour distances becomes nearly a craft.

The more traditional and less flexible functions remove most of

the ambiguity about the large regions away from any information carrying points.

A general analytical single term pair potential function $v(r)$ may be factorised to its value v_0 at reference distance $r = r_0$ and a function normalised at r_0 . In most cases r_0 is set to or close to the nearest neighbour spacing, in this way we write, firstly,

$$v(r) = v_0 f_n(r) \quad (\text{III.2})$$

$$f_n(r_0) = 1 \quad (\text{III.3})$$

In a second step the normalised function f_n is further factorised to its simplest form f_{ts} , which does not in general pass through $(r_0, 1)$, and a normalisation constant $1/f_{ts}(r_0)$. This simplifies manipulation as well as implementation. For example the pair potential $A(r/r_0)^{-n}$ is replaced by r^{-n} which can be scaled back to its original value at the end of any analysis or during fitting. We therefore make the definition

$$f_n(r) = \frac{f_{ts}(r)}{f_{ts}(r_0)} \quad (\text{III.4})$$

$$f_n^{(m)}(r_c) = 0 \quad (\text{III.5})$$

in which the superscript (m) is used to denote the m^{th} derivative of the function.

The simpler function f_{ts} contains specific modifications in a given range $[r_1, r_c]$ or over the whole space so that it is cutoff smoothly to zero at r_c .

III.1 Cutoffs

A common modification cutting off an asymptotic function smoothly from a distance r_1 to a distance r_c is to replace it with a “tail” function, f_t , matching the original, “source”, function f_s up to the n^{th} and m^{th} derivative on the boundaries r_1 and r_c respectively. Using the Heaviside step function, we write this as

$$f_{ts}(r) = f_s(r)\Theta(r - r_1) + f_t(r)(1 - \Theta(r - r_1)) \quad (\text{III.6})$$

$$f_t^{(n)}(r_1) = f_s^{(n)}(r_1); \quad f_t^{(m)}(r_c) = 0 \quad (\text{III.7})$$

III.1.1 The Augmentative Cut-off

A naive way to construct such a tail would be to write a polynomial of $(n + m + 1)^{\text{th}}$ order in the form $P_n(r)(r_c - r)^{m+1}$, impose the boundary conditions and find its coefficients. The specified polynomial has the required behaviour and completely replaces the source function between r_1 and r_c . For this reason it is also often called augmentative f_a . We will have

$$f_t(r) = f_a \left(\frac{r - r_1}{r_c - r_1} \right) \quad (\text{III.8})$$

$$f_a^{(n)}(0) = f_s^{(n)}(r_1)(r_c - r_1)^n \equiv f_s^{(n_x)}(r(x=0)) \quad (\text{III.9})$$

$$f_a^{(n)}(1) = 0 \quad (\text{III.10})$$

Using the notation of (III.9), a solution for $n = m = 2$ is:

$$\begin{aligned} f_a^{(2,2)}(x) = & \left(\left(\frac{1}{2}f_s^{(2_x)}(r_1) + 3f_s^{(1_x)}(r_1) + 6f_s(r_1) \right) x^2 + \right. \\ & \left. + \left(f_s^{(1_x)}(r_1) + 3f_s(r_1) \right) x + f_s(r_1) \right) (1 - x)^3 \end{aligned} \quad (\text{III.11})$$

III.1.2 The Multiplicative Cut-off

The multiplicative method introduces a factor which preserves the original function but modifies it so it follows the prescriptions that it matches the function at r_1 and vanishes at r_c . A third step, after (eq. III.2) to (eq. III.5), taken for reasons of sanity is the linear mapping of $[r_1, r_c]$ to $[0, 1]$, which allows us to introduce the following tail function, defined for $r > r_1$, in which the source function is multiplied by the function f_m ,

$$f_t(r) = f_s(r)f_m\left(\frac{r - r_1}{r_c - r_1}\right) \quad (\text{III.12})$$

$$f_m(0) = 1; \quad f_m^{(n>0)}(0) = 0 \quad (\text{III.13})$$

$$f_m^{(n)}(1) = 0 \quad (\text{III.14})$$

There are many functions satisfying the requirements for a multiplicative cutoff factor. A simple and very general one can be constructed as a polynomial analogous to the augmentative case. We will refer to this as the general multiplicative polynomial, matching up to the n^{th} derivative on the left side and up to the m^{th} on the right side, and denoted by $f_I^{\{n,m\}}(x)$. The solution for $n = m = 2$ then is:

$$f_m(x) : f_I^{\{2,2\}}(x) = (6x^2 + 3x + 1)(1 - x)^3 \quad (\text{III.15})$$

An attractive property of this and all multiplicative cutoffs is the independence of the properties of the function to which they are applied. The derivatives of the original function need not enter in the expression because they are retained in the derivative of the product of functions and the requirements for the cutoff at r_1 , this is because if f represents the source function and g the tail function, we have

$$(fg)' = f'g + fg' = f'1 + f0 = f'$$

$$(fg)'' = f''g + 2f'g' + fg'' = f''1 + 2f'0 + f0 = f''$$

As we will see later the lack of direct dependence on the source function in practice does not exactly mean total independence from it.

A special case for the multiplicative cutoff is when r_1 is shifted near the beginning of the original function or even beyond. This is acceptable because the factor introduced is only a multiplier and the spirit of the original function is still present. The special, so called GSP function, introduced by Goodwin, Skinner and Pettifor[84], is a particular example of this approach which will be discussed later. Taking the line of thought slightly further one can completely forget about r_1 and even pick a cutoff factor which diverges on the left side e.g.:

$$(r_c - r)^{m+1} \Theta(r_c - r)$$

which vanishes smoothly at r_c up to its m^{th} derivative. The inevitable price to pay for modifying the whole function rather than a selected region is that the ratios f'_{ts}/f_{ts} , f''_{ts}/f'_{ts} etc.. increase with the order of the factor. This is not always detrimental and in certain cases it is beneficial to the model .

The general form for the polynomial $f_I^{(n,m)}(x)$ is:

$$f_I^{(n,m)}(x) = (1-x)^{m+1} \sum_{i=0}^n \binom{m+i}{m} x^i \quad (\text{III.16})$$

It was proposed after following the pattern of the coefficients in (III.15) and other explicit expressions for higher n and m .

This general expression will be referred to later as the binomial

cutoff polynomial.

The coefficients are very simple to calculate because they happen to be the first n elements of the m^{th} diagonal of Pascal's triangle. The sum part of the expression can be quickly evaluated with fused multiply-add instructions using Horner's method.

After a few transformations one can arrive at a simpler form for the derivative, than may naively be expected from the above, namely,

$$f_I^{(n,m)'}(x) = -(m+n+1) \binom{m+n}{m} x^n (1-x)^m \quad (\text{III.17})$$

$$f_I^{(n,m)''}(x) = -(m+n+1) \binom{m+n}{m} (n - (n+m)x) x^{n-1} (1-x)^{m-1} \quad (\text{III.18})$$

III.1.3 Proof of eligibility

The roots of the first derivative and their multiplicity prove that the definition in (eq. III.16) satisfies the boundary conditions for the derivatives. The conditions for the values at 0 and 1 are evident from the definitions itself having in mind $0^0 = 1$.

The proof for the left boundary conditions may be written more elaborately by presenting the definition in (eq. III.16) as product of two functions and subsequently writing the general binomial formula for arbitrary derivative of product of functions and evaluating the expressions at $x = 0$. If everything is properly carried out eventually the answer is 0 for any positive derivative k . Indeed,

$$f_I^{(k>0)}(x) = (fg)^{(k)} = \sum_{i=0}^k \binom{k}{i} f^{(i)} g^{(k-i)} \quad (\text{III.19})$$

$$f^{(k)}(x) = ((1-x)^{m+1})^{(k)} \quad (\text{III.20})$$

$$= \begin{cases} \frac{(-1)^k (m+1)!}{(m+1-k)!} (1-x)^{m+1-k} & \text{if } k < m+2 \\ 0 & \text{otherwise} \end{cases} \quad (\text{III.21})$$

$$f^{(k)}(0) = \begin{cases} \frac{(-1)^k (m+1)!}{(m+1-k)!} & \text{if } k < m+2 \\ 0 & \text{otherwise} \end{cases} \quad (\text{III.22})$$

$$g^{(k)}(x) = \left(\sum_{i=0}^n \binom{m+i}{m} x^i \right)^{(k)} = \sum_{i=k}^n \frac{(m+i)!}{m!(i-k)!} x^{i-k} \quad (\text{III.23})$$

$$g^{(k)}(0) = \begin{cases} \frac{(m+k)!}{m!} & \text{if } k < n+1 \\ 0 & \text{otherwise} \end{cases} \quad (\text{III.24})$$

(III.25)

Then to substitute into (eq. III.19), we use (eq. III.22) with $k \rightarrow i$ and (eq. III.24) with $k \rightarrow (k-i)$. We also find

$$(fg)^{(k)} = \sum_{i=0}^k \binom{k}{i} \frac{(-1)^i (m+1)!}{(m+1-i)!} \frac{(m+k-i)!}{m!} = \begin{cases} 0 & \text{if } k > 0 \\ 1 & \text{otherwise} \end{cases} \quad (\text{III.26})$$

The last expression (eq. III.26) is vanishing because it can be represented as the derivative of a polynomial at its root with multiplicity an order higher than the derivative:

$$f_I^{(k>0)}(0) = \sum_{i=0}^k \binom{k}{i} \frac{(-1)^i (m+1)!}{(m+1-i)!} \frac{(m+k-1)!}{m!} \quad (\text{III.27})$$

$$= (m+1) \sum_{i=0}^k \binom{k}{i} \frac{(-1)^i (m+k-i)!}{(m+1-i)!} \quad (\text{III.28})$$

$$= (m+1) \left((x^m - 1)^k \right)_{|x=1}^{(k-1)} = 0 \quad (\text{III.29})$$

$$\left((x^m - 1)^k \right)^{(k-1)} = \sum_{i=0}^k (-1)^i \binom{k}{i} \frac{(m+k-i)!}{(m+1-i)!} x^{m-i+1} \quad (\text{III.30})$$

III.1.4 Type II

The expressions above from (eq. III.27) to (eq. III.30) lead to another potentially useful polynomial which is shorter to write but likely harder to evaluate,

$$f_{II}^{\{n,m\}}(x) = (1 - x^n)^m \quad (\text{III.31})$$

for which the following approximate relation holds,

$$f_I^{\{2,2\}}(x) \approx f_{II}^{\{2.454, 3.398\}}(x) \quad (\text{III.32})$$

The n and m in this formula do not have the clear meaning they had in the previous one. The first derivative of the binomial polynomial exposes symmetry at $n = m$ which is lacking here. The symmetric binomial polynomial, taken in the region of $[0, 1]$ and rescaled and shifted as necessary, may be practical in other applications as an approximant to the step function with guaranteed decay. Its first derivative may be useful as a delta function approximation holding non-zero value only in a clearly defined range and integrating to 1 over its definition and the whole space by extension. It is interesting to note the kernel in (eq. III.17) for $n = m$

remapped from $[0, 1]$ to $[-1, 1]$ is:

$$(1 - x^2)^n = f_{II}^{(2,n)}(x) \quad (\text{III.33})$$

which is exactly the value of $f_{II}\{2, n\}$ in the same region.

Here are the first and second derivatives of f_{II} for reference:

$$f'_{II}(x) = -nm(1 - x^n)^{m-1}x^{n-1} \quad (\text{III.34})$$

$$f''_{II}(x) = nm(1 - x^n)^{m-2}x^{n-2}(1 - x^n - n(1 - mx^n)) \quad (\text{III.35})$$

One interesting representation of the binomial polynomial is easily obtained from integration of the kernel of (eq. III.17), $x^n(1 - x)^m$, by parts and subsequent normalisation,

$$f(x) = (m + n + 1)!(1 - x)^{m+1} \sum_{i=0}^n \frac{x^i(1 - x)^{n-i}}{i!(m + n + 1 - i)!} \quad (\text{III.36})$$

$$= \sum_{i=0}^n \binom{m + n + 1}{i} x^i (1 - x)^{m+n+1-i} \quad (\text{III.37})$$

This appears to be an incomplete binomial expansion of $((1 - x) + x)^{m+n+1}$ which, if taken completely, is 1.

III.1.5 Comparison

Comparison between the cutoffs, mentioned so far, applied to a few commonly used functions at two different ranges, are presented in (fig. III.1) and (fig. III.2). The first column plots the functions and the second and the third respective derivatives with consistent colours and appropriate scaling on the ordinate. The source

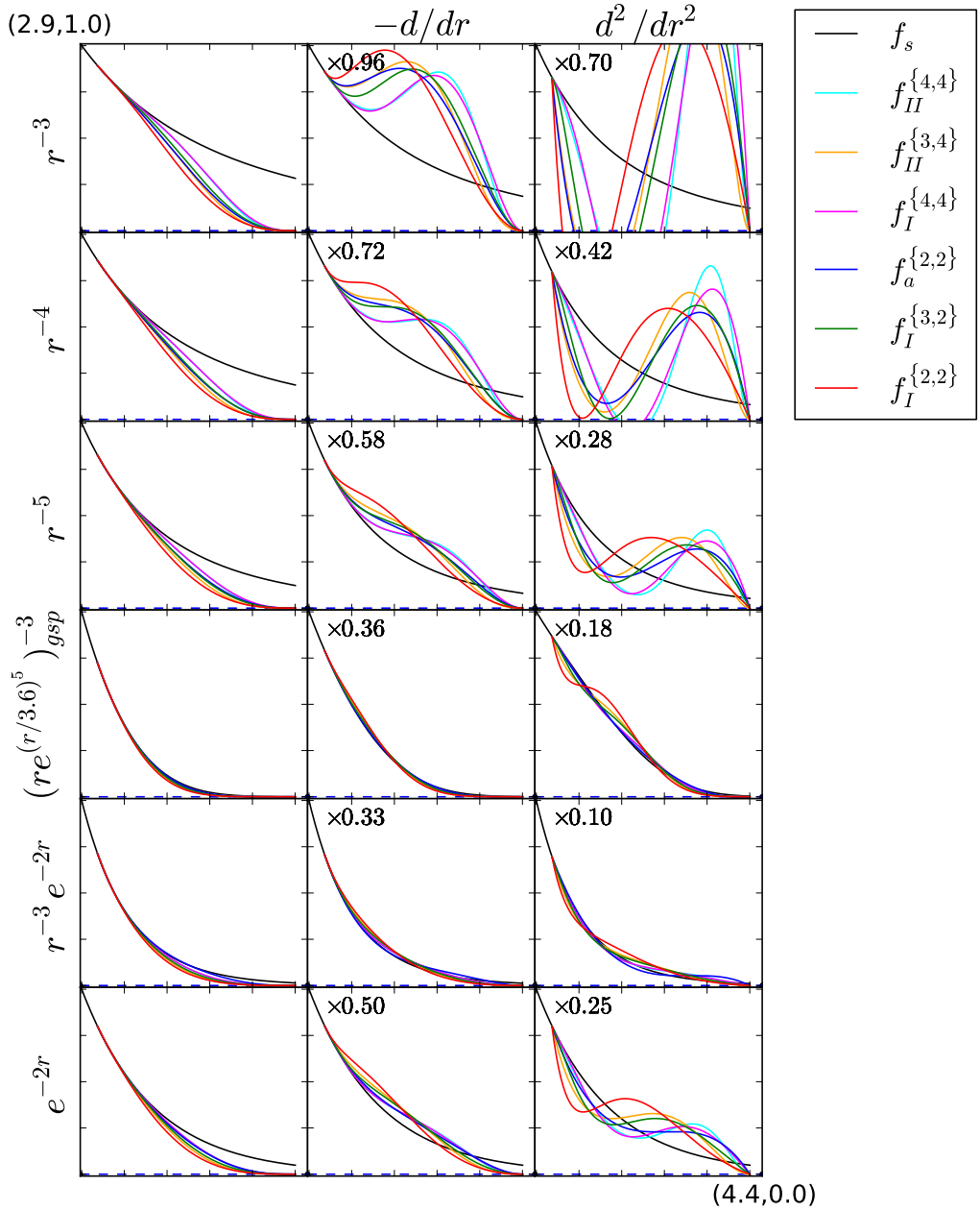


Figure III.1: Comparison between different cutoffs applied to different functions between 3 and 4.4 Å. f_I is (eq. III.16), f_{II} : (eq. III.31) and f_a is from (eq. III.12)

functions and derivatives are shown alongside the various cutoffs.

The first striking observation is the huge divergences in the

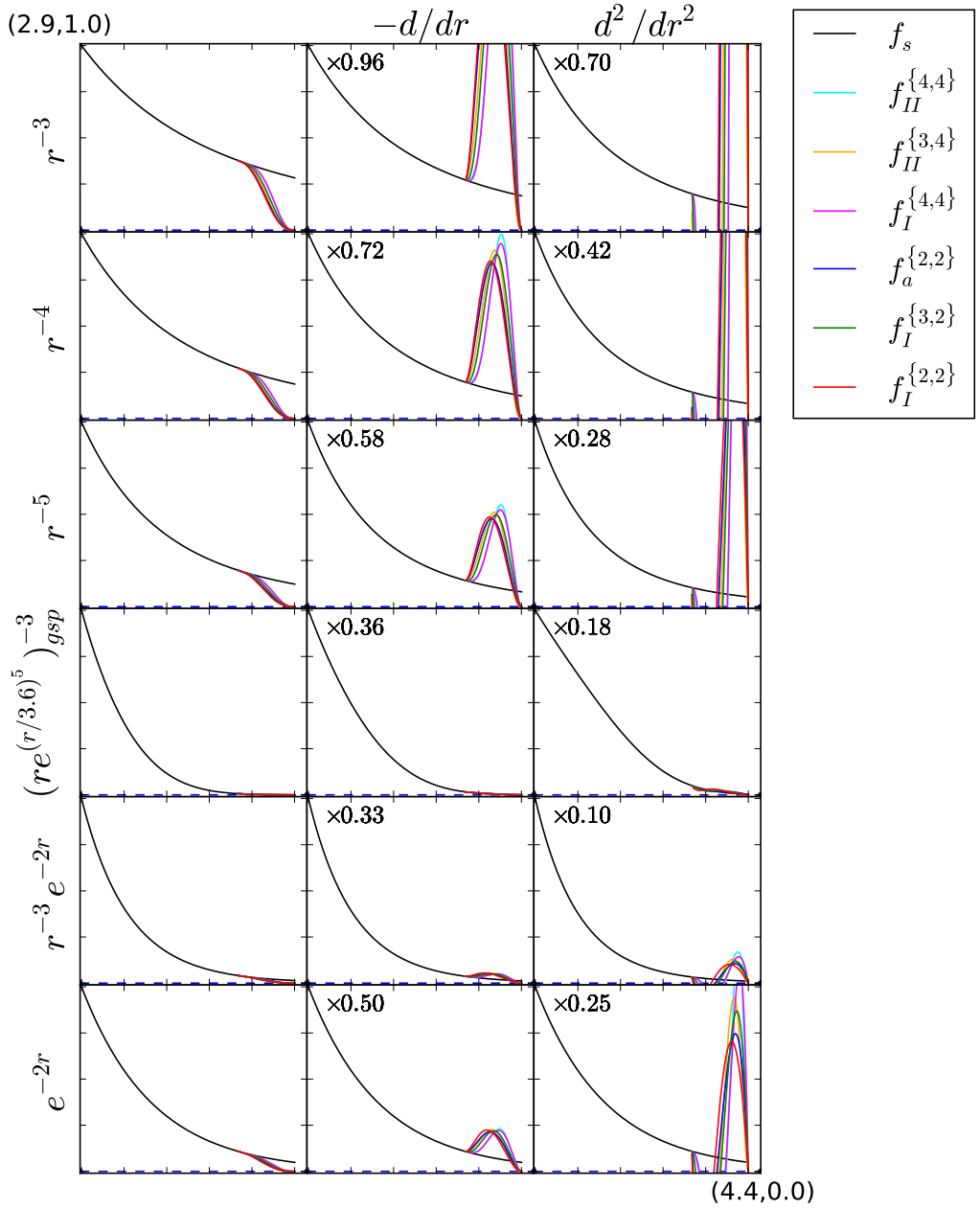


Figure III.2: Comparison between different cutoffs applied to different functions between 4 and 4.4 Å. f_I is (eq. III.16), f_{II} : (eq. III.31) and f_a is from (eq. III.12)

derivatives of the inverse power law functions, very commonly used for hopping integrals and overlap scalings, and pretty much all cut-

offs. The effects are more acute and are visible not only on the inverse power laws when the recommended strategy of choosing a short cutoff range is used as in (fig. III.2). A few solutions to this problem may be proposed. A simple one is to follow the trend of smoothing the step by increasing the range of the cutoff either to the left or the right. Extending the range to the right will include more neighbours and slow down a real space method like BOP significantly. Another complication arising with a number of cutoffs is that far away from r_1 and near r_c there may be an unphysical undesirable increase of the value of the second derivative which may be detrimental to credible description of the elastic properties. The cutoffs to be avoided if such decision is to be made are the augmentative and the multiplicative ones whose smoothness at zero is too high. The damage to the properties may be significant if many neighbours happen to live this far from the central atom. These neighbours are supposed to have little to no influence instead of the observed greatly exaggerated cutoff derivatives.

Extending the range to the left will result in general steepening of the final function. The augmentative cutoff in this case will be have particularly poor effect on the derivatives around the right end (r_c) and a low order multiplicative polynomial is recommended in this case. The steepening effect is similar to what happens if an inverse power law is modified by multiplying with some exponential as is the case in the GSP and row 5 of the tables. If this is not detrimental to the model it may be worth experimenting with adding an $(r_c - r)^3$ factor. This will avoid the issues of the ranges of the cutoffs plotted here.

III.2 GSP revisited

Another solution comes from a closer look at the construction of the GSP potential[84]. If written as f_s in our convention it is:

$$f_{gsp}(r) = r^{-n} e^{-n\left(\frac{r}{d}\right)^{n_c}} \quad (\text{III.38})$$

But it may also be written as f_t where the source function f_s is r^{-n} and the exponential factor is a global multiplicative cutoff function.

$$f_m : f_g(r) = e^{-n\left(\frac{r}{d}\right)^{n_c}} \quad (\text{III.39})$$

In the region $[0, \infty]$ the cutoff factor f_g behaves like an asymmetric asymptotic step function. The stretching parameter d defines the approximate location after which it is close to vanishing and the power n_c influences strongly the rate of decay. The function is always centred at the beginning of the coordinate system and has exponential growth in the negative direction of r . If asymptoticity is neglected and instead arbitrary points r_1 and r_c , left and right of d respectively, are considered for which the following conditions apply,

$$f_g(r_1) \approx 1 \quad (\text{III.40})$$

$$f_g^{(n>0)}(r_1) \approx 0 \quad (\text{III.41})$$

$$f_g^{(n)}(r_c) \approx 0 \quad (\text{III.42})$$

then the GSP factor can be equated with our multiplicative polynomials applied for the same range $[r_1, r_c]$. Its advantage over the binomial polynomial is that it can produce arbitrary steepness of the step. The binomial function is restricted to the discrete choice of number of derivatives (n) and (m) which are integers. This advantage is most pronounced for low values of $1 < n_c < 3$. This continuity in the steepness is however covered by the type II polynomials. A GSP factor with arbitrary choice of d and n_c can be approximated very well by f_{II} within accurately defined region $[r_1, r_c]$.

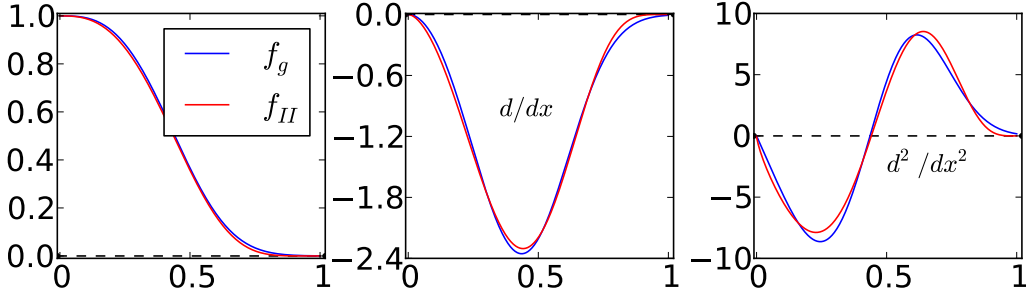


Figure III.3: Values and the first two derivatives of $f_g(x) = e^{-3(x/0.72)^3}$ from (eq. III.39), selected to reside within $[0, 1]$, approximated by $f_{II}(x) = (1 - x^{2.75})^{6.4}$ from (eq. III.31)

The explanation for the relative ease with which the type II polynomial fits the GSP factor is evident if f_{II} is represented in exponential form and Taylor expansion of the logarithmic exponent around 0 is performed:

$$(1 - x^n)^m = e^{\ln(1-x^n)m} = e^{m \ln(1-x^n)} \approx \text{(III.43)}$$

$$e^{m(-x^n - \frac{x^{2n}}{2} - \frac{x^{3n}}{3} - \dots)} = e^{-mx^n(1 + \frac{x^n}{2} + \frac{x^{2n}}{3} + \dots)} \approx e^{-mx^n}$$

The parameters n and m in f_{II} correspond to n_c and n in f_g respectively. The terms $\frac{x^n}{2} + \frac{x^{2n}}{3} + \frac{x^{3n}}{4} \dots$ are much smaller than 1 for x near 0 and quickly vanish for $n >> 1$ but converge much more slowly for x near 1 and are thus the necessary ingredient for complete vanishing at 1 instead of asymptoticity. The GSP factor is then simply a first order approximation of our type II polynomial. If the type II function is stretched by replacing x with x/x_{cut} and m increased appropriately to keep the step in place then x_{cut} stretched to infinity the quadratically faster vanishing infinite sum would be negligible indeed and the two functions will be identical.

The disadvantage of f_g compared with the multiplicative polynomials of both types presented here is that it is not a strict step function but asymptotic hence it does not remove the need for a

strict cutoff. Looking back at the GSP as a source function presented in the tables above its cutoff friendliness is not surprising since it is actually an inverse power law with two cutoffs applied at different scales. In most cases a simpler result with the same properties may be obtained by using a strict multiplicative cutoff which approximates the chosen GSP factor well and avoids the additional cutoff. There may also be cases where the second cutoff applied on more localised region is needed.

III.3 Matching cosines

Expressions could be developed giving the dependence of the extrema in the second derivative on the source function properties and cutoff region, determining its appropriate size which may be useful in automated fitting.

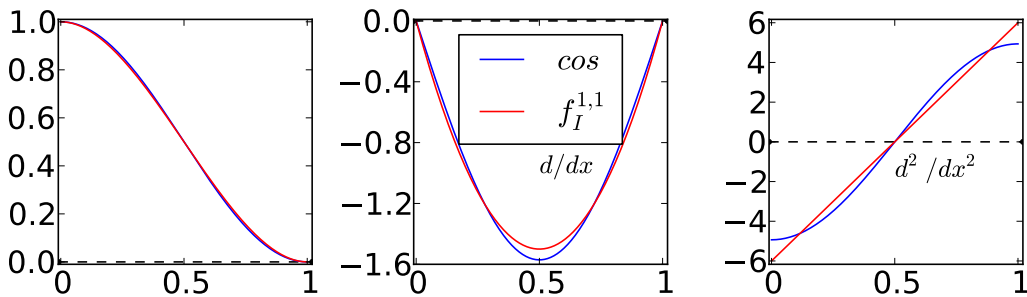


Figure III.4: Comparison between the values and the first two derivatives of $(\cos(\pi x) + 1)/2$ and $(1 - x)^2(1 + 2x) : f_I^{1,1}$ from (eq. III.16)

In cases where the second derivative is of no importance a simple cosine function has been used as multiplicative cutoff in the past[110]. Its similarity to the binomial polynomial set to match up to first derivatives only, is shown in (fig. III.4). The polynomial is practically the same but it and its derivatives have the benefit of being much faster to compute.

The comparisons here have been limited to the more traditional functions used in not only classical central potentials but also in the construction of Hamiltonian and overlap matrices and also in the many body classical environment dependent terms described in the previous chapter (II.94)-(II.97). The classical environment dependent potential uses plain exponentials in its screening terms illustrated in the 6th rows of figures III.1 and III.2 while $e^{-\lambda x}/r$ in the central term is not unlike the expression in the 5th rows. Having in mind that the environmental screening potential was introduced specifically to deal with the notorious negative Cauchy pressures[107] it is of utmost importance that the cutoffs' second derivatives are carefully controlled.

Chapter IV

Finding Parameters

The one and two-centre integrals in the TB Hamiltonian are included as parameters. The two repulsive classical potentials also require a handful of parameters. Generally there is neither 'one right set' nor a single guaranteed path of finding a good set of parameters. Part of the reason for the ambiguity lies in the definition of 'good' or 'appropriate'. Since TB is a significant approximation to the electronic structure problem, transferability and general applicability is often constrained. Depending on the specific problem at hand a balance has to be struck between accurate representation of specific properties of interest and transferability requirements. Appropriately weighting the testing properties and finding the appropriate set of parameters is probably the major barrier to using TB.

IV.1 Introduction

The number of parameters needed for the Hamiltonian can be reduced considerably if the atoms are granted only one type of orbitals. For most transition metals and intermetallics p and d orbitals are enough to provide decent models. In this case parameters for the on-site energies are not necessary due to the mandatory

LCN in BOP and only initial guesses have to be provided. If more than one type of orbitals are used then the separations between the on-site energies of different orbital types on one atom are required.

When the Hamiltonian parameters are not many it is possible to find acceptable set with the help of a few rules, intuition, experience and "intelligent guesswork"[111]. Such models were developed in the past for Ti[112], Mo, Re, Nb, and Fe[113, 114]. Useful sources for starting are Harrison's solid state table[115] and Spanjaard and Desjonquères's prescriptions[116].

The manual trial and error approach may still be viable for binary compounds but increasing further the number of elements in the system may lead to "combinatorial explosion". In such cases other more streamlined strategies may be preferable.

Another approach is to adjust the parameters with some algorithm until a suitably policed objective function is minimised. When the Hamiltonian is concerned the objective function may contain information for the energy bands calculated with more precise method usually a DFT flavour. The objective function may also include energy differences between comparable structures, deformation paths and bond contributions to a variety of experimental or calculated physical properties. The algorithms used often vary from simple brute-force, downhill simplex and simulated annealing[117] to the more complex genetic evolution and neural networks[118]. Being dynamic unpredictable systems these methods may take a life of their own and frequently produce erroneous results, such as non physical parameter sets. Often the steps towards the final solution are more significant than the solution itself. They may give ideas for starting points or policy adjustments. Indeed writing good policies for the objective function may become the most important activity. Different minima of the function in

the configuration space may be found and the decision which one to pick may not be easy at first sight.

A recent method[119] which improves transferability and avoids many of the ambiguities and uncertainties of the properties and bands fitting is to optimise the projection of DFT wavefunctions on TB atomic-like basis orbitals.

A quick and straightforward technique to find a decent set of Hamiltonian parameters is to use the linear muffin-tin orbitals (LMTO) [42]. DFT method implemented within the Atomic Spheres Approximation (ASA). LMTO-ASA is probably the most transparent and chemically intuitive DFT implementation available. Its Hamiltonian is assembled in a way which provides for easier separation between one-, two- and three-centre integrals. The possibility to balance between locality and orthogonality is useful for the preparation of a TB-like Hamiltonian. While it is fiddly error prone work the bond integrals can be extracted from this TB-like Hamiltonian without too much uncertainty. If not perfect they can at least be used as initial guesses for fitting procedures. A major portion of the present work has been to write a general and robust code to extract TB models from the LMTO-ASA program.

The quantum mechanical part is the one carrying most of the interesting physics. The classical repulsive potentials are fitted to reproduce exactly the formation energies, lattice parameters and elastic constants. The classical potentials represent mostly ion-ion electrostatics, core orbitals repulsion and correct previous approximations if possible. They depend strongly on reasonable behaviour of the bond contribution in order to fit well the observable physical properties. There is a variety of expressions which can be used[84]. The usual approach is to use fitting algorithms but for some smartly chosen expressions mathematical tricks can be helpful. For example the sum of splines [109] half of the param-

eters can be determined automatically to exact fit of the properties for selected set of independent parameters.

Next the building of TB Hamiltonian with LMTO-ASA will be visited then a few more will be said on the fitting of all parameters. Afterwards models for Ti-Al alloys developed with these techniques will be presented and discussed.

IV.2 From LMTO-ASA

The LMTO method[80, 120] is an efficient and approximate implementation of the DFT. The problem is solved by partitioning the space in spheres, usually centred on the atom sites, and interstitial space. In the conventional LMTO the potential is assumed to have spherical symmetry around the atomic sites and flat elsewhere much like the shape of some cookie baking tray or dish, from which it probably takes its name. The Schrödinger equation (SE) is governing in the muffin tin (MT) sphere and the Laplace equation in the interstitial space. It is similar to the Linear Augmented Plane Waves (LAPW)[80] method in that the radial SE is solved numerically in the sphere but differs in that atom centred modified Hankel functions (eq. IV.2) are attached to the spheres. The Hankel tails from site R spreading in other MT spheres at R' are expanded in terms of modified Bessel functions centred at R' . The expansion coefficients are known as "structure constants" (eq. IV.1) because they only depend on the positions of the spheres. The numerical solution in the sphere is matched, by value and logarithmic derivative with respect to the energy at the boundary, to the combination of Hankel and Bessel functions. The matching condition yields a few parameters called "potential parameters". The structure constants are

$$B_{R'L'RL}^0 = -8\pi \sum_{L''} (-1)^\ell \frac{(2\ell'' - 1)!!}{(2\ell - 1)!!(1\ell' - 1)!!} C_{L''LL''} K_{L''}(R - R') \quad (\text{IV.1})$$

where

$$K_L(r) = r^{-(l+1)} Y_L(r) \quad (\text{IV.2})$$

The index 0 denotes bare or first generation LMTO ($\kappa = 0$) structure constants[121] which are later converted to screened ones. The double factorials " $n!!$ " represent the product of all odd numbers from 1 to n . The $C_{L''LL''}$ are Gaunt coefficients defined as the expansion coefficients of the product of $Y_{L''}$ and $Y_{L'}$ in terms of Y_L ,

$$Y_{L'} Y_{L''} = \sum_L C_{LL'LL''} Y_L \quad (\text{IV.3})$$

$$C_{L''LL'} = \int Y_{L''} Y_{L'} Y_L d\Omega \quad (\text{IV.4})$$

Real spherical harmonics are used.

Effectively the Slater-Koster table is contained in these coefficients and the structure constants rotate like the hopping integrals. The ratios of the integrals according to the canonical band theory are the same as the ratios of the corresponding bare structure constant matrix elements when the bond is oriented along the z axis[122, 123],

$$B_{ss\sigma} = -2/d$$

$$B_{sp\sigma} = 2\sqrt{3}/d^2$$

$$B_{pp\{\sigma,\pi\}} = 6[2, -1]/d^3$$

$$B_{sd\sigma} = -2\sqrt{5}/d^3$$

$$B_{pd\{\sigma,\pi\}} = 6\sqrt{5}\{-\sqrt{3}, 1\}/d^4$$

$$B_{dd\{\sigma,\pi,\delta\}} = 10\{-6, 4, -1\}/d^5 \quad (\text{IV.5})$$

The bond length measure d is relative to the Wigner-Seitz radius of the lattice $d = r/s$.

The ASA simplifies the problem further by neglecting the interstitial space. Then the total volume of all spheres is required to match the volume of the unit cell to minimise the error caused by the neglect. Small overlaps are allowed to satisfy the volume filling. The overlaps and the tiny leftover free spaces are least significant for close-packed lattices FCC, HCP and their derivatives for example L1₂, L1₀, D0₁₉, D0₂₂, D0₂₄ etc. with near ideal axial ratios. The formal neglect of the interstitial space in ASA means that any point in the system is associated with a single atom only. The potential parameters then have physical meaning: C is the centre of the band, Δ is the bandwidth γ is a band distortion parameter representing the deviation from canonical bands and p is third order eigenvalue correction parameter. The band structure is then dependent only on these sets of potential parameters and the structure constants which are solely determined by the positions of the spheres.

The basis functions give the name of the method itself. The LMTOs are localised orbital-like functions centred on the atomic sites. One is assigned to each site, R , and angular momentum $L = \{\ell m\}$ which, in comparison to plane wave basis, leads to very small Hamiltonian and a certain level of chemical intuitiveness. An ASA-LMTO (linear mutffin-tin orbital)[120] χ in the sphere at site R is a linear combination of the radial solution ϕ and its energy derivatives $\dot{\phi}$ entering from all other sites R' . An LMTO is assigned to each orbital on each atom. Very few LMTOs are needed for fairly accurate description of the band structure.

$$\chi_{RL}(r - R) = \phi_{RL}(r - R) + \sum_{R'L'} \dot{\phi}_{R'L'}(r - R') h_{R'L', RL} \quad (\text{IV.6})$$

The coefficients h are obtained from the structure constants and the potential parameters[124, 123]. Every site and angular momentum has its set of potential parameters so that for every bond they form diagonal matrices. They are shown below to have a major contribution to the ASA Hamiltonian (eq. IV.20),

$$h_{RL,R'L'} = \delta_{RL,R'L'}(C_{RL} - \varepsilon_{v,RL}) + \sqrt{\Delta_{RL}} B_{RL,R'L'}^0 \sqrt{\Delta_{R'L'}} \quad (\text{IV.7})$$

The tails $\dot{\phi}$ can be chosen to be those that are orthogonal to ϕ and can be combined further with radial solutions originating at their sites R' . The orthogonal derivatives are indexed with γ for a reason which will become apparent later. The o potential parameter stands for overlap, and is defined through

$$\dot{\phi}_{R'L'}(r - R') = \dot{\phi}_{R'L'}^\gamma(r - R') + \phi_{R'L'}(r - R') o_{R'L'} \quad (\text{IV.8})$$

The structure constants are unfortunately rather long ranged[121]. To bring the LMTO closer to TB an electrostatics analogy is applied. Tails coming from spheres not close to the head are being screened by the nearby spheres. A similarity transformation can be applied on the LMTOs producing shorter ranged but equivalent basis set[121]. The transformation is performed by screening the structure constants with screening constants and converting the potential parameters appropriately. The screening constants are a new set of parameters named α and linked to the overlap parameter o [124]. The structure constants are screened by α using a Dyson type equation:

$$B^\alpha = B^0 + B^0 \alpha B^\alpha$$

$$B^\alpha = B^0 (1 - \alpha B^0)^{-1} \quad (\text{IV.9})$$

$$\frac{1}{o_{RL}} = C_{RL} - \varepsilon_{v,RL} - \frac{\Delta_{RL}}{\gamma_{RL} - \alpha_{RL}} \quad (\text{IV.10})$$

The following screening values

$$\alpha_s = 0.3485; \quad \alpha_p = 0.05304; \quad \alpha_d = 0.010714 \quad (\text{IV.11})$$

have been found empirically [120], to give the most localised TB like basis set for angular momentum up to $\ell = 2$. This usually includes only first and optionally second nearest neighbours.

The potential parameters C and Δ can be converted[124] easily with the help of the auxiliary variables ξ_{RL} .

$$\xi_{RL} = 1 + (C_{RL} - \varepsilon_{v,RL}) \frac{\alpha_{RL}}{\Delta_{RL}} \quad (\text{IV.12})$$

C and Δ are named c and d respectively in the new representation.

$$c_{RL} = \varepsilon_{v,RL} + (C_{RL} - \varepsilon_{v,RL})\xi_{RL} \quad (\text{IV.13})$$

$$d_{RL} = \xi_{RL}^2 \Delta_{RL} \quad (\text{IV.14})$$

$$p_{RL} = o_{\alpha RL}^2 - o_{RL}^2 \quad (\text{IV.15})$$

An interesting case appears when α_{RL} are set equal to γ_{RL} . Then $o_{RL} = 0$ and we have orthogonal basis functions only. This is said to be the γ -representation [120] and also denotes the γ index on the orthogonal tails. In this representation it is reasonable to expect the basis to be less localised because it is formed by combinations of localised basis functions.

While the first generation B^0 had spherical symmetry the screened B^α include some environment dependence. Another important difference is that nonzero on-site elements emerge containing a crys-

tal field splitting pattern induced by the surrounding charges.

Having the parameter and structure constants defined, the conditions:

$$\langle \phi | \phi \rangle = 1; \quad \langle \phi | \dot{\phi} \rangle = o; \quad \langle \dot{\phi} | \dot{\phi} \rangle = p \quad (\text{IV.16})$$

the LMTOs in bra-ket notation:

$$|\chi\rangle = |\phi\rangle + |\dot{\phi}\rangle h; \quad |\dot{\phi}\rangle = |\dot{\phi}^\gamma\rangle + |\phi\rangle o \quad (\text{IV.17})$$

and the Schrödinger equation in LMTOs [121]

$$(H - \varepsilon_v)|\phi\rangle = 0; \quad (H - \varepsilon_v)|\dot{\phi}^\gamma\rangle = |\phi\rangle \quad (\text{IV.18})$$

the Hamiltonian and overlap matrix elements can be written up to second order in $(\varepsilon - \varepsilon_v)$ [123] :

$$S = \langle \chi | \chi \rangle = 1 + ho + oh + hph \quad (\text{IV.19})$$

$$H = \langle \chi | H | \chi \rangle = \varepsilon_v + h + ho\varepsilon_v + \varepsilon_v oh + h(o + \varepsilon_v p)h \quad (\text{IV.20})$$

If written to first order in the deviation from the eigen values the overlap is the identity and the Hamiltonian is simply $\varepsilon_v + h$. This simple construction of the matrix elements is unique to the ASA method. The terms except the last in (eq. IV.19) and (eq. IV.20) contain only one and two centre integrals. The last terms contain all the three centre integrals, two centre on- and intersite terms. In the γ representation the overlap parameters o vanish together with the second order terms.

The significance of the different terms for a specific system can be evaluated by crafting the required matrices. Only the terms bilinear in h require a little more care:

$$(hph)_{RL,R'L'} = \sum_{R''L''} h_{RL,R''L''} p_{R''L''} h_{R'L',R''L''} \\ = \delta_{RR'} \sum_{L''} h_{RL,RL''} p_{RL''} h_{RL',RL''} \quad (IV.21)$$

$$+ \delta_{RR'} \sum_{R''L''} h_{RL,R''L''} p_{R''L''} h_{RL',R''L''} (1 - \delta_{RR''}) \quad (IV.22)$$

$$+ (1 - \delta_{RR'}) \sum_{L''} (h_{RL,RL''} p_{RL''} h_{R'L',RL''} + h_{RL,R'L''} p_{R'L''} h_{R'L',R'L''}) \quad (IV.23)$$

$$+ (1 - \delta_{RR'}) \sum_{R''L''} h_{RL,R''L''} p_{R''L''} h_{R'L',R''L''} (1 - \delta_{RR''}) \quad (IV.24)$$

The one centre terms are (eq. IV.21), the two centre on-site in (eq. IV.22) and intersite in (eq. IV.23). The three centre terms are in (eq. IV.24).

The simple operation of the spherical approximation to the potential comes at a price of reduced accuracy that is hopefully small for the systems of interest due their close packed structure. Before proceeding with the application part it is useful to find out how the ASA compares with the more accurate full potential (FP) methods[125, 126, 127]. The cohesive energies of the different lattices will be calculated with FP-LMTO as implemented in the NFP code[125] and FP-LAPW as implemented in the Elk code[128]. FP programs do not assume spherically symmetric potential in the muffin-tin spheres and allow it to vary in the interstitial space too. The basis functions of FP-LMTO are similar to the LMTO-ASA ones but the Hankel functions are "smoothed"[129] by convoluting them with Gaussian functions. The FP-LAPW uses an augmented plane wave basis. Both programs handle semi-core states as local orbitals. The MT spheres in the FP methods are smaller and do not overlap as in ASA.

There are four competing lattices with the Ti₃Al stoichiometry: D0₁₉, L1₂, D0₂₂ and D0₂₄. Ideal geometries will be assumed to avoid error from overlapping spheres in ASA. The nearest neighbour distance is 2.89 Å. It was chosen to be the one experimentally observed in D0₁₉, the only experimentally observable phase. The MT radii for both atom types was 2.0 and 2.5 bohrs for FP-LAPW and FP-LMTO, respectively.

The k-point meshes are approximately commensurate with about 12 points per reciprocal unit lattice vector length. The FP-LMTO calculation utilises double basis set. The primary includes s, p, and d orbitals and the secondary only s and p on the Al atoms and only d on the Ti atoms. The 3p orbital on Ti is included as local orbital in both FP calculations. These semi-core orbitals can safely be retained in the core in the ASA due to the larger sphere radii employed.

	FP-LAPW		FP-LMTO	
	PW92/CA	vBH	CA	vBH
D0 ₁₉	-13.5	-10.3	-9.5	-9.7
D0 ₂₄	-2.2	-0.2	-1.7	-1.8
D0 ₂₂	20.9	22.3	23.8	23.7

Table IV.1: Cohesive energy in meV/atom with respect to the L1₂ structure. Full potential LDA calculations with different exchange-correlation functionals.

The FP-LMTO and FP-LAPW results are close and the cohesive energy differences between the structures is quite small, only a few meV per atom. Other ab-initio cohesive energy calculations[130, 54] agree with the calculations. The small difference between the phases has led to attempts to stabilise the L1₂ phase by doping with scandium[131].

IV.2.1 Structural Energy Difference and RS-LMTO-ASA

The structural energy difference theorem [132, 133] has to be used in order to use ASA to compare the stability of the phases. A self-consistent potential is prepared from a chosen crystal structure. A potential for each of the other competing structure is then assembled from the self-consistent atomic potential by rigidly moving the spheres. The band energy is evaluated in this potential without further modifying it by making any self-consistency steps. This is the frozen potential method illustrated in [134]. To be able to assemble unambiguous potentials it is preferable to choose a starting cell which does not have symmetrically nonequivalent positions of the same atom type. For example, the suitable choices for Ti₃Al are L1₂ or D0₁₉, but not D0₂₂ or D0₂₄.

The energy difference between two structures can be expressed as

$$\Delta E = \Delta E_{\text{band}} + \Delta E(\Delta \rho) + \sum_{R,R'} q_2(R) q_2(R') \left(\frac{1}{(R - R')_2} - \frac{1}{(R - R')_1} \right) \quad (\text{IV.25})$$

The first term is the difference between the bandstructure energies. It contains the difference in covalent bonding. The second term represents the energy changes due to charge redistribution, and the third term is the Madelung electrostatic energy for charge obtained from the nonselfconsistent calculation (structure index 2).

If the charge transfer is small the second term is dispensable. The radial distribution functions for the four lattices (fig. IV.1) are quite similar and the Madelung difference is expected to be negligible. Within these approximations the band energies must represent the cohesive energy differences well. This will be confirmed by the comparison to the FP calculations.

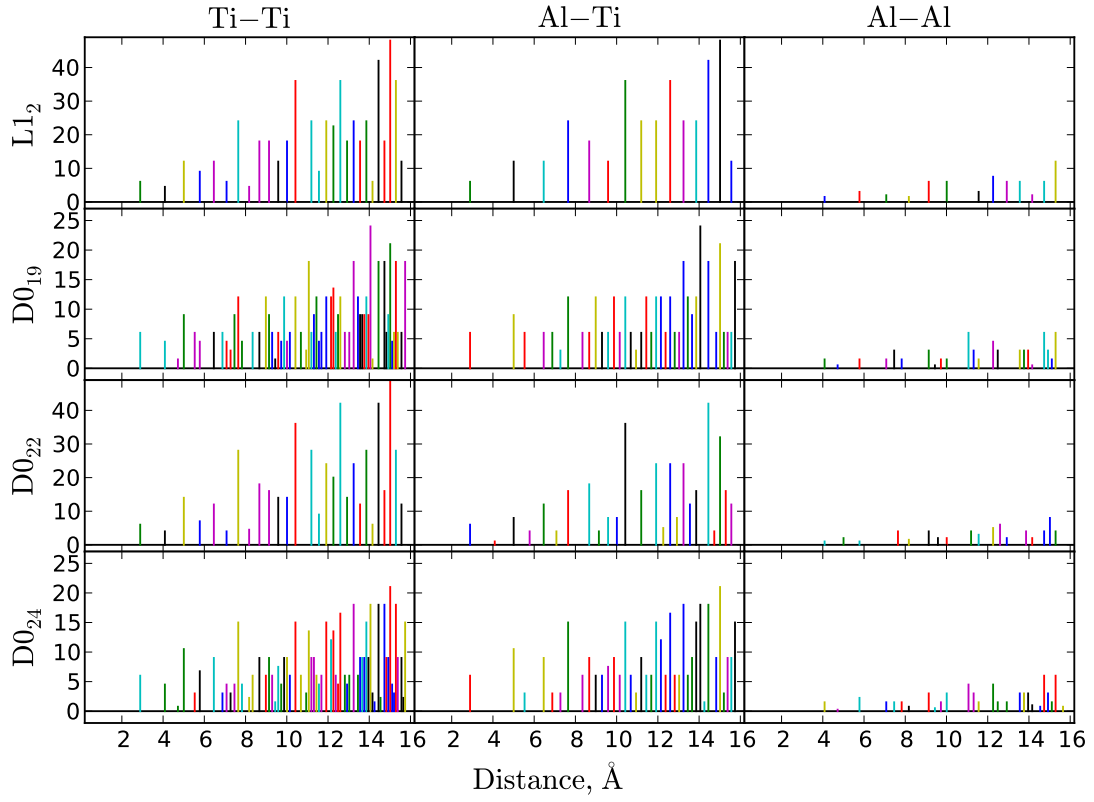


Figure IV.1: Average radial distribution of the atoms sorted by bond type.

Table (tbl. IV.2) shows the results of applying the ASA structural energy difference to the competing structures of Ti_3Al . Two choices of r_{cut} are made, restricting the range of the LMTO-ASA Hamiltonian matrix elements. Results are shown with and without combined correction (CC) and with and without the inclusion of three-centre terms in the Hamiltonian; these are omitted in the calculation by setting the third order parameter p^γ to zero.

The combined correction is a device within the ASA which allows the tails of the LMTOs to be augmented formally up to $\ell = \infty$ while at the same time taking some account of the error introduced from the overlapping spheres.

The competing structures are all close packed providing maxi-

LMTO-ASA	with CC		no CC	
r_{cut}	3.1Å	4.4Å	3.1Å	4.4Å
D0 ₁₉	-10.4	-15.3	-5.5	-14.9
D0 ₂₄	-2.9	-6.6	0.7	-5.1
D0 ₂₂	21.5	22.2	20.8	19.9
$p^\gamma = 0 :$				
D0 ₁₉	-10.8	-15.5	-6.3	-15.6
D0 ₂₄	-3.2	-6.8	0.1	-5.6
D0 ₂₂	21.3	21.7	20.0	19.1

Table IV.2: Cohesive energies in meV/atom with respect to the L1₂ structure at different cutoff radii. Frozen potential LMTO-ASA calculations with combined correction and 3 centre terms included or excluded($p^\gamma = 0$). The D0₂₂ energies at $r_{cut}=4.4\text{\AA}$ contain a small electrostatic term.

mal sphere filling ratio and it is not surprising to see how well the ASA energy differences from (tbl. IV.2) match the full-potential results. The first and second neighbour shells are virtually the same as can be seen from the radial distribution functions (fig. IV.1). The only exception is the small fraction of Ti-Al and Al-Al second neighbours in D0₂₂. Only first neighbours enter the 3.1Å cutoff while 4.4Å also includes the second neighbours. Further neighbours are not included because the environment they create varies significantly amongst the structures as seen in (fig. IV.1). The unknown part of the energy due to the neglect of the long ranged interactions is not included to keep the second and third terms in (eq. IV.25) small. These interactions are handled in TB model by a classical potential for practical performance reasons anyway. The combined correction is somewhat more important for the first neighbours only calculations leading to pretty good match with the FP energies. The difference between D0₂₄ and L1₂ is very small according to both FP methods and ASA+CC. Switching off CC swaps their places but it is still negligibly small. Adding the second neighbours increases the difference more than twice and stays consistent after switching off the CC. Performing the same calculations without the small p^γ parameter does change the results appreciably but it

further simplifies the model and is a welcome approximation. The combined correction is a complication inappropriate for a simple TB model. The second choice: whether to include the second nearest neighbours or not is not easy to decide. On the positive side the energy differences are closer to the FP ones except $D_{024} - L_{12}$ which has the correct sign but the wrong magnitude. On the other hand second nearest neighbour hoppings are severely screened in a close packed structure so one can expect severe discontinuity in the hopping integrals which may have to be addressed by introducing environment dependence.

The splitting of the contributions in the ASA Hamiltonian described in (IV.21)-(IV.24) was applied for the competing structures. The three-centre terms of (eq. IV.24) were additionally separated into two groups. The first group is composed of atoms R' which are within the reach of the central atom R , that is, the structure constant block $h_{RL,R'L'}$ is nonzero. The second group is composed of terms in which the R and R' atoms are sufficiently far apart that $h_{RL,R'L'} = 0$ and are only being linked through the R'' atom via structure constants $h_{RL,R''L''}$ and $h_{R'L',R''L''}$, that is to say, by double hops. This dissection was made for first and second neighbour models. The results are shown in tables (tbl. IV.3) and (tbl. IV.4). The first order approximations include only the first two terms in (IV.20) and thereby correspond to orthogonal Hamiltonians.

The last column in the tables contains the energy differences calculated with unmodified ASA Hamiltonian constructed after the structure constants are Bloch transformed, which is the normal modus operandi. In the other columns the matrices are assembled before Bloch transformation. Adding extra two-centre terms to the first order model evidently leads to significant reordering in the stability. The close three-centre terms partially cancel the jump in the differences and the distant three-centre contributions almost completely negate the effect. Indeed the results in (tbl. IV.3) and

ref: L1 ₂	1 st order 1c + 2c	2 nd order, 1c +				ref. ASA	
		2c		3c			
		inter	on-site	near	far		
D0 ₁₉	-1.1	7.3	11.6	25.8	-5.5	-5.5	
D0 ₂₄	3.5	-5.5	-3.5	14.1	0.7	0.7	
D0 ₂₂	14.0	32.3	22.0	21.7	20.8	20.8	
$p^\gamma = 0 :$							
D0 ₁₉	-1.8	2.4	6.4	17.5	-6.3	-6.3	
D0 ₂₄	3.1	-8.2	-5.9	10.0	0.1	0.1	
D0 ₂₂	14.4	35.8	23.8	21.6	20.0	20.0	

Table IV.3: TB-ASA structural energy differences dissected. No CC, $r_c = 3.1\text{\AA}$

ref: L1 ₂	1 st order 1c + 2c	2 nd order, 1c +				ref. ASA	
		2c		3c			
		inter	on-site	near	far		
D0 ₁₉	-11.1	13.7	14.0	4.9	-14.9	-14.9	
D0 ₂₄	-2.6	-1.0	-1.7	4.9	-5.1	-5.1	
D0 ₂₂	12.7	36.4	23.4	27.8	19.9	19.9	
$p^\gamma = 0 :$							
D0 ₁₉	-11.6	8.8	9.3	5.3	-15.7	-15.7	
D0 ₂₄	-3.0	-3.3	-3.8	5.4	-5.6	-5.6	
D0 ₂₂	13.2	39.8	25.5	29.4	19.1	19.1	

Table IV.4: TB-ASA structural energy differences dissected. No CC, $r_c = 4.4\text{\AA}$

(tbl. IV.4) from the first order two-centre orthogonal model are very close to the ones from the second order 3-centre non orthogonal model. The first order second nearest neighbour model (tbl. IV.4) does look like the best so far and it may even be unreasonable to ask for more but in the context of BOP having shorter, nearest neighbours only hoppings. Therefore this model is very attractive from practical point of view, since far reaching hopping integrals will slow down the computations of the recursion coefficients significantly. Since the nearest neighbour model is not much worse it may be more beneficial to keep it and test it further. If the final

nearest neighbour TB model produces similar differences as ASA and keeps the relative order with this exception only then it may be tuned additionally or the longer ranged one may be revisited.

Since the orthogonal first order and nonorthogonal second order models show such small differences it is interesting to compare the band structures and see what is the effect of the overlap on the system.

Figure (fig. IV.2) shows the LMTO-ASA energy bands corresponding to the first and second order Hamiltonians, with and without overlap. The first order orthogonal model band structure is remarkably similar to the second order. Only the lower and higher energy bands are distorted. The low lying bands are primarily composed of s states as shown in (fig. IV.5a) and (fig. IV.5b). These states are also most influenced by the overlap in the second order comparisons.

IV.2.2 Less-Than-Minimal Basis

One of the requirements for our TB/BOP model is to reduce the basis to the minimum necessary for satisfactory description of the properties of interest. In the preceding comparisons between first and second order LMTO Hamiltonians, with and without overlap, an attempt may be made to remove the s orbitals from the model. Since there is no interstitial space in ASA the band energy may be easily projected on the atoms and orbitals. These projections may be used to set expectations for the contributions and dispensability of the different orbitals. Of course removing orbitals will change bonding in more complex ways so expectations may not or will not match reality.

According to results in (tbl. IV.5) it may be speculated that ne-

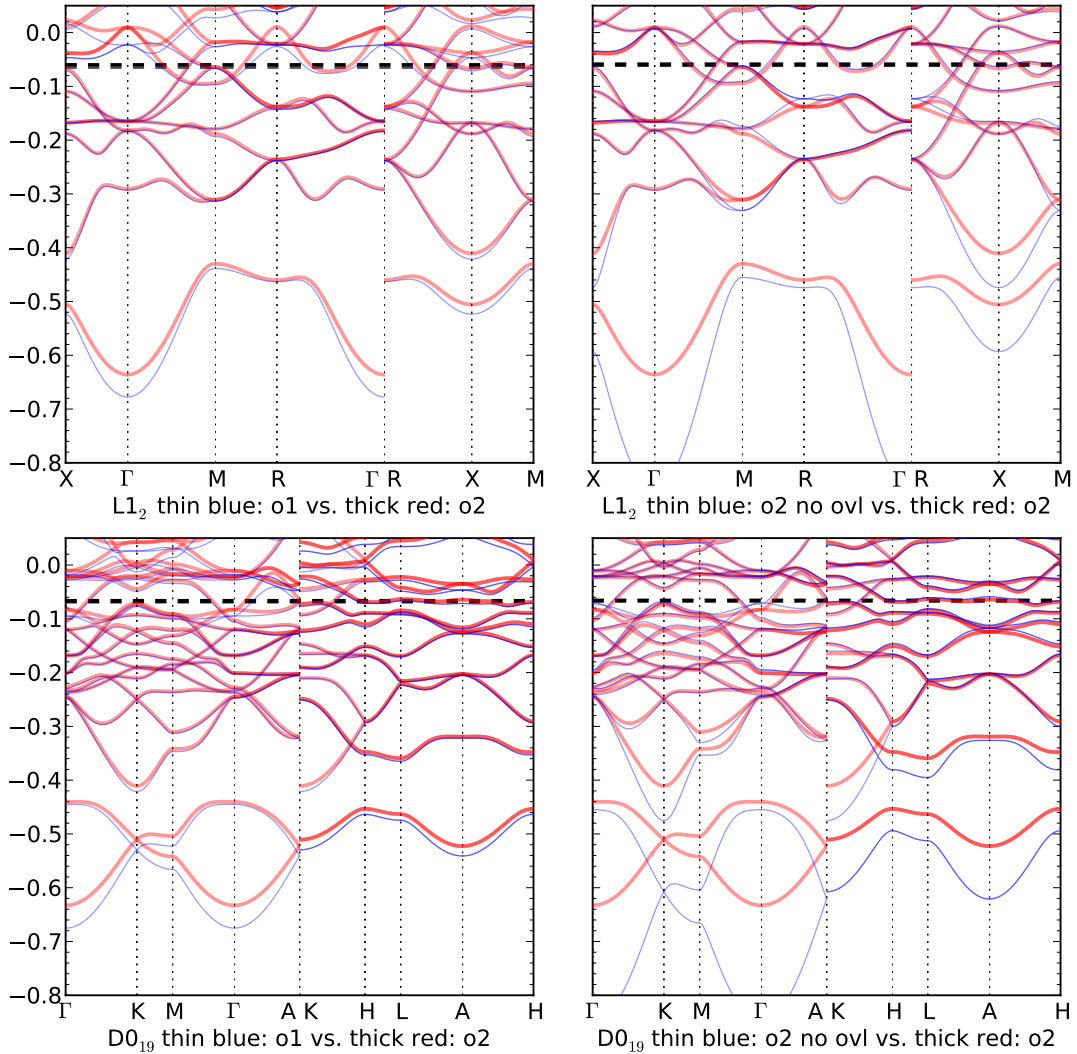


Figure IV.2: L1₂ and D0₁₉ Bandstructure comparisons: first order vs second order vs second order no overlap.

E _{band} ^{proj}	Al				Ti				Ti ₃ Al
	s	p	d	Al	s	p	d	3Ti	
D0 ₁₉	9.27	15.24	-8.11	16.39	-0.59	-22.77	1.73	-21.63	-5.24
D0 ₂₂	-7.16	-11.28	-2.93	-21.36	6.28	2.95	31.98	41.20	19.84

Table IV.5: Band energy contributions to the energy differences in Ti₃Al with respect to L1₂, projected on the orbitals according to ASA. The total is in units of meV/atom.

glecting s and d orbitals from Al together with the s orbital from Ti may not impact the structural energy difference considerably because they approximately cancel out. The significant part of the band energy difference is projected on the p orbitals on Al and p and d on the Ti atoms. The D₀₂₄ band energy is not included due to the rather approximate nature of this analysis and the small difference between the energies of the D₀₂₄ and L₁₀ lattices.

Similar projections of the electron density on the orbitals (tbl. IV.6) show that the charges accumulated are quite uniform across the different lattices.

N	Al				Ti				Ti ₃ Al
	s	p	d	Al	s	p	d	Ti	
D ₀ ₁₉	1.17	1.74	0.32	3.23	0.64	0.72	2.57	3.92	15.00
L ₁ ₂	1.17	1.78	0.30	3.24	0.64	0.70	2.57	3.92	15.00
D ₀ ₂₂	1.17	1.78	0.30	3.25	0.64	0.72	2.56	3.92	15.00

Table IV.6: Number of electrons accumulated in the orbitals in a few phases of Ti₃Al. The total is for 4 atom cluster.

A qualitative evaluation of the significance of the different orbitals may be acquired from the partial DOS plots for the four lattices (fig. IV.3) and the magnified region of the D₀₁₉ DOS below the Fermi energy (fig. IV.4).

The first observation is that all of the DOSs have a wide gap between approximately -0.45 and -0.4 Ry with a very steep left slope and a slower rise on the right side. The small isles on the left side start at approximately the same energy -0.63 Ry, have approximately the same area and are all dominated by the Al s orbital shown in red. Removing them by dropping the Al s orbital should not impact significantly the cohesive energies.

The second relatively common feature is the evenly elevated region between -0.39 and -0.21 Ry. The presence of Al s character is negligibly small here. The same applies to Al d plotted in light

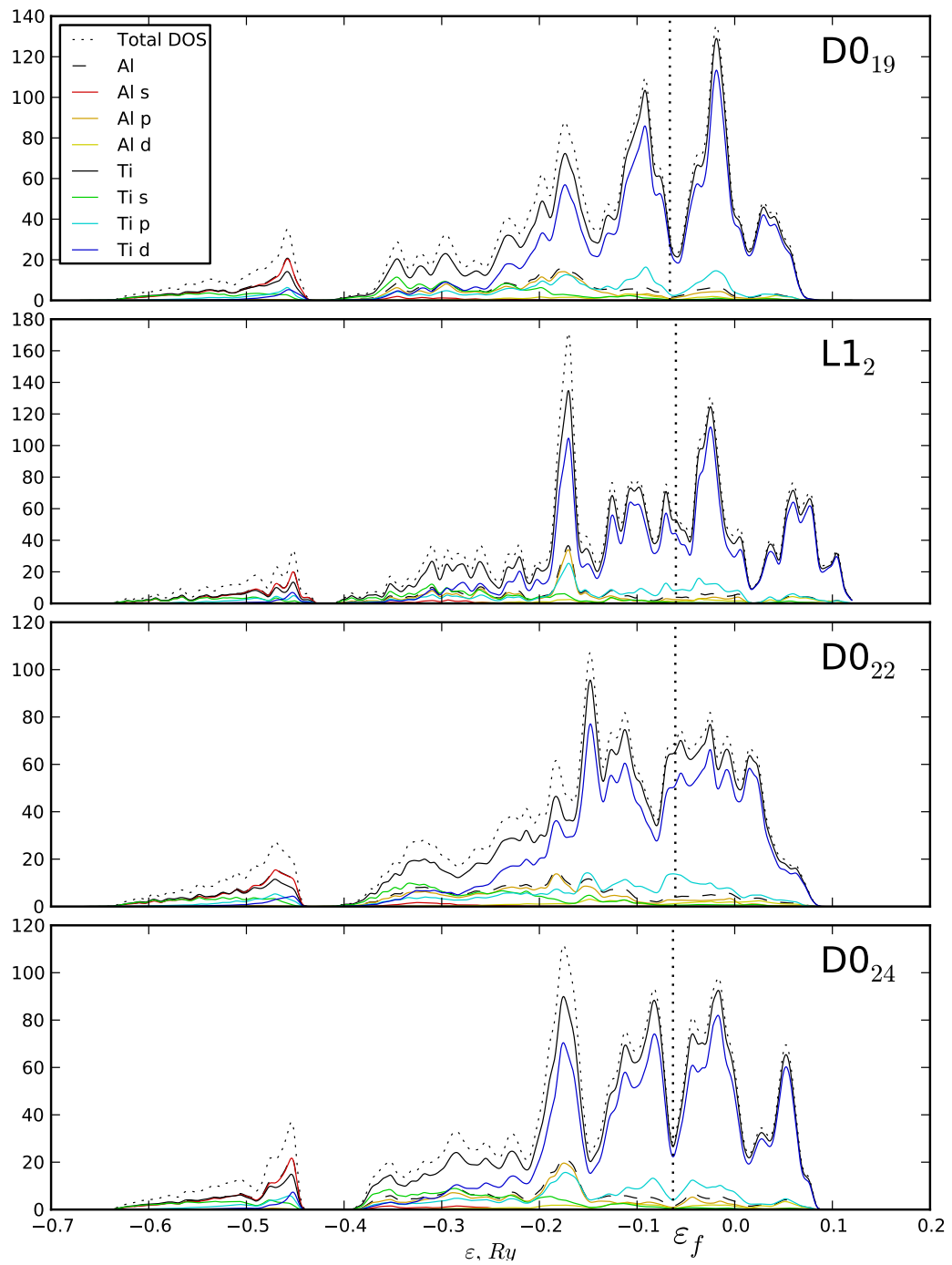


Figure IV.3: Comparison between the densities of states distributions in the compounds with stoichiometry Ti_3Al .

yellow. The rest of the orbitals have approximately equally small shares while Ti s and d prevail. The position, shape, area, and orbital projections of these ridges are quite similar across the different lattices so losing similar parts or the whole of it as a result of the removal of Ti s may not have large impact on the resultant band energies and, consequently, the cohesive energies.

The third part of the DOSs: the region above -0.2 Ry is occupied by large peaks and bulges where differences between the lattices are most pronounced. The Fermi energy of the hexagonal based lattices D₀₁₉ and D₀₂₄ falls in steep gaps while in the tetragonal, fcc based D₀₂₂ and L₁₀ it lies within peaks. The hexagonal lattices have more pronounced large peaks while the tetragonal lattices contain an assembly of peaks merged together to form continuous ridges. In all four lattices the d orbital on Ti is dominating the landscape together with the p from Al and Ti, painted in orange and cyan respectively.

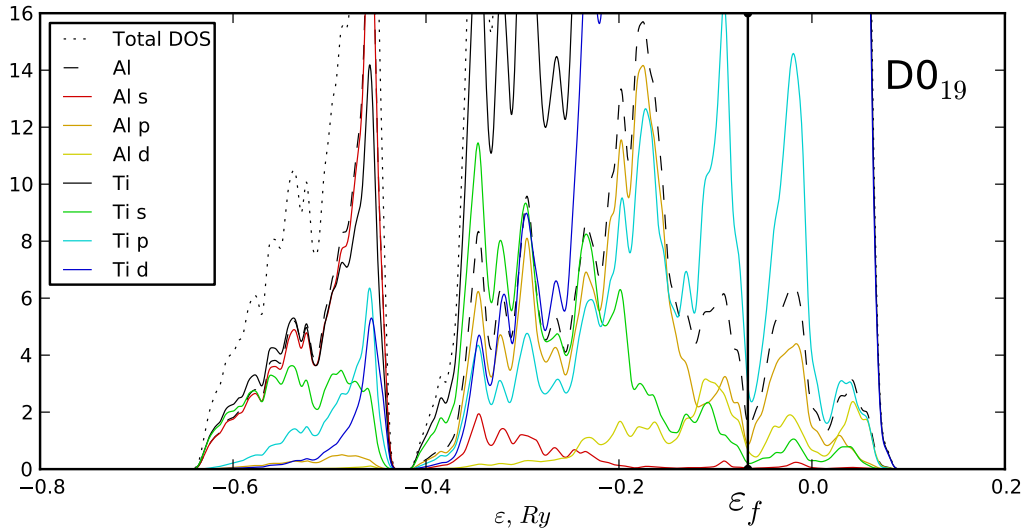


Figure IV.4: D₀₁₉ projected DOS. Magnified.

The DOS analysis confirms that the character defining orbitals are p on Al and p and d on Ti. To complete the analysis of the electronic structure the energy bands of D₀₁₉ are plotted in (fig. IV.5)

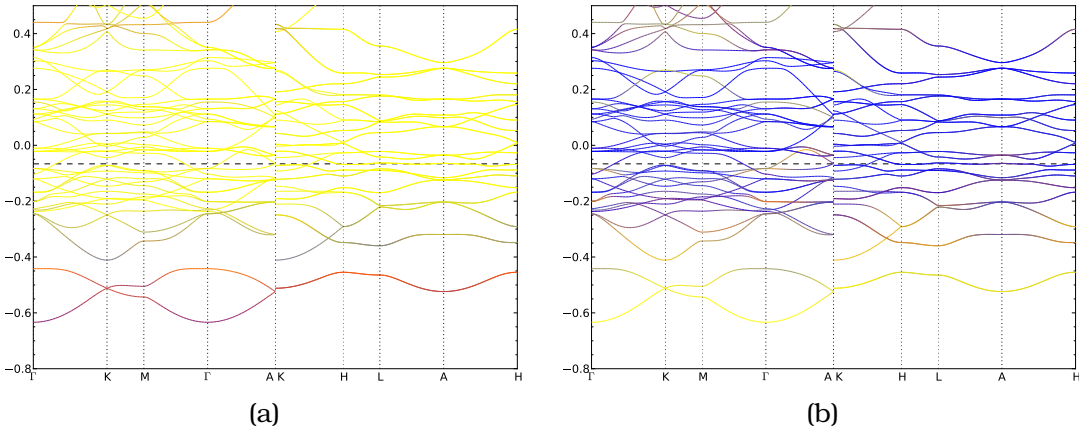


Figure IV.5: ASA band structure of D₀₁₉ with band character highlighting. Red and blue colours are used to highlight two groups of orbitals and yellow is used for the rest. a) Al s and Ti s are highlighted. b) Al p and Ti d are highlighted. Due to mixing with other colours the highlight may appear as neighbouring colour.

with varying colour representing the projection on two selected orbitals, Al s and Ti s in a), and Al p and Ti d in b), against the rest. Al d is negligible and is not worth distinguishing. The Ti p is spread across the whole graph as one can see from the DOS plot too and is not highlighted for reasons of sanity. The first graph (fig. IV.5a) shows the relative localisation and isolation of the Al s and Ti s orbitals. The gap separating their band from the rest is also noticeable. Another visible feature is the small semi gap starting from the Fermi energy.

The second graph (fig. IV.5b) highlights the major bonding orbitals d from Ti and p from Al in blue and red colours respectively, against yellow for all other orbitals. The Al p influence can be seen transforming the Ti d blue to magenta at places and changing the yellow background into orange.

IV.2.3 Moments Horizon

A TB model is prerequisite for construction of a BOP model. In BOP, the electronic structure is approximated up to certain moment of the DOS. For this purpose it is necessary to test how many moments may be required for an accurate reproduction of the DOS so that the structural energy differences are captured. The technique for calculating recursion coefficients from moments of a distribution developed in the previous chapter is used.

The total DOSs of the competing structures are taken as input. Their moments are calculated with a very high precision. From m moments $m/2 - 1$ recursion coefficient pairs are obtained. The DOS is then reconstructed from these recursion coefficients in fashion similar to that in the BOP method. The advantage of this formal reconstruction is that very high number of moments is achievable without any precision loss and that numerical errors are decoupled from all other effects specific to TB and BOP. The Beer-Pettifor terminator[135] is chosen as in the BOP calculations. The details of the DOS illustrated in (fig. IV.6) are demonstrated to be gradually developed to near perfect match with the addition of more moments.

Plotting the band energies of the competing structures calculated from the integration of the DOS reconstructions at different moments in (fig. IV.6) shows oscillatory behaviour which converges in the limit of a large number of moments. This is not very surprising considering the diverse and complex structure of the DOSs of the Ti_3Al phases.

The behaviour of the band energy with respect to the band filling from ASA D_{019} DOS is plotted and compared with reconstructions using 15 and 21 moments, the two lowest numbers of moments in (fig. IV.8) having correct stability order. The lines reconstructed up to the 21st moment (the right graph) closely follow the ASA lines within a constant shift.

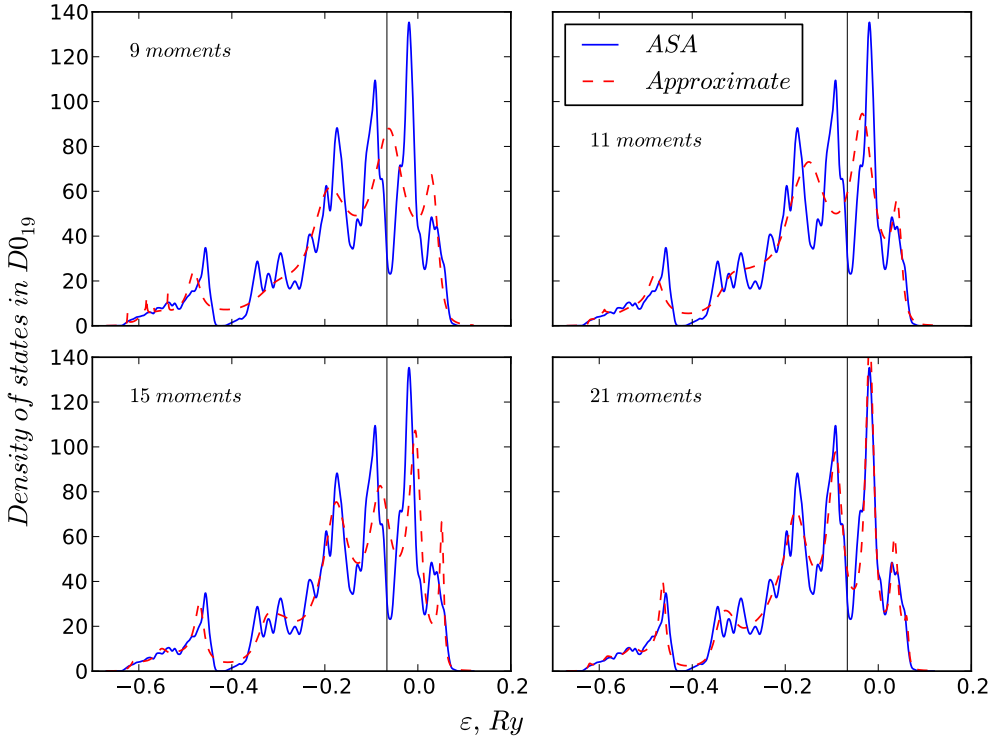


Figure IV.6: Reconstruction of D_{019} DOS with 9, 11, 15 and 21 moments.

The practically reachable number of moments in numerical BOPs with double precision arithmetic does not significantly exceed 15. Calculations are usually performed with 9 or 11 moments (4-5 recursion levels) for performance and stability reasons. The choice of a terminator then becomes very important. The recursion coefficients are hardly convergent even at levels as high as 200 (401m)(fig. IV.9).

The behaviour of the recursion coefficients in the different phases is largely similar with the exception of D_{024} , in which they have significantly larger amplitude of oscillation. It has a prominent band gap and the coefficients attain stable oscillatory trajectories instead. The main differences are in the first 20-30 levels. They are still well beyond the practical limits and thus are approximated by a constant in the Beer-Pettifor square root terminator or by a function in more advanced schemes[104]. The influence of the ter-

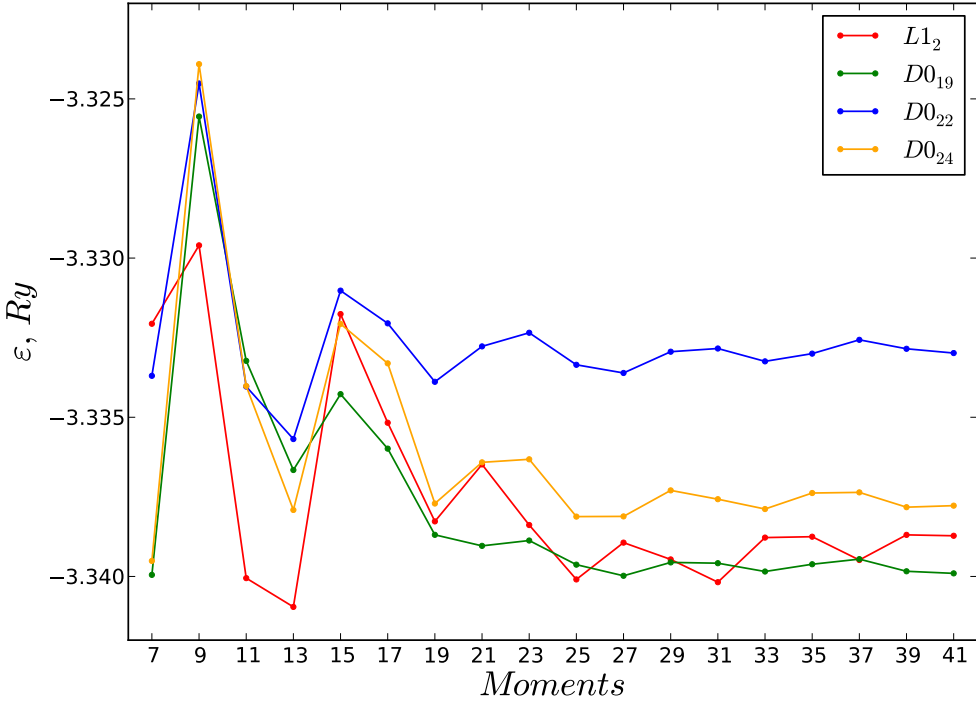


Figure IV.7: Band energies of $L1_2$, $D0_{19}$, $D0_{22}$ and $D0_{24}$ calculated by DOS integration reconstructed with up to the 41st moment.

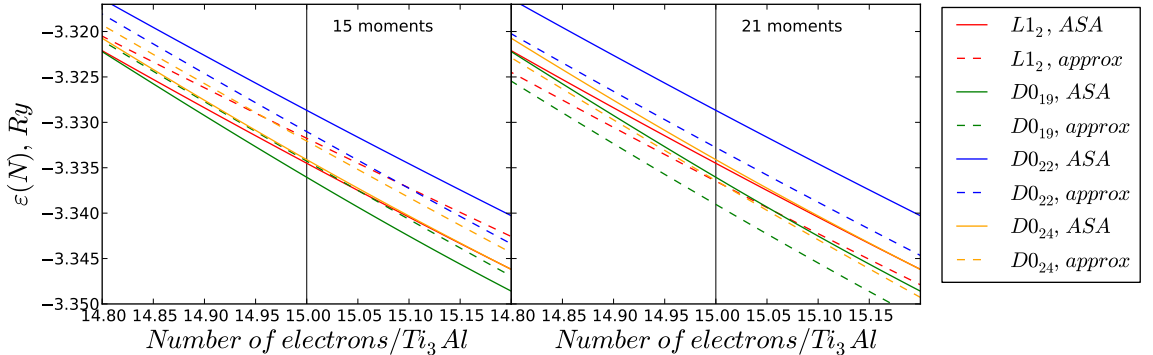


Figure IV.8: Band energy with respect to band filling, reconstructed up to 15 and 21 moments.

minator on the continued fraction decreases exponentially with the number of recursion pairs included exactly[136]. 4-5 levels however do not provide enough of the long term behaviour to make it

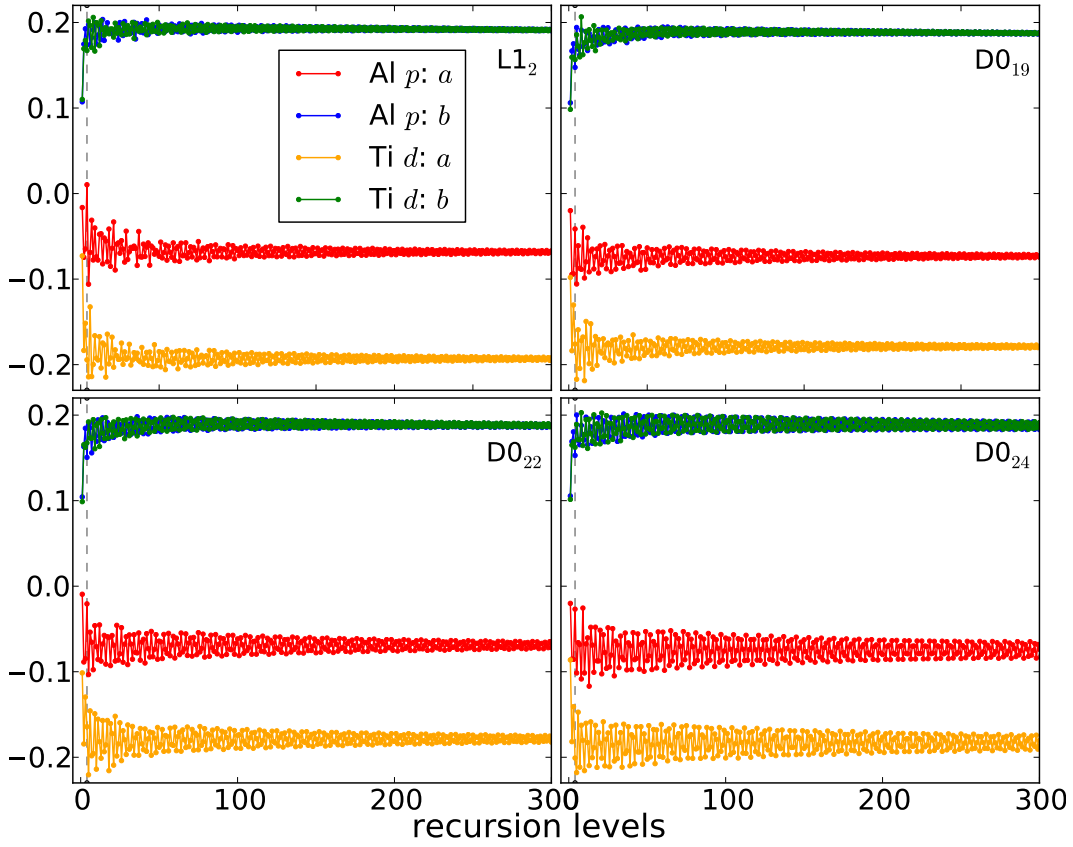


Figure IV.9: Recursion coefficients up to the 300th level. The dashed line marks the 4-th level.

possible to construct a good functional terminator. Within these limitation the Beer-Pettifor was found to be most suitable.

IV.2.4 TB-ASA fundamental integrals

As already discussed above, two-centre Hamiltonians can be obtained from the ASA, and the fundamental bond hopping integrals extracted to make a parametrised TB model. One approach is to use the self-consistent potential parameters in a chosen representation and the appropriately screened real space structure constants to construct a real space Hamiltonian matrix and overlap matrices according to the equations (IV.7)-(IV.14), (IV.20) and

(IV.19). Alternatively one may simply read the Hamiltonian and overlap matrices in reciprocal space and inverse Bloch transform them to real space using appropriate number of \vec{k} -points. The two approaches should provide identical results within a small numerical error. Once a real space Hamiltonian is obtained each small fragment of size $(\ell_R^{\max} + 1) \times (\ell_{R'}^{\max} + 1)$ referring to an atom pair is rotated to align the $R - R'$ line along the z axis. Then the independent two-centre hopping integrals can be picked up from the appropriate cells in (fig. IV.10). A more rudimentary procedure for obtaining the fundamental hopping integrals by rotation is to split the fragments into rectangular or trapezoidal subfragments made up of the different combinations of $\ell\ell'$, for example, sp , pp , pd , dd , and the trivial ss . A system of linear equations is written for each subfragment using the Slater-Koster table where the unknown variables are the particular σ , π , and δ hopping integrals. The systems of equations are generally overcomplete and the solution is ambiguous because different sets of equations lead to different answers. The ambiguity comes mainly from fact that the structure constants are not fully representable by spherical harmonics after the screening because they now contains contributions from other other sites and are thus slightly environmentally dependent[120].

The extraction procedure described was applied to the different Ti_3Al crystal structures, and to $L1_0$ at different volumes and the results plotted in (fig. IV.11). It is encouraging to see the different points of the same bond type and bond integral type, obtained from different structures falling so closely together that marking them separately in the graph is inconvenient. This points to a relatively small environment dependence of the hopping integrals. It should not be forgotten though that tiny differences do matter in the context of the order of stability.

The points from each structure and bond type were fitted with power law curves $v_0(r_0/r)^n$ in which v_0 is the hopping integral at

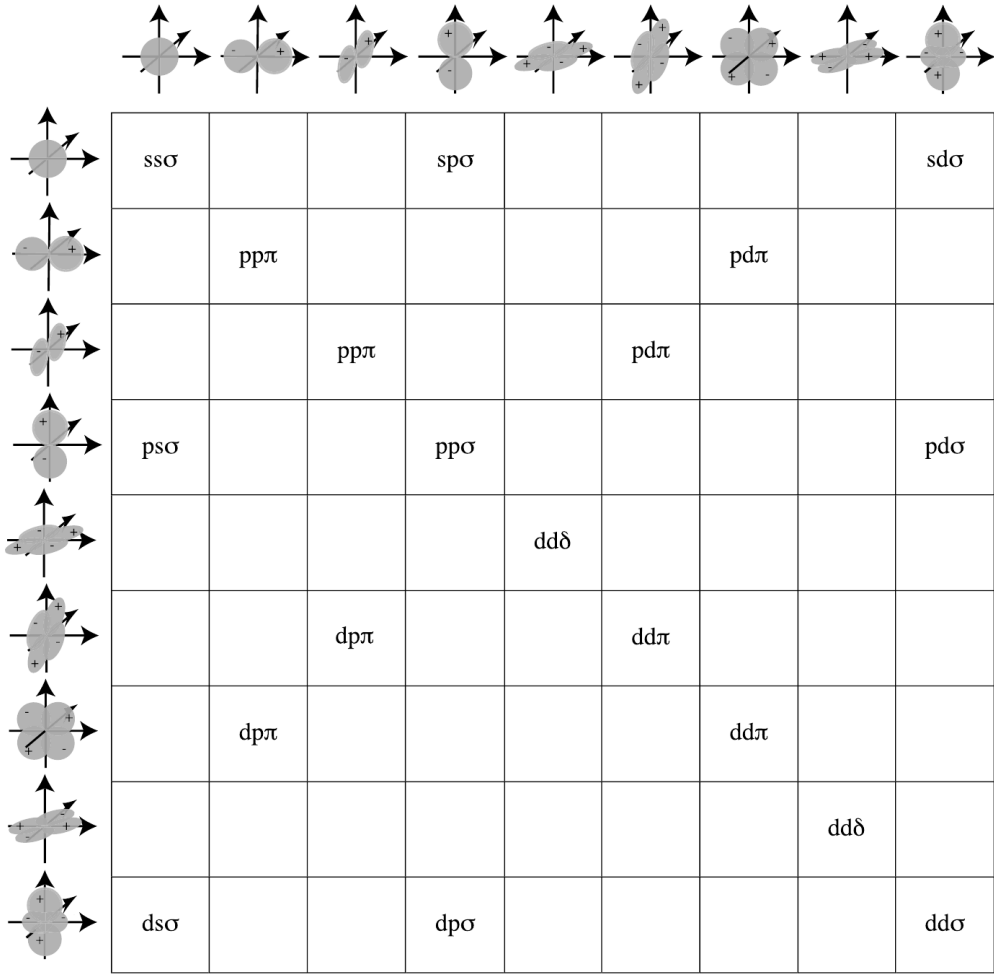


Figure IV.10: The independent fundamental hopping integrals positioned in a z-oriented pair fragment of a two-centre Hamiltonian.[118]

equilibrium distance r_0 set to 2.89 Å (5.46 Bohr radii). The averaged v_0 and n parameters are tabulated in (tbl. IV.7) together with the parameters obtained from D0₁₉, L1₂ and L1₀ for comparison.

The on-site elements similarly do not deviate too much but there is a notable difference in the crystal field splitting among the d orbitals.

The different parameter sets from (tbl. IV.7) and (tbl. IV.8) re-

$v_0(r_0/r)^n$ $\times 10 \text{mRy}$	Ti - Ti		Ti - Al		Al - Ti		Al - Al	
	v_0	n	v_0	n	v_0	n	v_0	n
D0 ₁₉	$ss\sigma$	-6.09	2.32	-6.38	2.81	-6.38	2.81	---
	$sp\sigma$	7.65	2.03	9.43	2.61	7.93	2.52	---
	$pp\sigma$	9.86	1.74	12.04	2.32	12.04	2.32	---
	$pp\pi$	-1.35	1.74	-1.64	2.32	-1.64	2.32	---
	$sd\sigma$	-6.00	3.13	-6.91	3.02	-6.45	3.63	---
	$pd\sigma$	-7.56	2.84	-8.64	2.73	-9.58	3.43	---
	$pd\pi$	1.87	2.84	2.14	2.73	2.37	3.43	---
	$dd\sigma$	-6.36	3.94	-7.53	3.83	-7.53	3.83	---
	$dd\pi$	2.85	3.94	3.37	3.83	3.37	3.83	---
	$dd\delta$	-0.22	3.94	-0.26	3.83	-0.26	3.83	---
L1 ₂	$ss\sigma$	-6.11	2.32	-6.39	2.81	-6.39	2.81	---
	$sp\sigma$	7.65	2.02	9.46	2.62	7.92	2.51	---
	$pp\sigma$	9.69	1.72	11.86	2.32	11.86	2.32	---
	$pp\pi$	-1.20	1.72	-1.47	2.32	-1.47	2.32	---
	$sd\sigma$	-5.86	3.14	-6.75	3.03	-6.30	3.63	---
	$pd\sigma$	-7.89	2.84	-9.00	2.73	-10.02	3.43	---
	$pd\pi$	1.90	2.84	2.16	2.73	2.41	3.43	---
	$dd\sigma$	-6.36	3.95	-7.52	3.85	-7.52	3.85	---
	$dd\pi$	2.78	3.95	3.29	3.85	3.29	3.85	---
	$dd\delta$	-0.19	3.95	-0.22	3.85	-0.22	3.85	---
L1 ₀	$ss\sigma$	-5.83	2.12	-6.19	2.65	-6.19	2.65	-6.29 3.18
	$sp\sigma$	7.22	1.84	9.10	2.47	7.60	2.37	9.23 3.01
	$pp\sigma$	9.05	1.56	11.30	2.19	11.30	2.19	13.71 2.83
	$pp\pi$	-1.12	1.56	-1.40	2.19	-1.40	2.19	-1.70 2.83
	$sd\sigma$	-5.97	2.99	-6.23	2.92	-6.08	3.52	-6.80 3.46
	$pd\sigma$	-7.55	2.71	-8.44	2.65	-9.88	3.34	-10.18 3.28
	$pd\pi$	1.75	2.71	2.06	2.65	2.41	3.34	2.37 3.28
	$dd\sigma$	-6.43	3.86	-7.18	3.79	-7.18	3.79	-7.73 3.73
	$dd\pi$	2.69	3.86	3.21	3.79	3.21	3.79	3.23 3.73
	$dd\delta$	-0.27	3.86	-0.17	3.79	-0.17	3.79	-0.32 3.73
D0 ₁₉ , L1 ₂ ... and L1 ₀	$ss\sigma$	-6.07	2.30	-6.37	2.80	-6.37	2.80	-6.29 3.18
	$sp\sigma$	7.62	2.01	9.41	2.60	7.91	2.50	9.23 3.01
	$pp\sigma$	9.73	1.71	11.91	2.31	11.91	2.31	13.71 2.83
	$pp\pi$	-1.26	1.71	-1.54	2.31	-1.54	2.31	-1.70 2.83
	$sd\sigma$	-5.90	3.12	-6.80	3.02	-6.37	3.62	-6.80 3.46
	$pd\sigma$	-7.74	2.83	-8.79	2.72	-9.80	3.43	-10.18 3.28
	$pd\pi$	1.88	2.83	2.14	2.72	2.38	3.43	2.37 3.28
	$dd\sigma$	-6.35	3.95	-7.51	3.84	-7.51	3.84	-7.73 3.73
	$dd\pi$	2.80	3.95	3.31	3.84	3.31	3.84	3.23 3.73
	$dd\delta$	-0.19	3.95	-0.24	3.84	-0.24	3.84	-0.32 3.73

Table IV.7: TB hopping integrals scaling parameters obtained from ASA D0₁₉, L1₂ and L1₀. The average section also includes D0₂₂ and D0₂₄ as plotted in (fig. IV.11).

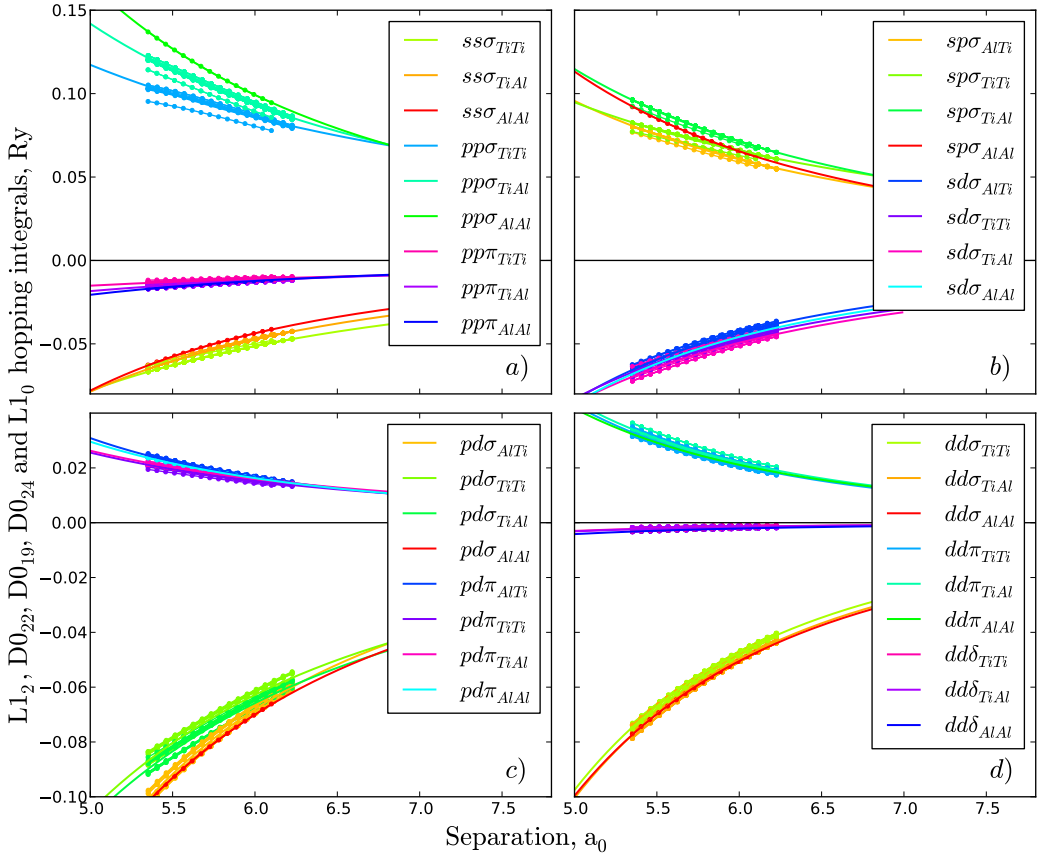


Figure IV.11: Hopping integrals from different cells as a function of distance, with power law fitted averages $v_0(r_0/r)^n$

sult in similar structural energy differences (tbl. IV.9) which are unfortunately even qualitatively very far from the correct ASA or FP ordering. One source of error may be the ambiguous solution of the the overcomplete systems of equations during the parameter extraction due to the screening of the structure constants. Another source may be the small environment dependence and the crystal field splitting. The screened structure constants have on-site off diagonal elements which are not taken into account in the TB parametrisation. Since the difference between the TB and the first order ASA energies even for the nearest neighbour only model (tbl. IV.3) are so large it looks highly unlikely that the inclusion of

$\varepsilon \times 100\text{mRy}$		s	p	d_{xy}	d_{yz}	d_{zx}	$d_{x^2-y^2}$	d_{3z^2-1}
L1 ₀	Al	-1.669	2.907	5.186	5.186	5.026	5.186	5.026
L1 ₂	Al	-1.869	2.696	5.136	5.136	4.979	5.136	4.979
D0 ₁₉	Al	-1.866	2.680	5.120	5.068	5.173	5.068	5.120
D0 ₂₄	Al	-1.851	2.698	5.115	5.062	5.167	5.062	5.115
	Al2	-1.888	2.675	5.096	5.043	5.149	5.043	5.096
D0 ₂₂	Al	-1.901	2.663	5.134	5.134	4.976	5.134	4.976
L1 ₀	Ti	2.331	4.369	1.242	1.242	1.086	1.242	1.086
L1 ₂	Ti	2.160	4.410	0.987	0.987	0.842	0.987	0.842
D0 ₁₉	Ti	2.137	4.416	0.934	0.885	0.982	0.885	0.934
D0 ₂₄	Ti	2.144	4.404	0.950	0.901	0.999	0.901	0.950
	Ti2	2.152	4.425	0.933	0.884	0.982	0.884	0.933
D0 ₂₂	Ti	2.159	4.476	0.941	0.941	0.797	0.941	0.797
D0 ₂₄	Ti2	2.145	4.446	0.996	0.996	0.851	0.996	0.851

Table IV.8: On-Site energies.

pm. src.	D0 ₁₉	L1 ₂	L1 ₀	avr.
D0 ₁₉	56.9	62.3	65.6	59.7
D0 ₂₂	20.8	16.7	22.5	18.5
D0 ₂₄	37.9	41.9	41.9	40.0

Table IV.9: TB structural energy differences from ASA parameters (tbl. IV.7) in meV/atom.

second neighbours will have any noticeable influence.

The influence of the crystal field splitting may be investigated on ASA level in the first order model. If all off diagonal on-site matrix elements are zeroed and the diagonal elements referring to the d orbitals are averaged then the crystal field on-site splitting will effectively be removed. Combinations of averaging the d and removing the offdiagonal elements were tested (tbl. IV.10) and all of them are far from the unmodified first order ASA results (tbl. IV.3).

It is still interesting to see what effect the removal of crystal field splitting will have on the band structure. A graph similar to (fig. IV.2) was plotted in (fig. IV.12). The influence on the band structure is tiny and hard to see despite the detrimental effect it

	avr d no + offd	avr d	no offd
D0 ₁₉	12.3	31.3	-21.3
D0 ₂₂	11.4	35.1	-21.4
D0 ₂₄	18.3	18.3	14.4

Table IV.10: First order ASA structural energy differences in meV/atom without crystal field splitting.

has on the structural energy differences.

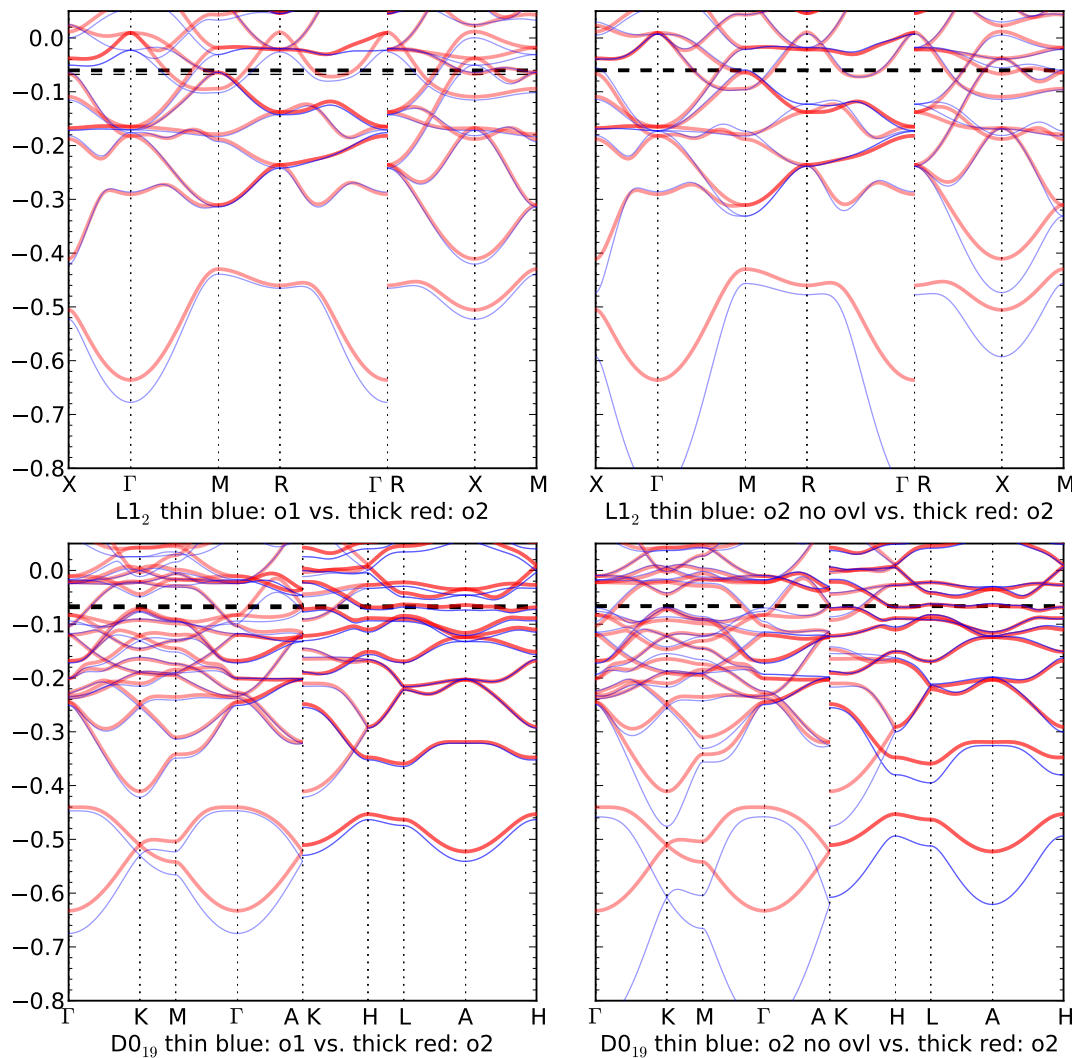


Figure IV.12: L1₂ and D0₁₉ Bandstructure comparisons: first order(o1) vs second order(o2) vs second order no overlap. No crystal field splitting

Extracting TB parameters from ASA with this approach has not resulted and is unlikely to result in practically useful model when the energies are very sensitive to small differences in the hopping integrals. It is still however an interesting exercise and the parameters obtained may be used as starting point for further refinement. For example a little adjustment may allow the bandstructure to be better matched. Further it is possible to not only fit to the bands but also the linear coefficient that make up a band character.

An alternative approach to that just described is to fit not the TB parameters but atomic-like radial wavefunctions to represent a predefined density, obtained from some DFT calculations[119]. After obtaining wavefunctions the matrix elements are calculated for z orientation of the bond and the fundamental hopping integrals selected. It is similar to the ASA in that LMTOs are also atomic like functions but unlike the ASA screened structure constants the angular and radial parts are kept separate and there is no error and ambiguity from the rotation. Unlike the first order ASA the arbitrary atomic orbitals are not orthogonal and ambiguity arises about the question when and how to orthogonalise the matrix. The idea of optimisation to match given density is similar to the fitting of the bands linear composition coefficients because both involve the eigen vectors. The idea is promising and was successfully applied to TiC in the cited paper. Another advantage over the ASA approach is that it is easier to model non-close packed systems but this is irrelevant in our case.

IV.2.5 Fitting to the ASA bandstructure

The electronic bands are energy surfaces which for periodic systems are conveniently sampled in the symmetrically irreducible Brillouin zone. Since the bandstructure holds the majority of information for even partially covalent systems it makes sense that

a TB model matching the correct DFT bandstructure has a good chance of having the correct Hamiltonian parameters. It only has a good chance and is not guaranteed to be perfect because other significant parts of the energy such as the exchange-correlation are represented in TB by the classical repulsive potentials. Saying "repulsive" is not strictly correct for cases where the basis for the Hamiltonian is reduced to beyond minimal and the rest absorbed in the classical potentials because they may no longer be guaranteed to be purely repulsive.

The problem of curve or surface fitting can be defined as nonlinear least squares functional minimisation of the difference between the desired and calculated eigenvalues of some chosen system. There is a number of methods of multi variable least squares functional minimisation. The popular Levenberg-Marquardt algorithm[137, 138] was used for this fitting. It bridges the inverse Hessian and the steepest descent methods with a single parameter adjusted in the course of the fitting. The least squares function for a parameter vector p with respect to some example eigenvalues ε^0 is

$$\chi^2(p) = r^t r; \quad r_i = \varepsilon_i^0 - \varepsilon_i(p) \quad (\text{IV.26})$$

The \vec{k} -point and band indices are combined in i . Not far from the minimum if quadratic approximation is reasonable then minimising step in the parameter vector δp is

$$\delta p = -D^{-1} d \quad (\text{IV.27})$$

where d is the gradient and D is the Hessian,

$$d = \chi^2(p)' = -2J^t r; \quad J_{ij} = \frac{\partial \varepsilon_i(p)}{\partial p_j} \quad (\text{IV.28})$$

$$D = \chi^2(p)'' = 2(J^t J - r^t H) \xrightarrow{r \rightarrow 0} 2J^t J; \quad H_{i,j,j'} = \frac{\partial^2 \varepsilon_i(p)}{\partial p_j \partial p_{j'}} \quad (\text{IV.29})$$

A steepest descent step on the other hand is

$$\delta p = -\text{const } d \quad (\text{IV.30})$$

To combine them one can write

$$\delta p = -(D + \lambda I)^{-1} d \quad (\text{IV.31})$$

In the limit of rather large λ the matrix $D + \lambda I$ will be diagonally dominant and its inverse approach the constant $1/\lambda$ approximating the steepest descent step.

Since the different parameters may be in different scales it is useful to replace the identity matrix I with a measure of the scale obtained by the diagonal elements of D .

$$\delta p = -(D + \lambda \text{ diag}(D))^{-1} d \quad (\text{IV.32})$$

The procedure usually starts with some λ which is then modified depending on the change in χ^2 eventually diminishing it to 0. If χ^2 increases λ shall be increased and if it decreases λ should also be decreased.

The eigenvalue fitting was performed on the different crystal structures separately, namely the $L1_0$ from TiAl and all the Ti_3Al phases. The Brillouin zone sampling meshes contained about 12 \vec{k} -points per reciprocal nearest neighbour distance. The fitting was restricted to eigenvalues up to 0.12Ry which is at a good margin above the Fermi levels of ≈ -0.06 Ry. The starting value of λ is 1. A wide variety of input parameters were tested on all the structures. Most converged to $\chi^2 \approx 0.01 - 1$. Surprisingly, the vast majority of the fitted results favoured the $D0_{22}$ as the most stable phase;

v_0 , $\times 10\text{mRy}$	Ti-Ti	Ti-Al	Al-Ti
ss σ	-6.3416	-6.2560	-6.2560
sp σ	8.9410	8.1244	8.6942
pp σ	10.9669	11.8341	11.8341
pp π	-1.1625	-3.7870	-3.7870
sd σ	-5.0178	-6.7686	-6.3020
pd σ	-5.7769	-9.4576	-8.8821
pd π	3.2298	0.4641	4.0088
dd σ	-6.2153	-5.5809	-5.5809
dd π	3.8533	4.2607	4.2607
dd δ	-0.6176	-1.4350	-1.4350

Table IV.11: TB hopping integrals fitted to L1₂ bands at 12x12x12 k-point mesh.

ref: L1 ₂ , meV	TB L1 ₂ bandfit				LMTO-ASA				FP	
	diag spd	BOP Alp Tid			3.1 Å		4.4 Å		LAPW	LMTO
		9 m	11 m	o1	3c	o1	3c			
D0 ₁₉	-17.3	-14.9	-20.9	-1.8	-6.3	-11.6	-15.7	-10.3	-9.7	
D0 ₂₄	6.2	-10.3	-11.3	3.1	0.1	-3.0	-5.6	-0.2	-1.8	
D0 ₂₂	24.0	34.9	38.4	14.4	20.0	13.2	19.1	22.3	23.7	

Table IV.12: Energy differences in meV with respect to L1₂. The TB results are obtained from the parameters in (tbl. IV.11). The other columns are replicated for comparison from (tbl. IV.3), (tbl. IV.4), and (tbl. IV.1) respectively.

however there were some exceptions (tbl. IV.11) that gave approximately correct structural energy difference ordering (tbl. IV.12). The TB energy differences (tbl. IV.12) are self consistent with respect to the charge transfers in the high Hubbard U limit which approximates the local charge neutrality very well judging by the tiny (≈ 0.01 mRy) and consistent second order energy terms.

If only the p orbitals on Al and the d orbitals on Ti atoms are kept and all other orbitals are removed without any other modifications, the TB results deteriorate, but the correct ordering is kept in BOP. The data in (tbl. IV.12) show results of calculations utilising

up to 9 and 11 moments. The correct order can be attributed to constructive cancellation with the various approximations in BOP. However different problems may appear during fitting of the classical part. The energy of D₀₂₄ with respect to L₁₂ is too low in contrast to the results of the reference calculations, and this will certainly have an impact on the γ -surfaces. The lowest and highest points however, should not be erroneously affected as far as the bonding part is concerned. Since the transformation paths from one phase to another will be influenced by the diminished difference between D₀₁₉ and D₀₂₄, it is likely that band contribution the certain elastic properties may be incorrect.

These problems may be alleviated to some extent by the repulsive potential and more specifically the new environment dependent terms[139]. The classical potentials however have their limits and a certain amount of further refining of the band parameters may be advisable. The next section covers the issues surrounding the fitting of the classical part of the TB model.

IV.3 Fitting the Classical Terms

The properties chosen for fitting are the cohesive energies, the lattice parameters and the elastic constants. The benchmark properties are the relative energy positions of the stacking faults and the energies along the γ -surface lines connecting them. The obvious way to start would be to calculate all these properties after relaxing the cells then calculate the objective function as least squares of the differences. This approach however is slow and acutely prone to very long and meaningless relaxations if the entry parameter set happens to be not particularly fit.

The first point of great importance is to circumvent the relaxations which can be avoided if the level of proximity to the relaxed

structure is judged by some proxy measure which is easier to calculate. Such measures are the stresses felt by the cell obtained from a trial set of parameters at fixed chosen experimental or precisely calculated coordinates of the atoms. This approach obviously removes the possibility to include the lattice parameters directly in the list of fitting properties. This is only a formality because when the stresses are vanishing at the given lattice parameters the cell is in or very close to equilibrium. Full relaxation can be performed afterwards to settle the other physical properties including the lattice parameters. If necessary the fitting procedure may be continued this time with relaxation at every step, replacing the stresses with the lattice parameters in the list of properties because the parameter vector is now known to point near a minimum and it is unlikely to escape the well. This approach was applied to Ti and γ -TiAl previously[112, 42].

The second important point is to design good constraints on the parameters in order to avoid inappropriate sets. The difficulty with the constraints is that rarely is the border between appropriate and inappropriate precisely definable. Instead of steep walls the parameters are better confined within valleys with smooth slopes starting beyond a chosen acceptable space. The least squares method is one such approach where smooth restrictions in terms of quadratic valleys are drawn around known points. It is acceptable for the target properties, but it is not very well applicable to input parameters because of its simplistic clearly defined minima. The best situations however are those for which the objective to be found is not a known quantity when it comes to input parameters. What is known is usually a vague reference to the regions they have to be found in and often some possibly vague interrelations they may have or it is preferable that they obey. These may be relations between different contributions to the properties or favourable relations between the input parameters and they can be introduced as new abstract

property and be subjected to similar applicable constraints. All of these require an elaborate curation of the landscape of the fitting parameter space.

For many fitting algorithms it is often useful to have the first derivatives of the fitted properties with respect to the fitting parameters. Precise values of these are not easy to obtain for the hoppings from the band term. The pairwise potential's formulation is significantly simpler and analytical expressions are quick to evaluate. The three body classical environment term also has exact analytic derivatives but they are often more time consuming to calculate than the numerical. As a result analytic derivatives of energies and the related analytic stresses and elastic strains are only used when fitting the pairwise potential alone. In non pathological cases the differences between the analytical and the numerical derivatives of the pairwise terms for a chosen constant small deformation step ($\approx 0.25\% - 0.5\%$) is insignificant.

Fitting procedures which do not require the availability of the derivatives with respect to the parameters were preferred for the bond and environmental part. Simplex and simulated annealing were used initially with the SA emerging as the more successful.

In the simplex method a simplex is built of the dimensionality of the parameter space and all vertices evaluated initially. A simple step consists of reflection of the worst point and evaluation. Depending on how the new value compares with its previous and the best and next worst a shrink or expansion step may be performed. The simplex thus rolls down the valley it is dropped at and shrinks down once the minimum is surrounded, until the specified tolerance is reached. It may take a significant number of steps to reach an even nearby minimum because of the constrained motion of the simplex.

The simulated annealing method performs a random walk starting from initial point in the parameter space. The maximal step for each parameter is specified and enforced either by reflection or simple limit. The length of the new vector is random as is its direction maximising the space explored. The value at each step is compared with a random pick deciding whether it is accepted or not. Usually if it is lower than the current it is guaranteed to be accepted, otherwise the probability of being accepted depends on how much worse the point is and the 'temperature' of the system. At high temperature the odds of accepting a more energetic state is higher reflecting the thermal motion of actual particles in a melt. The starting temperature is usually high allowing the 'particle' to browse through larger areas with various outlay while finding the wider valleys. As time passes and the system is cooled the particle becomes more conservative in its motion. With the more stringent acceptance probability the particle is localised further and further and hopefully finally finds a lower local minimum. The cooling schedule and starting temperature are important controls of the process and should be tuned for the specific fitting requirements by looking at the parameters' paths.

A simple parallel version of the simulated annealing was developed in which trial points were executed simultaneously. The consequences are decreased probability of escape the vicinity of local minimum together with decreased time for finding the local lowest point in comparison to the serial SA. If the maximal step is large there is also a benefit to the global minima search in the early stages when the acceptance probability is low and larger number of surrounding remote points can be tested at once. The position of the point in this simple parallelisation of SA may be viewed as an organism reproducing asexually in an environment defined by the cost function and frequent nearly total extinction events. The only source of variability are the random mutations which unnat-

urally decrease with time. This may be contrasted to the genetic algorithms where there is more advanced reproduction, formation of families and tribes, and rare or even no mass extinction events. The genetic algorithm is probably superior in finding different minima if nature to judge by.

The cost function defines the physical laws in the environment of evolution, the potential surface landscape and so on. During fitting of the bond part the first policy for the Ti₃Al was to introduce large penalty for violation of the structural energy difference order to D₀₁₉ < L₁₂ < D₀₂₂ and D₀₁₉ < D₀₂₄ < D₀₂₂. Then a small cost was added for deviation from a set of energy differences between pairs of the cells. The same rules were applied with respect to the TiAl's L₁₀ and B₁₉. Then a rather large penalty was applied in case the lowest cohesive energies were becoming too low, say, < -15eV/atom. Once these aims were achieved additional rules concerning the Cauchy pressures were imposed. While the environment dependent term does contribute to negative Cauchy pressures its influence is small and unless the bond part provides reasonable values to build upon the classical potential is not going to be very useful. 'Fees' are collected if C₁₃ - C₄₄ in D₀₁₉ becomes too high or when the differences within the pairs of pressures in both D₀₁₉ and L₁₀ are too large.

When the environmental term is fitted together with the bond one the same rules are kept for the bond contributions and new ones are added to attempt to steer the total CPs to their target positions. Adding the pair potential to the mix brings additional rules applied to the total energy differences, the independent elastic constants and, most importantly, to the stresses. Large weights are set to ensure the stresses are as close to vanishing as possible because the credibility for all other properties strongly depends on the chosen geometry of the cells. If the stresses are nonzero they will lead to change in the lattice parameters and subsequently in

the other properties.

Tables with fitting results can be found in the appendix. A single acceptable potential describing well the two phases γ and α_2 Ti-Al could not be found unfortunately. A set of parameters for α_2 -TiAl ($D0_{19}$) with significant deviations in the elastic constants is available. It should be noted that none of the Ti_3Al phases have Al-Al nearest neighbours. The parameters for this interaction are taken from TiAl cells from the best mixed potential.

Chapter V

Exact Embedding with BOP

The inability of BOPs to describe different phases in certain materials, with acceptable accuracy should not be too disappointing. BOP is still vastly more capable than the purely classical central force field methods and has vastly greater performance than any of the other quantum methods. The origins of its performance are two fold: 1) the time for one step is linearly dependent on the number of atoms in the system and 2) the procedures are naturally parallelisable over the atoms or orbitals with minimal communication necessary leading to linear speedup on parallel machines with many processing units. These two features are hardly achievable with TB and DFT implementation when applied to metallic systems.

BOP's failures can be alleviated and its attractive features utilised for many practical calculations for which long range effects are important, for example: point-defect diffusion, dislocation motion, grain boundaries and so on.

The presented work was initiated by Dr. I. Katzarov. My contribution consist of the alternative interpretation and implementation methodology, the extension to surfaces and the generalised inclusion of the overlap.

V.1 Introduction

A common feature in solid state simulation boxes is that relatively little is happening in very large parts of the volume. Most of the interesting action is concentrated in a relatively small region around the defects. The field provided by and the interactions with the large, less active regions however are important.

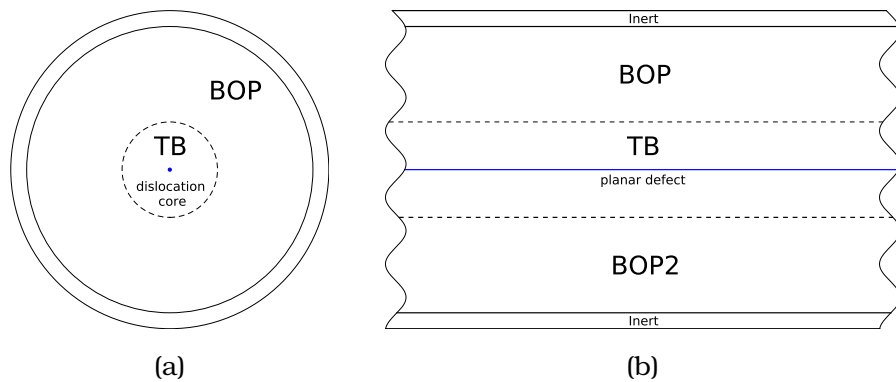


Figure V.1: Schematic depiction of a (a) slab with dislocation line (blue dot) normal to the viewing plane and (b) planar defect possibly separating 2 different phases with different BOP models. The thin outer regions in (a) and (b) represents inert atoms which emulate infinite medium spanning the rest of the space.

For such systems a fictitious surface may be drawn separating the two regions. Afterwards different methods can be applied to the different pieces and then used to construct the Green matrix for the whole box. There are two general viewpoints for implementing this scheme reviewed in [140]. One is to represent the more active area as a perturbation to the otherwise ideal crystal. The other is to see the important cluster as being embedded within the effective field potential. If no other approximations are applied both lead to the very same expressions.

The BOP method is particularly appropriate for this kind of embedding since its framework is entirely build upon moments approximation to the Green distribution and thus the DOS.

Let's consider a large slab possibly emulating infinite periodic crystal hosting or interfacing with a cluster of impurities or other defects (fig. V.1a). BOP can treat the vast regions with no dangerous phase transitions fairly well with just a single basis orbital and local charge neutrality condition. All operators concerned with this area will be denoted with sub- or superscript B. The more sophisticated dynamics of the atoms in the cluster of interest, containing impurities and defects, are better described with more complete TB or other quantum mechanical models. Matrices describing this region will be indexed by T. BT and TB may be used only for the rectangular pieces of the matrices relating the two spaces.

V.2 Perturbative representation

One idea is to present the whole system as a sum of its non interacting parts with quantities labelled with 0. Solve the parts separately and introduce the correlating blocks BT afterwards through perturbative addition Δ . The Hamiltonian matrix of the whole system H is then written as:

$$H = H_0 + \Delta H \quad (\text{V.1})$$

The Hamiltonian of the sum of the isolated systems H_0 and the perturbative ΔH have the following structure:

$$H_0 = \begin{pmatrix} H_B & \cdot \\ \cdot & H_T \end{pmatrix} \quad (\text{V.2})$$

$$\Delta H = \begin{pmatrix} \cdot & H_{BT} \\ H_{TB} & \cdot \end{pmatrix} \quad (\text{V.3})$$

The dots replace 0s. The system is defined in direct (real) space so H , H_0 and ΔH are symmetric and the H_{TB}, H_{BT} blocks are transposes of each other.

$$H_{TB} = H_{BT}^\dagger \quad (V.4)$$

The Green matrix of the interacting system $G(z)$ then can be written as a perturbation of its value $G_0(z)$ for the noninteracting system. The Green function is defined as an inverse operator. A minimalist illustration will be its value for the null energy operator:

$$G^\circ(z) = z^{-1} \quad (V.5)$$

Adding an arbitrary potential $-V$ in matrix form the scalar energy z turns into a diagonal square matrix with the dimension of V . Then the new Green matrix G^V

$$G^V(z) = (zI - V)^{-1} \quad (V.6)$$

can be represented as the original null one G° modified by the potential V :

$$G^V(z) = (zI - V)^{-1} = (I - (zI)^{-1}V)^{-1}(zI)^{-1} = (I - G^\circ(z)V)^{-1}G^\circ(z) \quad (V.7)$$

Applying $I - G^\circ(z)V$ to the left side and representing $G^V(z)$ without inversions leads to the Dyson equation:

$$\begin{aligned} G^V(z) &= G^\circ(z) + G^\circ(z)VG^V(z) \\ &= G^\circ(z) + G^\circ(z)V(G^\circ(z) + G^\circ(z)VG^V(z)) \\ &= G^\circ(z) + G^\circ(z)V(G^\circ(z) + G^\circ(z)V(G^\circ(z) + G^\circ(z)VG^V(z))) \end{aligned} \quad (V.8)$$

Its iterative expansion is formally equivalent to the power series expansion of (eq. V.7) for small V .

The equations can be applied recursively to any successive changes to V local and nonlocal.

If the starting point is the noninteracting system then its total Green matrix is the sum of the matrices for the separate parts since H_0 is itself block diagonal:

$$\begin{aligned} G_0 = (zI - H_0)^{-1} &= \left(\begin{pmatrix} zI & \cdot \\ \cdot & zI \end{pmatrix} - \begin{pmatrix} H_B & \cdot \\ \cdot & H_T \end{pmatrix} \right)^{-1} \\ &= \begin{pmatrix} Q_{B0} & \cdot \\ \cdot & Q_{T0} \end{pmatrix}^{-1} = \begin{pmatrix} Q_{B0}^{-1} & \cdot \\ \cdot & Q_{T0}^{-1} \end{pmatrix} = \begin{pmatrix} G_{B0} & \cdot \\ \cdot & G_{T0} \end{pmatrix} \end{aligned} \quad (\text{V.9})$$

Where the following shorthand notation is adopted:

$$Q(z) = zI - H = zI - H_0 - \Delta H = Q_0 - \Delta H \quad (\text{V.10})$$

$$G \equiv G(z) = (zI - H)^{-1} \equiv Q(z)^{-1} \equiv Q^{-1} \quad (\text{V.11})$$

while keeping in mind the energy dependence of the respective quantities.

The Green matrix for the interacting system will then be written, following (eq. V.7) or (eq. V.9), as:

$$G = Q^{-1} = (Q_0 - \Delta H)^{-1} = (I - G_0 \Delta H)^{-1} G_0 \quad (\text{V.12})$$

The product $G_0 \Delta H$ has a particular pattern making it quite simple to calculate:

$$G_0 \Delta H = \begin{pmatrix} G_{B0} & \cdot \\ \cdot & G_{T0} \end{pmatrix} \cdot \begin{pmatrix} \cdot & H_{BT} \\ H_{TB} & \cdot \end{pmatrix} = \begin{pmatrix} \cdot & G_{B0} H_{BT} \\ G_{T0} H_{TB} & \cdot \end{pmatrix} \quad (\text{V.13})$$

The subsequent matrix for inversion also has a pattern allowing significant simplification and it will be examined later too.

Achieving charge transfer self consistency or local neutrality requires adding a local potential or simply adjusting the onsite energies. Both activities equate to adding a new diagonal or block diagonal potential $\Delta\epsilon$ and updating the Green matrix as in (eq. V.7) and (eq. V.9):

$$G_{\text{new}}(z) = (I - G(z)\Delta\epsilon)^{-1}G(z) \quad (\text{V.14})$$

One could solve this equation and later integrate but there are unfortunately no particular patterns or simple and exact simplifying tricks. The interacting system matrix $G(z)$ is dense and inverting it is in the order of difficulty of diagonalising it if not higher. Further, integration over a number of points will require hundreds of times the effort needed for simply diagonalising once. Including $\Delta\epsilon$ in ΔH does not help either since $G_0\Delta H$ becomes dense.

A better approach is to return to (eq. V.12), recalculate $G_0(z)$ and proceed as before. This is more efficient because $G_{B0}(z)$ is very fast to compute because this is BOP's core competency and $G_{T0}(z)$ is not slow because it is supposedly much smaller.

V.3 Direct block-matrix solution

Since the justification for the embedding is to combine BOP's speed with with TB's richer basis and more accurate description of the small region, easing the difficulty of the inversion and subsequent multiplication steps in (eq. V.12) is crucial.

The matrices have simple block pattern (fig. V.2) and it pays off to treat these blocks separately. The inversion of a 2×2 block matrix may be written analytically:

$$a^{-1} = \begin{pmatrix} a_{11} & a_{12} \\ a_{12}^\dagger & a_{22} \end{pmatrix}^{-1} = \begin{pmatrix} a_{11}^{-1} + A C A^\dagger & -A C \\ -(A C)^\dagger & C \end{pmatrix} \quad (\text{V.15})$$

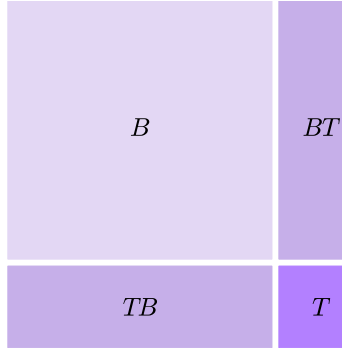


Figure V.2: Hamiltonian matrix blocking pattern for embedding cluster T in the larger block B . The connecting surface is fully contained in the $TB = BT^\dagger$ rectangles.

where a_{ij} are the matrix subblocks corresponding to the the pattern in (fig. V.2). a_{ii} are symmetric or hermitian matrices in general and A , B and C are shorthand substitutions:

$$A = a_{11}^{-1} a_{12} \quad (\text{V.16})$$

$$C = (a_{22} - a_{12}^\dagger A)^{-1} \equiv (I - a_{22}^{-1} a_{12}^\dagger A)^{-1} a_{22}^{-1} \quad (\text{V.17})$$

Modifying the inversion to suit the asymmetric matrix $I - G_0 \Delta H$ will require additional storage and extra writing. Applying it to the first form of (eq. V.12) would require the same amount of operations and also relaxes the dependence on G_{T0} by allowing Q_{T0} to be used directly instead.

$$G(z) = \begin{pmatrix} Q_{B0}(z) & -H_{BT} \\ -H_{BT}^\dagger & Q_{T0}(z) \end{pmatrix}^{-1} \quad (\text{V.18})$$

The expression for C ,

$$C : G_T = \left(Q_{T0} - H_{BT}^\dagger G_{B0} H_{BT} \right)^{-1} \quad (\text{V.19})$$

then reveals the energy dependent embedding potential for the cluster region:

$$Q_T = Q_{T0} - H_{BT}^\dagger G_{B0} H_{BT} \quad (V.20)$$

$$H_T = H_{T0} + H_{BT}^\dagger G_{B0}(z) H_{BT} = H_{T0} + \Sigma(z) \quad (V.21)$$

The difficulty of the problem may seem of $O(N_B^2)$ for $N_B \gg N_T$ due to the matrix products forming A and ACA^\dagger from (eq. V.17) and (eq. V.15). The A product corresponds to $G_B H_{BT}$ and it can be sped up significantly by exploiting the sparsity of H_{BT} . If the system is composed of two semi infinite slabs and an appropriate permutation of the whole matrix is taken, the nonzero values of H_{BT} would be concentrated in its lower left corner. Optimisation for the second product is harder to find.

The description of the cluster may also be provided as a Green matrix instead of a Hamiltonian. In this case a second form of C is used:

$$C : G_T(z) = (I - G_{T0}(z)\Sigma(z))^{-1} G_{T0}(z) \quad (V.22)$$

The inversion of C may be carried through initial diagonalisation to avoid problems when z happens to be an eigenvalue.

The energy dependent embedding potential requires full inversion or diagonalisation of the cluster matrix for every evaluation of energy z during Fermi level search, and at every integration point for charges and indeed everything else. The Fermi trialing may be avoided by making the reasonable assumption that it is not influenced by the presence of the defect cluster.

To simplify the integration one may make further assumptions for the Green function of the BOP region which will have to be carefully tested. The integration points are independent calculations and they can be performed on a distributed parallel computer. If

the system is large and such hardware is used anyway for BOP then the effort can be amortised because the processors are likely to be idle while C is solved.

The direct solution and the perturbative view results are the same. The advantage of the direct method is in the flexibility gained by not having to use large matrices, the removal of the necessity to handle G_{T0} and its particular blocking pattern.

V.4 Extension to embedded surface

Splitting the simulation box in three regions is useful in cases where the system under consideration consists of two different phases interfaced with an interphase boundary, and there is no good BOP potential describing both phases and their transition. The two phases may be described well by separate BOP models I and II, and the interface between together with reasonably sized region around it may be served well by more complete TB model. A schematic view is presented in (fig. V.1b)

Assuming the two BOP pieces do not have direct hopping the blocking pattern of the whole Hamiltonian allows for relatively simple Green matrix solution. The Q matrix is:

$$Q = \begin{pmatrix} Q_{B_I} & Q_{B_I T} & 0 \\ Q_{TB_I} & Q_T & Q_{TB_{II}} \\ 0 & Q_{B_{II} T} & Q_{B_{II}} \end{pmatrix} \quad (V.23)$$

with $Q_{TB_I} = Q_{B_I T}^\dagger$ and $Q_{B_{II} T} = Q_{TB_{II}}^\dagger$.

This is a tridiagonal symmetric matrix and the model symbolic inversion is:

$$\mathbf{a}^{-1} = \begin{pmatrix} \mathbf{a}_{11}^{-1} + \mathbf{A}\mathbf{C}\mathbf{A}^\dagger & -\mathbf{AC} & \mathbf{ACB} \\ -\mathbf{CA}^\dagger & \mathbf{C} & -\mathbf{CB} \\ \mathbf{B}^\dagger\mathbf{CA}^\dagger & -\mathbf{B}^\dagger\mathbf{C} & \mathbf{a}_{33}^{-1} + \mathbf{B}^\dagger\mathbf{CB} \end{pmatrix} \quad (\text{V.24})$$

where the substitutions are:

$$\mathbf{A} = \mathbf{a}_{11}^{-1} \mathbf{a}_{12} \quad (\text{V.25})$$

$$\mathbf{B} = \mathbf{a}_{23} \mathbf{a}_{33}^{-1} \quad (\text{V.26})$$

$$\mathbf{C} = \left(\mathbf{a}_{22} - (\mathbf{a}_{12}^\dagger \mathbf{A} + \mathbf{B} \mathbf{a}_{23}^\dagger) \right)^{-1} \quad (\text{V.27})$$

The total embedding potential for the cluster is just the sum of the potentials provided by the isolated BOP regions:

$$\Sigma(z) = \Sigma_I(z) + \Sigma_{II}(z) = H_{B_1 T}^\dagger G_{B_1 0}(z) H_{B T} + H_{T B_{II}}^\dagger G_{B_{II} 0}(z) H_{T B_{II}}^\dagger \quad (\text{V.28})$$

and the performance observations from the 2×2 case apply to this system inductively.

V.5 Overlap

If the TB model necessitates the consideration of an overlap matrix only within its region the changes to the above equations are minimal.

Writing $S = S_T$ as the overlap matrix, the Green function we need to use for the generalised eigenproblem is:

$$G_T(z) = (z - S^{-1} H_T)^{-1} = (zS - H_T)^{-1} S \quad (\text{V.29})$$

which also redefines Q_T . The step calculating C can still be performed either through inversion (eq. V.19), (eq. V.27) or through the Green function (eq. V.22). If the eigenvectors are the precursors

the only difference to the orthogonal basis case is that there is 1 additional matrix multiplication.

$$G(z) = W(zI - \Lambda)^{-1}W^\dagger S \quad (\text{V.30})$$

Here W is a matrix which columns are the eigenvectors of a Hamiltonian H and Λ is a diagonal matrix containing its eigenvalues in the same order. This equation and all following in this section are concerned with the T region specifically but are generally applicable and the index will be skipped. To prove the relation in (V.30) holds for nonorthogonal basis the general systems of secular equations can be written in matrix form as:

$$HW = SW\Lambda \quad (\text{V.31})$$

The orthogonality of the eigenvectors for the so defined problem is:

$$W^\dagger SW = I \quad (\text{V.32})$$

then the following relations,

$$W^\dagger S = W^{-1} \quad (\text{V.33})$$

$$S = W^{\dagger-1}W^{-1} = (WW^\dagger)^{-1} \quad (\text{V.34})$$

$$SW = W^{\dagger-1} \quad (\text{V.35})$$

can be obtained by multiplying from right and/or left by $W^{\dagger-1}$ and W^{-1} respectively. From these it follows that $W^\dagger = W^{-1}$ in the orthogonal case $S = I$.

The Hamiltonian matrix decomposition can be obtained by multiplying W^{-1} on the right side and substituting with (eq. V.35):

$$H = SW\Lambda W^{-1} = W^{\dagger-1}\Lambda W^{-1} \equiv SW\Lambda W^\dagger S \quad (\text{V.36})$$

The G matrix can be constructed with the help of (V.34):

$$\begin{aligned} G(z) &= (zI - S^{-1}H)^{-1} = (WzW^{-1} - W\Lambda W^{-1})^{-1} = \\ &= W(zI - \Lambda)^{-1}W^{-1} = W(zI - \Lambda)^{-1}W^\dagger S \end{aligned}$$

as in (V.30).

Chapter VI

Conclusions

Of fundamental importance to the progress of this project was the finding of an appropriately fitted BOP model describing both of the constituent phases of PST-TiAl, including fairly accurate matching of the experimental elastic properties. The success of the model for pure γ -TiAl [42] was very encouraging; especially its surprisingly well behaved results for α_2 considering this phase was not included in the fitting procedure. The trivial improvements to the potential, envisaged at the beginning turned out not to be successful. The long search for parameters proved fruitless. A variety of strategies and minimisation algorithms were attempted and the results ranged from inane insistence on the very wrong order of stability to deviations from the target elastic values impossibly large to reconcile. The necessity to perform large amounts of calculations during fitting led to technical and algorithmically improvements to the code, namely revamped input data handling execution order, parallelisation, critical path optimisations and a move to an order of magnitude faster secant/Newton-Raphson mixing scheme.

After repeated failures with carefully tuned fitting procedures the focus shifted to trying to understand the source of the difficulty. The method of obtaining bond integrals from LMTO-ASA was revisited and a real space ASA version was developed to separate the

1, 2 and 3-centre integrals and their contributions of different orders with quite a surprising result. The first order contributions are adequately accurate but further terms are not asymptotically convergent. The root problem of the ASA inversion method is the detrimental reshaping of the structure constants after screening and the inevitable problems with their rotations.

Another avenue of thought led to the development of the formal DOS reconstruction $\text{DOS} \Rightarrow \text{moments} \Rightarrow \text{recursion coefficients} \Rightarrow \text{DOS}$ procedure which proved useful in quantifying the amount of information lost due to the incomplete moment expansion, and analysing the behaviour of the recursion coefficients in the tail. All from a given model DOS without having to deal with any complications like atoms, neighbours, sparse products and every other pesky but non-neglectable detail of carrying out a calculation for actual atoms. It showed how volatile is the order when structural energy differences are tiny. More importantly, it showed the that fair amount of luck is needed to reproduce the order in the Ti_3Al without requesting impractical amount of moments.

The arbitrary moment DOS reconstruction gave us opportunity to look at the behaviour of the far reaching recursion coefficients and gain insight into the implications of the choice of terminator. As it stands, intermetallics composed of atoms with partially covalent bonding tendencies together with atoms of clearly metallic character are not described well by any terminator within reasonably low number of recursion levels. This is because a terminator invariably assumes certain pattern of behaviour based on few datapoints far from asymptoticity. This mismatch to reality together with the exponentially larger importance of the terminator in the low moment models means that the systems which will be well described should have either fairly standard metallic DOS distribution or have permanent well defined band gap.

The good matching of the bands from 2-centre first order LMTO-

ASA Hamiltonian coupled with the issues surrounding its rotation convinced us that a successful set of bond parameters should be found by relegating the error of rotation by avoiding the procedure altogether and instead fit a model to the band structure directly.

An often neglected and thus longstanding problem in TB simulations is the choice of scaling functions for the hopping integrals and classical potentials. The wisdom of pursuing no direct interaction with the second or third neighbour, respectively, is in conflict with long range scalings such as $1/r^{2,3,4}$. Simply discarding the interactions beyond any given neighbour would render TB useless for molecular dynamics when these atoms move and cross the boundary. The peculiarities of the tail function, introduced to smear the hopping, have sometimes been utilised to reproduce notorious properties like the negative Cauchy pressures in some intermetallics, rather than being kept to minimal interference as is common in the classical potential MD simulations.

The GSP potential has been fairly successful at shortening the hopping distance while improving the TB energy-volume curves and thus it is fairly popular and widely deployed. It is however still reliant on a cut-off tail function. Our improvements to the GSP and the cut-offs in general preserve most or, in case of GSP, all positive aspects and provide a solution to the smooth cut-off problem.

Faced by the prospects of having two separate BOP models for the γ and α_2 phases we found the general framework of embedding, of regions with different basis sizes using Green functions, particularly suitable for application to interfacing BOP with TB. It is still a work in progress and we are hopeful it will also applicable for more complex systems with larger variety of atoms, for which developing a BOP model may not be a feasible task.

Appendix

Bond part:

Al:

nel, l: 2.9000, 1

Ti:

nel, l: 2.4974 2

AlAl:

	Vscr	r0	r1	rcut	n
sss	0.0000	0.0000	0.0	0.0	0.00000
sps	0.0000	0.0000	0.0	0.0	0.00000
pps	1.7402	2.8547	0.5	4.8	3.10725
ppp	-1.5329	2.8547	0.5	4.8	3.10725
pds	0.0000	0.0000	0.0	0.0	0.00000
pdp	0.0000	0.0000	0.0	0.0	0.00000
sds	0.0000	0.0000	0.0	0.0	0.00000
dds	0.0000	0.0000	0.0	0.0	0.00000
ddp	0.0000	0.0000	0.0	0.0	0.00000
ddd	0.0000	0.0000	0.0	0.0	0.00000

AlTi:

	Vscr	r0	r1	rcut	n
sss	0.0000	0.0000	0.0	0.0	0.00000
sps	0.0000	0.0000	0.0	0.0	0.00000
pps	0.0000	0.0000	0.0	0.0	0.00000
ppp	0.0000	0.0000	0.0	0.0	0.00000
pds	-1.7979	2.8547	1.5	4.8	3.78715
pdp	1.0138	2.8547	1.5	4.8	3.78715
sds	0.0000	0.0000	0.0	0.0	0.00000
dds	0.0000	0.0000	0.0	0.0	0.00000
ddp	0.0000	0.0000	0.0	0.0	0.00000
ddd	0.0000	0.0000	0.0	0.0	0.00000

TiTi:

	Vscr	r0	r1	rcut	n
sss	0.0000	0.0000	0.0	0.0	0.00000
sps	0.0000	0.0000	0.0	0.0	0.00000
pps	0.0000	0.0000	0.0	0.0	0.00000
ppp	0.0000	0.0000	0.0	0.0	0.00000
pds	0.0000	0.0000	0.0	0.0	0.00000
pdp	0.0000	0.0000	0.0	0.0	0.00000
sds	0.0000	0.0000	0.0	0.0	0.00000

dds	-1.2062	2.8547	1.0	4.8	4.88590
ddp	0.4174	2.8547	1.0	4.8	4.88590
ddd	-0.1289	2.8547	1.0	4.8	4.88590

Environmental part add and bond part fixed:

12	name	sw	val	scl	mnsw	min	mxsw	max
	Al_10	T	0.501968281352	0.010000	T	0.500000	T	5.000000
	Al_m	T	1.00007808183	0.010000	T	1.000000	T	3.000000
	Al_rcore	T	0.999574456733	0.010000	T	0.400000	T	1.000000
	Ti_10	T	0.685832894252	0.010000	T	0.500000	T	5.000000
	Ti_m	T	1.09204444340	0.010000	T	1.000000	T	3.000000
	Ti_rcore	T	1.08543111744	0.010000	T	0.400000	T	1.100000
	AlAl_a	T	392.912419890	1.000000	T	2.000000	T	500.000000
	AlAl_c	T	89.9639599578	1.000000	T	0.500000	T	500.000000
	AlAl_nu	T	1.72535835586	0.010000	T	1.500000	T	5.000000
	TiTi_a	T	100.512242837	1.000000	T	2.000000	T	500.000000
	TiTi_c	T	48.9812862673	1.000000	T	0.500000	T	500.000000
	TiTi_nu	T	1.51048814222	0.010000	T	1.500000	T	5.000000
14	name	sw	target	val	weight			
	d19_en	T	-4.74400000000	-5.02416240501	1.000000000000			
	d24_en	T	0.00000000000	-5.01423662601	1.000000000000			
	l12_en	T	0.00000000000	-5.00524697998	1.000000000000			
	d22_en	T	0.00000000000	-4.99980913145	1.000000000000			
	l10_en	T	-4.52000000000	-6.97357604162	1.000000000000			
	b19_en	T	0.00000000000	-6.93130150863	1.000000000000			
	l10_c1344	T	-0.21300000000	-0.218415098546	1.000000000000			
	l10_c1266	T	-0.45000000000E-01	-0.450513087842E-01	1.000000000000			
	d19_c1344	T	-0.12500000000E-01	-0.126851125407E-01	1.000000000000			
	d19_c1266	T	0.26200000000	0.260931364843	1.000000000000			
	l10_s11	T	0.00000000000	0.893851262834	1.000000000000			
	l10_s33	T	0.00000000000	1.22457580968	1.000000000000			
	d19_s11	T	0.00000000000	0.852214584146	1.000000000000			
	d19_s33	T	0.00000000000	0.875499439166	1.000000000000			

Environmental and pairwise parts together:

24	name	sw	val	scl	mnsw	min	mxsw	max
	Al_10	T	1.04279509255	0.010000	T	0.500000	T	5.000000
	Al_m	T	1.31322218513	0.010000	T	1.000000	T	3.000000
	Al_rcore	T	0.994804323776	0.010000	T	0.400000	T	1.000000
	Ti_10	T	0.550545397879	0.010000	T	0.500000	T	5.000000
	Ti_m	T	1.11808230593	0.010000	T	1.000000	T	3.000000
	Ti_rcore	T	1.05906222842	0.010000	T	0.400000	T	1.100000
	AlAl_a	T	369.684460521	1.000000	T	2.000000	T	500.000000
	AlAl_c	T	107.707453516	1.000000	T	0.500000	T	500.000000
	AlAl_nu	T	1.70733119732	0.010000	T	1.500000	T	5.000000
	TiTi_a	T	105.118329927	1.000000	T	2.000000	T	500.000000
	TiTi_c	T	62.9324577622	1.000000	T	0.500000	T	500.000000
	TiTi_nu	T	1.53514049559	0.010000	T	1.500000	T	5.000000

	AlAl_pwp_v	T	0.249729241946E-01	5.000000	T	0.000000	T	2500.000000
	AlAl_pwp_n	T	4.60447526331	0.200000	T	1.000000	T	5.000000
	AlAl_pwp_rc	T	5.31626787054	0.500000	T	0.100000	T	8.000000
	AlAl_pwp_nc	T	0.365624094885E-01	0.050000	T	0.000000	T	5.000000
	AlTi_pwp_v	T	1.27518945962	5.000000	T	0.000000	T	2500.000000
	AlTi_pwp_n	T	3.71120378983	0.200000	T	1.000000	T	5.000000
	AlTi_pwp_rc	T	3.03091043472	0.500000	T	0.100000	T	8.000000
	AlTi_pwp_nc	T	2.06464235119	0.050000	T	0.000000	T	5.000000
	TiTi_pwp_v	T	0.745718524622	5.000000	T	0.000000	T	2500.000000
	TiTi_pwp_n	T	3.57497632926	0.200000	T	1.000000	T	5.000000
	TiTi_pwp_rc	T	3.70037257328	0.500000	T	0.100000	T	8.000000
	TiTi_pwp_nc	T	0.519459471783	0.050000	T	0.000000	T	5.000000
26	name	sw	target	val		weight		
	d19_en	T	-4.74400000000	-4.19927908747		2.00000000000		
	d24_en	F	-4.72540000000	0.00000000000		2.00000000000		
	l12_en	T	-4.70700000000	-4.09692246043		2.00000000000		
	d22_en	T	-4.65150000000	-4.06721845391		2.00000000000		
	l10_en	T	-4.52000000000	-4.58591780080		2.00000000000		
	b19_en	T	-4.48000000000	-4.53048695432		2.00000000000		
	l10_c1344	T	-0.213000000000	-0.181414594326		1.00000000000		
	l10_c1266	T	-0.450000000000E-01	-0.447029710782		1.00000000000		
	d19_c1344	T	-0.125000000000E-01	-0.341497312501		1.00000000000		
	d19_c1266	T	0.262000000000	0.275850356866		10.0000000000		
	l10_s11	T	0.00000000000	0.865127901125E-01		10.0000000000		
	l10_s33	T	0.00000000000	0.441365474101E-01		10.0000000000		
	d19_s11	T	0.00000000000	0.344823040979		10.0000000000		
	d19_s33	T	0.00000000000	0.316158311557		10.0000000000		
	l10_c11	T	1.16700000000	2.07328568728		1.00000000000		
	l10_c33	T	1.13600000000	6.80489412496		1.00000000000		
	l10_c12	F	0.00000000000	0.197344107458		1.00000000000		
	l10_c13	F	0.00000000000	2.36568480896		1.00000000000		
	l10_c44	T	0.68000000000	2.57976173766		1.00000000000		
	l10_c66	T	0.50700000000	0.687630213296		1.00000000000		
	d19_c11	T	1.14230000000	1.63351856782		1.00000000000		
	d19_c33	T	1.40450000000	2.37240709562		1.00000000000		
	d19_c12	F	0.00000000000	0.613649896613		1.00000000000		
	d19_c13	F	0.00000000000	0.295594185288		1.00000000000		
	d19_c44	T	0.39950000000	0.802336835923		1.00000000000		
	d19_c66	T	0.29300000000	0.510211060237		1.00000000000		
24	name	sw	val	scl	mnsw	min	mxsw	max
	Al_10	T	1.04342058324	0.010000	T	0.500000	T	5.000000
	Al_m	T	1.30828116230	0.010000	T	1.000000	T	3.000000
	Al_rcore	T	0.994181280286	0.010000	T	0.400000	T	1.000000
	Ti_10	T	0.555219201832	0.010000	T	0.500000	T	5.000000
	Ti_m	T	1.11423397036	0.010000	T	1.000000	T	3.000000
	Ti_rcore	T	1.05604103674	0.010000	T	0.400000	T	1.100000
	AlAl_a	T	370.131976843	1.000000	T	2.000000	T	500.000000
	AlAl_c	T	107.725812351	1.000000	T	0.500000	T	500.000000
	AlAl_nu	T	1.70303695425	0.010000	T	1.500000	T	5.000000

TiTি_a	T	105.135543929	1.000000	T	2.000000	T	500.000000
TiTি_c	T	62.5413165833	1.000000	T	0.500000	T	500.000000
TiTি_nu	T	1.53425410418	0.010000	T	1.500000	T	5.000000
AlAl_pwp_v	T	0.767969804815E-01	5.000000	T	0.000000	T	2500.000000
AlAl_pwp_n	T	4.56145641293	0.200000	T	1.000000	T	5.000000
AlAl_pwp_rc	T	5.33420382331	0.500000	T	0.100000	T	8.000000
AlAl_pwp_nc	T	0.355009073126E-01	0.050000	T	0.000000	T	5.000000
AlTi_pwp_v	T	1.21548445735	5.000000	T	0.000000	T	2500.000000
AlTi_pwp_n	T	3.66245159665	0.200000	T	1.000000	T	5.000000
AlTi_pwp_rc	T	3.13741772013	0.500000	T	0.100000	T	8.000000
AlTi_pwp_nc	T	2.05239387554	0.050000	T	0.000000	T	5.000000
TiTि_pwp_v	T	0.826039741963	5.000000	T	0.000000	T	2500.000000
TiTि_pwp_n	T	3.65575566340	0.200000	T	1.000000	T	5.000000
TiTि_pwp_rc	T	3.55896961264	0.500000	T	0.100000	T	8.000000
TiTि_pwp_nc	T	0.514869507537	0.050000	T	0.000000	T	5.000000
26	name	sw	target	val	weight		
d19_en	T	-4.74400000000	-4.25883475423	2.00000000000			
d24_en	F	-4.72540000000	0.00000000000	2.00000000000			
l12_en	T	-4.70700000000	-4.14326861005	2.00000000000			
d22_en	T	-4.65150000000	-4.11377161430	2.00000000000			
l10_en	T	-4.52000000000	-4.73387978248	2.00000000000			
b19_en	T	-4.48000000000	-4.72298816904	2.00000000000			
l10_c1344	T	-0.213000000000	-0.367078597859E-01	1.00000000000			
l10_c1266	T	-0.450000000000E-01	-0.312999137128	1.00000000000			
d19_c1344	T	-0.125000000000E-01	-0.181119536720	1.00000000000			
d19_c1266	T	0.262000000000	0.422885559093	10.0000000000			
l10_s11	T	0.00000000000	0.141539022685	10.0000000000			
l10_s33	T	0.00000000000	0.210210156240	10.0000000000			
d19_s11	T	0.00000000000	0.393676504955	10.0000000000			
d19_s33	T	0.00000000000	0.375956060369	10.0000000000			
l10_c11	T	1.16700000000	1.48020869902	1.00000000000			
l10_c33	T	1.13600000000	5.48018890062	1.00000000000			
l10_c12	F	0.00000000000	0.289769343319	1.00000000000			
l10_c13	F	0.00000000000	1.69557435813	1.00000000000			
l10_c44	T	0.68000000000	1.82021951265	1.00000000000			
l10_c66	T	0.50700000000	0.673537991789	1.00000000000			
d19_c11	T	1.14230000000	0.851093239173	1.00000000000			
d19_c33	T	1.40450000000	1.42779008233	1.00000000000			
d19_c12	F	0.00000000000	0.434560654562	1.00000000000			
d19_c13	F	0.00000000000	0.162880999394	1.00000000000			
d19_c44	T	0.39950000000	0.536408677445	1.00000000000			
d19_c66	T	0.29300000000	0.208513347947	1.00000000000			

Bibliography

- [1] Chester Thomas Sims and William C. Hagel. *The Superalloys*. Wiley-Interscience, 1972. 1
- [2] Chester Thomas Sims, N. S. Stoloff, and William C. Hagel. *Superalloys II*. Wiley, 1987. 1
- [3] http://www.arabianoilandgas.com/pictures/gallery/Offshore/300x200/GE_SteamTurbine_For-Web.jpg. 2
- [4] <http://uk.photos.com/royalty-free-images/please-visit-my-lightboxes-from-here/147695509>. 2
- [5] http://www.rolls-royce.com/Images/Trent%20900_tcm92-11346.pdf. 2
- [6] edited by Cahn R.W. D.P. Pope and Haasen P. volume 3, chapter 24. Elsevier, 1996. 1
- [7] G.W Goward. Progress in coatings for gas turbine airfoils. *Surface and Coatings Technology*, 108–109(0):73 – 79, 1998. 2
- [8] D. M. Dimiduk. Gamma titanium aluminide alloys—an assessment within the competition of aerospace structural materials. *Materials Science and Engineering A*, 263(2):281 – 288, 1999. 2, 3

- [9] J.J. Petrovic and A.K. Vasudevan. Key developments in high temperature structural silicides. *Materials Science and Engineering: A*, 261(1–2):1 – 5, 1999. 2
- [10] D. M. Dimiduk, D.B. Miracle, and C. H. Ward. Development of intermetallic materials for aerospace systems. *Materials Science and Technology*, 8(4):367–375, 1992. 2, 3
- [11] F. Appel and R. Wagner. Microstructure and deformation of two-phase γ -titanium aluminides. *Materials Science and Engineering*, R22:187–268, 1998. 3, 4, 5
- [12] Fujiwara T., Nakamura A., Hosomi M., Nishitani S. R., Shirai Y., and Yamaguchi M. Deformation of polysynthetically twinned crystals of TiAl with a nearly stoichiometric composition. *Philosophical Magazine A*, 61(0141-8610):591–606, 1990. 3
- [13] Guy Norris. Power House. <http://www.flightglobal.com/articles/2006/06/13/207148/power-house.html>, 2006. 3
- [14] F.J.J van Loo and G.D Rieck. Diffusion in the Titanium-Aluminium System-II. Interdiffusion in the composition range between 25 and 100 at.% Ti. *Acta Metallurgica*, 21(1):73 – 84, 1973. 4
- [15] T. Namboodhiri, C. McMahon, and H. Herman. Decomposition of the α -phase in titanium-rich Ti-Al alloys. *Meturgical and Materials Transactions B*, 4:1323–1331, 1973. 10.1007/BF02644528. 4
- [16] M. Heckler. Löslichkeit von Titan in Flüssigem Aluminium./Solubility of Titanium in Molten Aluminum. *Aluminium, Germany*, 50:405–407, June 1974. 4

- [17] Kimihiro Shibata, Tamotsu Sato, and Goro Ohira. The solute distributions in dilute Al-Ti alloys during unidirectional solidification. *Journal of Crystal Growth*, 44(4):435 – 445, 1978. 4
- [18] Larry Kaufman and Harvey Nesor. Coupled phase diagrams and thermochemical data for transition metal binary systems – V. *Calphad*, 2(4):325 – 348, 1978. 4
- [19] Abdel-Hamid, Ahmed, Allibert, Colette H., Durand, and Francis. Equilibrium between $TiAl_3$ and molten Al: results from the technique of electromagnetic phase separation. *Zeitschrift für Metallkunde/Materials Research and Advanced Techniques*, 75:455–458, 1984. 4
- [20] J. L. Murray. *Phase Diagrams of Binary Titanium Alloys*, pages 354–366. ASM International, Metal Park, OH, 1987. 4
- [21] J.P. Gros, B. Sundman, and I. Ansara. Thermodynamic modeling of the Ti-rich phases in the TiAl system. *Scripta Metallurgica*, 22(10):1587 – 1591, 1988. 4
- [22] C McCullough, J.J Valencia, C.G Levi, and R Mehrabian. Phase equilibria and solidification in Ti-Al alloys. *Acta Metallurgica*, 37(5):1321 – 1336, 1989. 4
- [23] U. Kattner, J. Lin, and Y. Chang. Thermodynamic Assessment and Calculation of the Ti-Al System. *Metallurgical and Materials Transactions A*, 23:2081–2090, 1992. 10.1007/BF02646001. 4
- [24] J. Ding, Q. Qin, S. Hao, X. Wang, and G. Chen. Partial phase diagram of the Ti-Al binary system. *Journal of Phase Equilibria*, 17:117–120, 1996. 10.1007/BF02665786. 4

- [25] F. Zhang, S. L. Chen, Y. A. Chang, and U. R. Kattner. A thermodynamic description of the Ti—Al system. *Intermetallics*, 5(6):471 – 482, 1997. 4
- [26] I. Ohnuma, Y. Fujita, H. Mitsui, K. Ishikawa, R. Kainuma, and K. Ishida. Phase equilibria in the Ti-Al binary system. *Acta Materialia*, 48:3113–3123, 2000. 4
- [27] V. Raghavan. Al-Ti (Aluminum-Titanium). *Journal of Phase Equilibria and Diffusion*, 26:171–172, 2005. 10.1007/s11669-005-0137-x. 4
- [28] R. Kainuma, M. Palm, and G. Inden. Solid-phase equilibria in the Ti-rich part of the Ti—Al system. *Intermetallics*, 2(4):321 – 332, 1994. 4
- [29] M. Werwer and A. Cor nec. The role of superdislocations for modeling plastic deformation of lamellar tial. *International Journal of Plasticity*, 22:1683–1698, 2006. 5
- [30] Pearson. *Handbook of Crystallographic Data for Intermetallic Phases*, volume 2. American Society for Metals, Metals Park, OH, 1967. 4
- [31] Charles Kittel, editor. 1996. 6
- [32] Helmut Föll and Bernd Kolbesen. Agglomerate von Zwischengitteratomen (Swirl-Defekte) in Silizium – ihre Bedeutung für Grundlagenforschung und Technologie. *Jahrbuch der Akademie der Wissenschaften in Göttingen*. 7
- [33] A. Kelly and G. W. Groves. *Crystallography and crystal defects*. TechBooks with permit from Addison-Wesley, 2600 Sesky Glen Court, Herndon, VA 22071, USA, 1970. 7, 9, 10, 11
- [34] V. Vítek. Intrinsic stacking faults in body-centred cubic crystals. *Philosophical Magazine*, 18(154):773–786, 1968. 10

- [35] J. P. Hirth and J. Lothe. *Theory of Dislocations*. McGraw-Hill Book Company, 1968. 11, 62
- [36] E. N. da C. Andrade. The cry of tin. *Nature*, 129:651–651, 1932. 11
- [37] M. H. Yoo and M. Yamaguchi. *Interfacial Structures and Mechanical Properties of Titanium Aluminides*, volume 2, chapter 2. World Scientific Publishing Co. Pte. Ltd, 57 Shelton Street, Covent Garden, London WC2H 9HE, 2000. 12
- [38] H. Inui, M. Matsumuro, D. H. Wu, and M. Yamaguchi. Temperature dependence of yield stress, deformation mode and deformation structure in single crystals of TiAl (Ti-56 at.% Al). *Philosophical Magazine A*, 75(0141-8610):395–423, 1997. 12
- [39] M. Yamaguchi, H. Inui, K. Kishida, M. Matsumuro, and Y. Shirai. Gamma Titanium Aluminide Alloys. In *MRS Symposium Proceedings*, volume 364. Materials Research Society, 1995. 12, 13
- [40] I. H. Katzarov, M. J. Cawkwell, A. T. Paxton, and M. W. Finnis. Atomistic study of ordinary [image omitted] screw dislocations in single-phase and lamellar-TiAl. *Philosophical Magazine*, 87(12):1795–1809, 2007. 12, 13, 14
- [41] C. Woodward and S.I. Rao. *Phil. Mag. A*, 84:401–413, 2004. 12
- [42] S. Znam, D. Nguyen-Manh, DG Pettifor, and V. Vitek. Atomistic modelling of TiAl I. Bond-order potentials with environmental dependence. *Philosophical Magazine*, 83(4):415–438, 2003. 12, 14, 80, 115, 132

- [43] Y. Minonishi and M. H. Yoo. Anomalous temperature dependence of the yield stress of Ti₃Al by {1121} ⟨1126⟩ slip. *Philosophical Magazine Letters*, 61(0950-0839):203–208, 1990. 14
- [44] Yasuhide Minonishi. Plastic deformation of single crystals of Ti₃Al with D019 structure. *Philosophical Magazine A*, 63(0141-8610):1085–1093, 1991. 14
- [45] Y. Umakoshi, T. Nakano, T. Takenaka, K. Sumimoto, and T. Yamane. Orientation and temperature dependence of yield stress and slip geometry of Ti₃Al and Ti₃Al-V single crystals. *Acta Metallurgica et Materialia*, 41(4):1149 – 1154, 1993. 14, 15
- [46] Inui H., Toda Y., and Yamaguchi M. Plastic deformation of single crystals of a DO19 compound with an off-stoichiometric composition (Ti-36.5 at.% Al) at room temperature. *Philosophical Magazine A*, 67:1315–1332, 1993. 14
- [47] H. Inui, Y. Toda, Y. Shirai, and M. Yamaguchi. Low-temperature deformation of single crystals of a DO19 compound with an off-stoichiometric composition (Ti-36.5 at.% Al). *Philosophical Magazine A*, 69(0141-8610):1161–1177, 1994. 14
- [48] Y. Minonishi. Dissociation of 1/3⟨1̄126⟩{11̄21} superdislocations in TiAl single crystals deformed at high temperatures. *Materials Science and Engineering: A*, 192:830–836, 1995. 15
- [49] Ping Wang, D. Veeraraghavan, and Vijay K. Vasudevan. Observation of twins in the [alpha]2 phase in a quenched Ti-46.54 at.% Al alloy. *Scripta Materialia*, 34(10):1601 – 1607, 1996. 15

- [50] K. Kishida, Y. Takahama, and H. Inui. Deformation twinning in single crystals of a D019 compound with an off-stoichiometric composition (Ti-36.5at.%Al). *Acta Materialia*, 52(16):4941 – 4952, 2004. 15
- [51] K. Kishida, J. Yoshikawa, H. Inui, and M. Yamaguchi. c-Axis tensile deformation of Ti₃Al with the DO19 structure at room temperature. *Acta Materialia*, 47(12):3405 – 3410, 1999. 15
- [52] Y. Umakoshi, T.Nakano, K.Sumimoto, and Y.Maeda. Plastic Anisotropy of Ti₃Al Single Crystals. In *MRS Symposium Proceedings*, volume 288. Materials Research Society, 1993. 16
- [53] C. L. Fu, J. Zou, and M. H. Yoo. Elastic constants and planar fault energies at the Ti₃Al, and interfacial energies at the Ti₃Al/TiAl interface by first-principles calculations. *Scripta Metallurgica et Materialia*, 33(6):885–891, 1995. 15
- [54] T. Hong, T. J. Watson-Yang, X. Q. Guo, A. J. Freeman, T. Oguchi, and Jian hua Xu. Chrystal structure, phase stability, and electronic tructure of Ti-Al intrmetallics: Ti₃Al. *Physical Review B*, 43, 1991-II. 15, 88
- [55] Y. L. Liu, L. M. Liu, S. Q. Wang, and H. Q. Ye. First-principles study of shear deformation in TiAl and Ti₃Al. *Intermetallics*, 15:428–435, 2007. 15
- [56] S. Rao, C. Woodward, and P. M. Hazzledine. The interaction between dislocations and lamellar grain boundaries in PST γ TiAl. In *MRS Symposium Proceedings*, volume 319. Materials Research Society, 1994. 17
- [57] I.H. Katzarov and A.T. Paxton. Atomistic studies of interactions between the dominant lattice dislocations and γ/γ -lamellar boundaries in lamellar γ -tial. *Acta Materialia*, 57(11):3349 – 3366, 2009. 17

- [58] Katzarov, Ivaylo H. and Paxton, Anthony T. Microscopic Origin of Channeled Flow in Lamellar Titanium Aluminide. *Phys. Rev. Lett.*, 104:225502, Jun 2010. 17
- [59] Murray S. Daw and M. I. Baskes. Semiempirical, Quantum Mechanical Calculation of Hydrogen Embrittlement in Metals. *Phys. Rev. Lett.*, 50:1285–1288, Apr 1983. 19
- [60] MW Finnis and JE Sinclair. A simple empirical N-body potential for transition metals. *Philosophical Magazine A*, 50(1):45–55, 1984. 19
- [61] F. Ducastelle and F. Cyrot-Lackmann. *J. Phys. Chem. Solid.*, 31, 1970. 20
- [62] F. Ducastelle and F. Cyrot-Lackmann. *J. Phys. Chem. Solid.*, 32, 1970. 20
- [63] I. I. Oleinik and D. G. Pettifor. Analytic bond-order potentials beyond tersoff-brenner. ii. application to the hydrocarbons. *Physical Review B*, 59(13), 1999. 20
- [64] D. G. Pettifor and I. I. Oleinik. Analytic bond-order potentials beyond tersoff-brenner. i. theory. *Physical Review B*, 59(13), 1999. 21
- [65] Ralf Drautz and D. G. Pettifor. Valence-dependent analytic bond-order potential for transition metals. *Phys. Rev. B*, 74:174117, Nov 2006. 21
- [66] Ralf Drautz and D. G. Pettifor. Valence-dependent analytic bond-order potential for magnetic transition metals. *Phys. Rev. B*, 84:214114, Dec 2011. 21
- [67] Inderjit Singh Dhillon. *A New $O(n^2)$ Algorithm for the Symmetric Tridiagonal Eigenvalue/Eigenvector Problem*. PhD thesis, University of California, Berkeley, 1997. 21

- [68] MW Finnis, AT Paxton, M Methfessel, and M van Schilfgaarde. Self-consistent tight-binding approximation including polarisable ions. 491:265–274, 1997. 21, 36
- [69] E. Schrödinger. An undulatory theory of the mechanics of atoms and molecules. *Phys. Rev.*, 28:1049–1070, Dec 1926. 22
- [70] Peter J. Mohr, Barry N. Taylor, and David B. Newell. Codata recommended values of the fundamental physical constants: 2006. *Rev. Mod. Phys.*, 80:633–730, Jun 2008. 24
- [71] M. Born, with emendations by Brian Sutcliffe J. R. Oppenheimer, English translation by S. M. Blinder, and Wolf Gepert (2002). Zur quantentheorie der moleküle (on the quantum theory of molecules). *Ann. Physik*, 84:457–484, January 1927. 24
- [72] E. Fermi. Eine statistische methode zur bestimmung einiger eigenschaften des atoms und ihre anwendung auf die theorie des periodischen systems der elemente. *Zeitschrift für Physik A Hadrons and Nuclei*, 48:73–79, 1928. 10.1007/BF01351576. 25
- [73] P. Hohenberg and W. Kohn. Inhomogeneous electron gas. *Phys. Rev.*, 136:B864–B871, Nov 1964. 25
- [74] W. Kohn and L. J. Sham. Quantum density oscillations in an inhomogeneous electron gas. *Phys. Rev.*, 137:A1697–A1705, Mar 1965. 25
- [75] W. Kohn and L. J. Sham. Self-consistent equations including exchange and correlation effects. *Phys. Rev.*, 140:A1133–A1138, Nov 1965. 25

- [76] Donald G. Anderson. Iterative procedures for nonlinear integral equations. *Journal of the Association for Computing Machinery*, 12(4):547–560, October 1965. 28
- [77] C. G. Broyden. *Math. Comp.*, 19:577–593, 1965. 28
- [78] J. Harris. Simplified method for calculating the energy of weakly interacting fragments. *Phys. Rev. B*, 31:1770–1779, Feb 1985. 29
- [79] W. Matthew C. Foulkes and Roger Haydock. Tight-binding models and density-functional theory. *Phys. Rev. B*, 39:12520–12536, Jun 1989. 29
- [80] O. Krogh Andersen. Linear methods in band theory. *Phys. Rev. B*, 12:3060–3083, Oct 1975. 31, 81
- [81] Felix Bloch. Über die quantenmechanik der elektronen in kristallgittern. *Zeitschrift für Physik A Hadrons and Nuclei*, 52(7-8):555–600, 1928. 34
- [82] JC Slater and GF Koster. Simplified LCAO Method for the Periodic Potential Problem. *Physical Review*, 94(6):1498–1524, 1954. 36, 37
- [83] A P Sutton, M W Finnis, D G Pettifor, and Y Ohta. The tight-binding bond model. *Journal of Physics C: Solid State Physics*, 21(1):35, 1988. 36, 41
- [84] L. Goodwin, A. J. Skinner, and D. G. Pettifor. Generating Transferable Tight-Binding Parameters: Application to Silicon. *Europhys. Lett.*, 9:701–706, 1989. 37, 66, 73, 80
- [85] J. A. Majewski and P. Vogl. *The Structures of Binary Compounds, F. R. de Boer and D. G. Pettifor*. Elsevier Science Publishing, 1989. 38

- [86] H. Haas, C. Z. Wang, M. Fähnle, C. Elsässer, and K. M. Ho. Environment-dependent tight-binding model for molybdenum. *Phys. Rev. B*, 57:1461–1470, Jan 1998. 39
- [87] M. Mrovec, D. Nguyen-Manh, D. G. Pettifor, and V. Vitek. Bond-order potential for molybdenum: Application to dislocation behavior. *Phys. Rev. B*, 69:094115, Mar 2004. 39, 44
- [88] D. Nguyen-Manh, DG Pettifor, and V. Vitek. Analytic Environment-Dependent Tight-Binding Bond Integrals: Application to MoSi_2 . *Physical Review Letters*, 85(19):4136–4139, 2000. 39
- [89] M. Mrovec, R. Gröger, A. G. Bailey, D. Nguyen-Manh, C. Elsässer, and V. Vitek. Bond-order potential for simulations of extended defects in tungsten. *Phys. Rev. B*, 75:104119, Mar 2007. 39
- [90] R Haydock, V Heine, and M J Kelly. Electronic structure based on the local atomic environment for tight-binding bands. *Journal of Physics C: Solid State Physics*, 5(20):2845, 1972. 42, 48
- [91] CA Coulson. The Electronic Structure of Some Polyenes and Aromatic Molecules. VII. Bonds of Fractional Order by the Molecular Orbital Method. *Proceedings of the Royal Society of London. Series A, Mathematical and Physical Sciences (1934-1990)*, 169(938):413–428, 1939. 42
- [92] Wolfgang Pauli. Exclusion principle and quantum mechanics. 10 1946. Nobel Lecture. 43
- [93] L E Ballentine and M Kolar. Recursion, non-orthogonal basis vectors, and the computation of electronic properties. *Journal of Physics C: Solid State Physics*, 19(7):981, 1986. 44

- [94] F. Cyrot-Lackmann. Sur le calcul de la cohesion et de la tension superficielle des metaux de transition par une methode de liaisons fortes. *J. Phys. Chem. Solids*, 29:1235–1243, 1968. 44
- [95] T. J. Stieltjes. Recherches sur les fractions continues. *Annales de la Faculte des Sciences de Toulouse*, 8:1, 1894. 46
- [96] T. J. Stieltjes. Recherches sur les fractions continues. *Annales de la Faculte des Sciences de Toulouse*, 9:5, 1894. 46, 48
- [97] Robert M. Mnatsakanov and Artak S. Hakobyan. Recovery of Distributions via Moments. In *Optimality: The Third rich L. Lehmann Symposium*, volume 57 of *IMS Lecture Notes-Monograph Series*, pages 252–265. Institute of Mathematical Statistics, 2009. 46
- [98] Parthapratim Biswas and Arun K. Bhattacharya. Function reconstruction as a classical moment problem: a maximum entropy approach. *J. Phys. A: Math. Theor.*, 43, 2010. 46
- [99] R Haydock, V Heine, and M J Kelly. Electronic structure based on the local atomic environment for tight-binding bands. ii. *Journal of Physics C: Solid State Physics*, 8(16):2591, 1975. 48
- [100] C. Lanczos. An iteration method for the solution of the eigenvalue problem of linear differential and integral operators. *J. Res. Nat. Bur. Standards*, 45(4):255–282, 1950. 48
- [101] C. C. Paige. Error analysis of the lanczos algorithm for tridiagonalizing a symmetric matrix. *J. Inst. Maths Applics.*, 18:341–349, 1976. 50
- [102] Taisuke Ozaki. Bond-order potential based on the lanczos basis. *Phys. Rev. B*, 59:16061–16064, Jun 1999. 52

- [103] P. Turchi, F. Ducastelle, and G. Treglia. 15:2891, 1982. 53
- [104] P. Turchi and F. Ducastelle. *Band gaps and asymptotic behaviour of continued fraction coefficients, in The Recursion Method and Its Applications.* Springer-Verlag, Berlin - Heidelberg - New York - Tokyo, 1985. 53, 101
- [105] AP Horsfield, AM Bratkovsky, M. Fearn, DG Pettifor, and M. Aoki. Bond-order potentials: Theory and implementation. *Physical Review B*, 53(19):12694–12712, 1996. 55
- [106] AP Horsfield, AM Bratkovsky, DG Pettifor, and M. Aoki. Bond-order potential and cluster recursion for the description of chemical bonds: Efficient real-space methods for tight-binding molecular dynamics. *Physical Review B*, 53(3):1656–1666, 1996. 55, 57
- [107] D. Nguyen-Maxh, D. G. Pettifor, S. Znam, and V. Vitek. Negative cauchy pressure within the tight-binding approximation. 491, 1997. 59, 77
- [108] Masato Aoki and Tatsuya Kurokawa. A simple environment-dependent overlap potential and cauchy violation in solid argon. *Journal of Physics: Condensed Matter*, 19(23):236228, 2007. 60
- [109] G. J. Acklandab, G. Tichy, V. Vitek, and M. W. Finnis. Simple n-body potentials for the noble metals and nickel. *Philosophical Magazine A*, 56:735–756, 1987. 61, 80
- [110] Georg K. H. Madsen, Eunan J. McEniry, and Ralf Drautz. Optimized orthogonal tight-binding basis: Application to iron. *Phys. Rev. B*, 83:184119, May 2011. 76
- [111] Anthony T. Paxton. An Introduction to the Tight Binding Approximation - Implementation by Diagonalisation. In Johannes Grotendorst, Norbert Attig, Stefan Blügel, and Do-

- minik Marx, editors, *Multiscale Simulation Methods in Molecular Sciences*, volume 42 of *Publication Series of the John Neumann Institute for Computing (NIC)*, chapter 1. Jülich Supercomputing Centre, 2009. 79
- [112] A. Girshick. Atomistic simulation of titanium I. A bond-order potential. *Philosophical Magazine A*, 77(4):981–997, 1998. 79, 115
- [113] A. T. Paxton. *J. Phys. D: Appl. Phys.*, 29, 1996. 79
- [114] A. T. Paxton and M. W. Finnis. *Phys. Rev. B*, 77, 2008. 79
- [115] W. A. Harrison. *Electronic structure and the properties of solids: the physics of the chemical bond*. W. H. Freeman, San Francisco, 1980. 79
- [116] D. Spanjaard and M. C. Desjonquères. *Phys. Rev. B*, 30, 1984. 79
- [117] Anders G. Froseth, Peter Derlet, and Ragnvald Hoier. Determination of total energy tight binding parameters from first principles calculations using adaptive simulated annealing. *MRS Proceedings*, 700, 2001. 79
- [118] M. Finnis. *Interatomic Forces in Condensed Matter*. Oxford University Press, USA, 2003. 79, 105
- [119] A. Urban, M. Reese, M. Mrovec, C. Elsässer, and B. Meyer. Parameterization of tight-binding models from density functional theory calculations. *Phys. Rev. B*, 84:155119, Oct 2011. 80, 110
- [120] O. K. Andersen and O. Jepsen. Explicit, First-Principles Tight-Binding Theory. *Phys. Rev. Lett.*, 53(27):2571–2574, Dec 1984. 81, 83, 85, 104

- [121] OK Andersen, Z. Pawlowska, and O. Jepsen. Illustration of the linear-muffin-tin-orbital tight-binding representation: Compact orbitals and charge density in Si. *Physical Review B*, 34(8):5253–5269, 1986. 82, 84, 86
- [122] D G Pettifor. First principle basis functions and matrix elements in the H-NFE-TB representation. *Journal of Physics C: Solid State Physics*, 5(2):97, 1972. 82
- [123] O. K. Andersen, O. Jepsen, and M. Šob. *Electronic band structure and its applications*, M. Yusouff. Springer, Berlin, 1987. 82, 84, 86
- [124] *Canonical description of the band structures of metals*, Proc. Intl. Sch. Phys. LXXXIX Corso, F. Basani, F. Fumi and M. P. Tosi, Varenna, 1984. 84, 85
- [125] M. Methfessel, Mark van Schilfgaarde, and R. A. Casali. A *full-potential LMTO method based on smooth Hankel functions*. Lecture Notes in Physics, H. Dreysse. Springer-Verlag, Berlin, 2000. 87
- [126] E. Wimmer, H. Krakauer, M. Weinert, and A. J. Freeman. Full-potential self-consistent linearized-augmented-plane-wave method for calculating the electronic structure of molecules and surfaces: O_2 molecule. *Phys. Rev. B*, 24:864–875, Jul 1981. 87
- [127] M. Weinert, E. Wimmer, and A. J. Freeman. Total-energy all-electron density functional method for bulk solids and surfaces. *Phys. Rev. B*, 26:4571–4578, Oct 1982. 87
- [128] The Elk FP-LAPW Code. 87
- [129] E. Bott, M. Methfessel, W. Krabs, and P. C. Schmidt. Non-singular Hankel functions as a new basis for electronic struc-

ture calculations. *Journal of Mathematical Physics*, 39, June 1998. 87

- [130] *Recent advances in non self-consistent total energy calculations in alloys*, volume 186 of *Alloy Phase Stability and Design*, G. M. Stocks, A.F. Giamei and D.P. Pope. MRS. Symp. Proc., 1990. 88
- [131] *The Effect of Scandium on the Microstructure of Ti₃Al*, volume 288. Materials Reserch Society, 1993. 88
- [132] D. G. Pettifor. *Commun. Phys.*, 1, 1976. 89
- [133] A. R. Mackintosh and O. K. Andersen. Cambridge University Press, 1979. 89
- [134] N. E. Christensen. Structural phase stability of B2 and B32 intermetallic compounds. *Phys. Rev. B*, 32(1):207–228, Jul 1985. 89
- [135] N. Beer and D. G. Pettifor. volume 113 of *NATO ASI*, page 769. Plenum, New York, 1982. 100
- [136] Roger Haydock and Ronald L. Te. Accuracy of the recursion method. *Physical Review B: Condensed Matter*, 49, 1994. 102
- [137] K. Levenberg. A method for the solution of certain non-linear problems in least squares. *The Quarterly of Applied Mathematics*, pages 164–168, 1944. 111
- [138] D. W. Marquardt. An algorithm for least-squares estimation of nonlinear parameters. *J. Society for Industrial and Applied Mathematics*, 11:431–441, 1963. 111
- [139] D. Nguyen-Manh, DG Pettifor, S. Znam, and V. Vitek. Tight-Binding Approach to Computational Materials Science. *Ma-*

terials Research Society Symposium Proceedings, 491, 1998.
114

- [140] A J Fisher. Methods of embedding for defect and surface problems. *Journal of Physics C: Solid State Physics*, 21(17):3229, 1988. 121

Acknowledgements

The journey over the years had its ups and downs and offered no shortage of disappointments and joy. It was also a time of rethinking, introspection and positive personal transformation which I fear may not have happened had I not taken the challenge of starting another life.

Firstly I would like to thank the people who had most to do with the completion, my supervisors Ivo Katzarov and Tony Paxton for the opportunity, guidance, ideas and encouragement they gave me, and especially for their seemingly endless patience. I know I would have hardly had enough of it to put up with a student like myself.

I cannot thank enough to the people who have helped me in the beginning: Matthias Meister, Alin Elena, till the end: Sasha Lozovoi, for the insightful discussions on physics, science, politics and everything else. Special thanks goes to Sasha for the ideas he gave me on the functional cutoffs and the numerous puzzles, to Matthias for making me understand the usefulness of \TeX and \LaTeX , and to Alin for taking the time to show me the benefits of mastering the seemingly negligible intricacies of coding, linking, compiling etc..

I should also thank Robin, Nancy, Claire, Tristan, Jorge, Malachy, Peter, Tchavdar and all other member of the ASC for the friendly and cheerful atmosphere.

Since the first week in Belfast I was lucky to meet good housemates and friends Fernando and Tej. The Sunday mornings' Magi Mays adventures, the new cuisine, the fierce debates on pretty

much everything, and everything else has made the first half of my stay an indispensable experience.

I would like to express my gratitude to my teachers and lecturers who cared deeply about teaching despite the headaches it usually brought them.

The entire adventure of academic life would most certainly not have been possible without the support from my parents and my brother during the more or less permanently murky times of hardship and austerity.

At last I shall aknowledge EPSRC's financial support.